1

INTRODUCTION TO LC–MS TECHNOLOGY

Interpretation of MS–MS Mass Spectra of Drugs and Pesticides, First Edition. Wilfried M. A. Niessen and Ricardo A. Correa C.

1.1 INTRODUCTION

In order to separate and quantify ions using mass spectrometry (MS), one must first generate and then send them to the mass analyzer, which is no easy task by any means. This process takes place in the ion source, where the introduced neutral atoms or molecules (the sample) are rendered ionized and in the gas phase. From there, they are sent into the mass analyzer and separated according to their m/z (mass-to-charge ratio (Section 2.2), where m is the mass number of an ion and z is the number of elementary charges regardless of sign). The order in which ionization and vaporization happen depends on the chosen technique, but ultimately the ions will have to find themselves under vacuum so that the mean free path between them is long enough to avoid random collisions, for example, fragment–fragment reactions. This is essential for the tenet of unimolecular reactions in MS to hold, whereby all the ions seen in the mass spectrum arise from the initially ionized sample in question. The ions generated can be odd-electron ions ($OE^{+\bullet}$ or $OE^{-\bullet}$) or even-electron ions (EE^+ or EE^-). Providing the m/z for all ions and especially for the ions related to the intact molecule, for example, molecule ion or (de)protonated molecule, is the main reason of MS success as an analytical technique. In general, one can say that there are two main types of ionization techniques: hard and soft ionization techniques. In the former case, the molecular ion undergoes significant fragmentation (even with no molecular ion detection), whereas in the latter case ions do not undergo extensive (or any) fragmentation and an ion related to the intact molecule is readily detected.

In practice, chemical analysis begins with two critical steps that determine the ultimate quality of the experiments: sample collection and preparation, which should always strive at getting the highest purity specimen possible. The ion source contribution to the overall instrumental sensitivity arises from the two main events taking place within: sample ionization and ion transmission to the mass analyzer. Ionization efficiency is defined as the ratio of the number of ions generated to the number of molecules consumed in the ion source of a mass spectrometer: the method for determining the number of molecules consumed has to be clearly stated. The transmission efficiency is defined as the ratio of the number of ions leaving a region of a mass spectrometer to the number of ions entering that region. Since the performance

of a source is tightly related to its actual components and their operating principles, sensitivity optimization depends on the kind and model of instrument used.

Sample introduction to the source is done by several methods: the most common being directly via a direct vapor inlet, or a direct insertion or exposure probe; indirectly via hyphenated techniques such as gas chromatography–mass spectrometry (GC–MS) and liquid chromatography–mass spectrometry (LC–MS), or surface-related desorption techniques such as thermally or laser-assisted techniques. Hyphenated techniques refer to the coupling of two (or more) separate analytical techniques by means of an appropriate hardware interface. In such cases, the instruments used in the hyphenated techniques work together in an automated manner as a single integrated unit (Hirschfeld, 1980). Particularly interesting is the coupling of powerful separation techniques, for example, GC, LC, thin-layer chromatography, electrophoresis, with spectrometry-related methods, for example, MS, infrared, ultraviolet–visible, atomic absorption, fluorescence, light scattering, Raman, nuclear magnetic resonance, for the analysis and characterization of all kinds of known matter.

1.2 ANALYTE IONIZATION: ION SOURCES

1.2.1 Electron Ionization

Electron ionization (EI) is a hard ionization technique and one of the oldest ionization methods in existence, yet still one the most widely used (Märk & Dunn, 1985). Vaporization of sample molecules must take place before their ionization, and therefore this limits the scope of the technique to volatile and thermostable compounds. EI furnishes ions by extracting one (or more) electron (e^-) out of the neutral sample molecule (M), according to Eq. 1.1. This process is carried out with high-energy electrons produced by means of thermionic emission from a heated (tungsten or rhenium) filament inside the source. Typically, the electrons are accelerated with a potential difference of 70 V. The energetic electrons interact with the analyte molecules, transfer part of their energy to the molecules, and render them ionic. The result is the production of a radical cation $M^{+\bullet}$ (molecular ion) and two electrons: the electron ejected from the neutral molecule and the ionizing electron after transferring part of its energy to M.

$$M + e^- \rightarrow M^{+\bullet} + 2e^- \tag{1.1}$$

The fate of the radical cation ($M^{+\bullet}$) produced depends on its internal energy at the moment of formation, which is determined by the kind and number of chemical bonds present in the sample molecule. It is $M^{+\bullet}$ and its fragmentation products (when present) that constitute the EI mass spectrum of the sample, and in principle for a given set of experimental conditions, each individual compound analyzed gives a unique mass spectrum (except for enantiomers).

1.2.1.1 Ionization Using Electrons The general operating components of an EI source are illustrated in Figure 1.1. These are contained within a heated (to avoid condensation of sample and ions) metal housing called the source block. EI uses thermionic emission as the main working principle for the production of high-energy (usually 70 eV, $1\,\text{eV} = 1.602177 \times 10^{-19}$ J) electrons under vacuum (0.1–1 Pa; 10^{-3}–10^{-2} mbar) in order to disrupt the nonbonding and bonding electrons of molecules.

An appropriately housed (coiled) tungsten or rhenium filament (cathode) is heated by passing a current through it (2–5 A). Once it reaches a certain temperature, the thermal energy of the electrons (greater than the work function of the metal) at the metal surface is sufficient to allow them to leave the metal thereby creating a flow of electrons. This is the thermionic emission of electrons from the filament. Concurrently, a negative potential (−70 V) is applied to the filament (e^- energy), and the electrons are thus accelerated

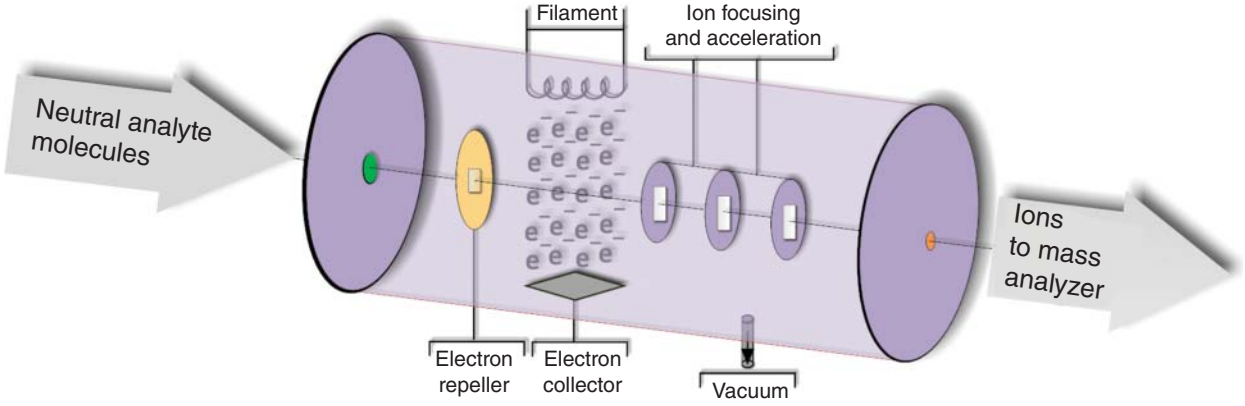

FIGURE 1.1 Schematic diagram of an electron ionization (EI) source.

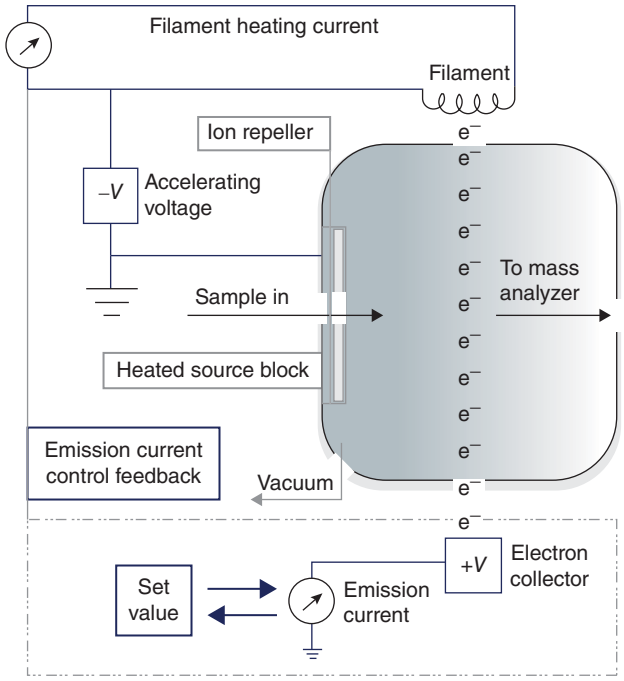

FIGURE 1.2 Scheme for the generation of ionizing electrons in an EI source.

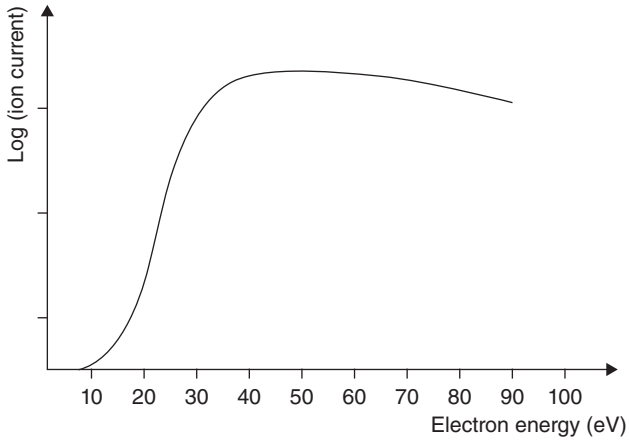

FIGURE 1.3 Relationship between ion current and electron energy.

and travel across from the surface of the metal filament to within the volume of the ion source. These electrons are attracted (by a positive voltage) to the e^- collector (anode) located opposite and on-axis to the filament. This filament current (emission current) is measured and kept constant (150 µA) via a feedback mechanism with the heating current driven through the filament. This ensures constant ionization conditions (the number of electrons emitted by the filament is constant). Effectively, this setup places a shower of electrons that analyte molecules must cross as they are transmitted from the inlet (sample in) to the outlet (to mass analyzer) of the EI source (Figure 1.2). Often, by using a magnet, the flight path of the electrons is made helical; since the electrons must travel a longer path, their interaction with analyte molecules is enhanced.

Fortunately, the value of 70 eV has been used for the electron energy (and to less extent 150 µA for the emission current) throughout the years, and this has allowed for the creation of searchable EI mass spectral libraries that are of critical importance to the analytical applications of MS. By controlling the energy of the electrons, one can achieve different ionizing conditions for a given sample. The plot of the ion current versus the electron energy for most atoms and molecules shows the general behavior illustrated in Figure 1.3. A rise in the ion current is observed once the analyte ionization energy (IE, minimum energy required to eject an e^- out of a neutral atom or molecule in its ground state) is reached. As the electron energy increases (≈20 eV), so does the ion current, mostly due to the formation of molecular ions. Further increase in energy (>30 eV) promotes fragmentation until a plateau is reached (around 70 eV); higher electronic energies actually cause a decrease in the ion current (Hübschmann, 2015). Operating the source at 70 eV for the electron energy, that is, at the plateau in Figure 1.3, ensures stable performance of the EI source. The EI efficiency is evaluated by the ratio of the number of ions formed to the number of electrons used in an ionization process.

Considering that helium has the highest ionization energy of any element (24.6 eV), along with the fact that the IE for most organic compounds lies between 5 and 12 eV, electrons with 70 eV will have more energy than the IE required to ionize incoming neutral species (Montalti et al., 2006). In chemistry, eV (non-SI unit) is expressed in molar terms and thus $70\,\text{eV} = 6{,}754\,\text{kJ mol}^{-1}$. The amount of excess energy transferred from the electron to the molecule, typically a few eV (≈5 eV), and the structure of the molecule will determine the degree of fragmentation. The general trend of atomic IE is the same as the one for electronegativity, for example, F > Cl > Br > I. For molecules, nonbonding (nb) electrons are easier to ionize than bonding electrons, for example, IE of F-nb > N-nb > O-nb > S-nb. The greater the s character of a covalent bond, the more the electronegative it is; thus, the IE of a sigma sp bond (alkynes) > sp^2 sigma bond (alkenes) > sp^3 sigma bond (alkanes) > nb electrons. Special molecular features, for example, conjugation, which can help stabilize the resulting radical cation, greatly influence the IE value of a molecule.

1.2.1.2 Ionization and Fragmentation As the sample is introduced into the source (perpendicular to the electron axis), electrons and neutral molecules interact. When the rapprochement of sample molecules and electrons is within the ionization cross-sectional area (area the electron must cross to lead to an effective ionization) of the analyte molecule and

the energy transferred is at least equal to the ionization energy, the loss of one (or more) electron is observed, along with the eventual fragmentation of the molecular ion thus produced. In the vacuum of the EI source, a random collision between an e^- and a sample molecule is extremely unlikely. Furthermore, the electrostatic repulsion of valence electrons makes it even more improbable. It is the electric field of the fast-moving charge (e^-) that causes a distortion in the orbits of the valence electrons. This interaction leads to a kinetic energy transfer from the e^- to the analyte cloud of electrons. If enough energy is transferred (IE) during this process, a valence electron is ejected from the analyte molecule, thereby forming an $M^{+\bullet}$. It is worthwhile noting that the de Broglie wavelength (λ) of the ionizing electrons must be of the same order as the bond length of the sample molecule, otherwise the energy transfer from the electrons to the analyte molecule will not happen effectively, for example, a 70 eV electron has a λ of 150 pm, an sp^2 hybridized C—C double bond has a bond length of ≈130 pm (Allen et al., 2006).

Approximately speaking, molecules have a diameter ranging from 0.1 nm for the smallest molecule (H_2), through macromolecules and supramolecular assemblies with diameters between 10 and 90 nm, for example, polymers, ATP synthase, to viruses and complex biological structures with >100 nm in diameter, for example, influenza virus, phages, chromosomes (Goodsell, 2009). Considering that the reaction in Eq. 1.1 is happening between two classical particles, an e^- with an energy of 70 eV travels approximately at a speed of 5000 km s^{-1} (0.017c, where c is the speed of light), which means that for a molecule like sucrose (nominal mass of 342 Da) with a 1 nm molecular diameter (Ramm et al., 1985), the electron will pass by the molecule in 2×10^{-16} s. In this timescale, the interaction between the electron and the molecule occurs much faster than that of an sp^3 O—H bond stretching vibration (10^{-14} s). As this electronic transition happens before any change occurs in the position of the nuclei involved (Franck–Condon principle), it can happen vertically from the electronic ground state of M to a (meta)stable excited electronic state of $M^{+\bullet}$ (or higher energy states) as illustrated in Figure 1.4. Taking a homodiatomic molecule as an example (Demtröder, 2010), its electronic ground state can be represented as shown in Figure 1.4a: the potential energy well is defined by the bond dissociation energy and the bond length. When the high-energy electrons match an electronic transition *i* (Figure 1.4b), the energy transfer leads to a stable excited electronic state (molecular ion), plus an e^- ejected off from the neutral sample. It is important to notice that electronic states higher than the ground state have potential energy wells with shallower minima and longer internuclear separations. Therefore, the bond is both weaker and elongated as a result of the ionization process (Figure 1.4b). Equally, if the energy of the electrons matches an electronic transition like *j* in Figure 1.4b, the formation of the radical cation will lead to an unstable excited state and fragmentation ensues.

What happens to the newly formed ions depends on their total energy and the ease with which they dissipate the excess energy among their other modes of motion, namely translational, vibrational, and rotational. Generally, the ions can be stable and last long enough to be detected, they can rapidly decompose producing fragment ions, or they can be

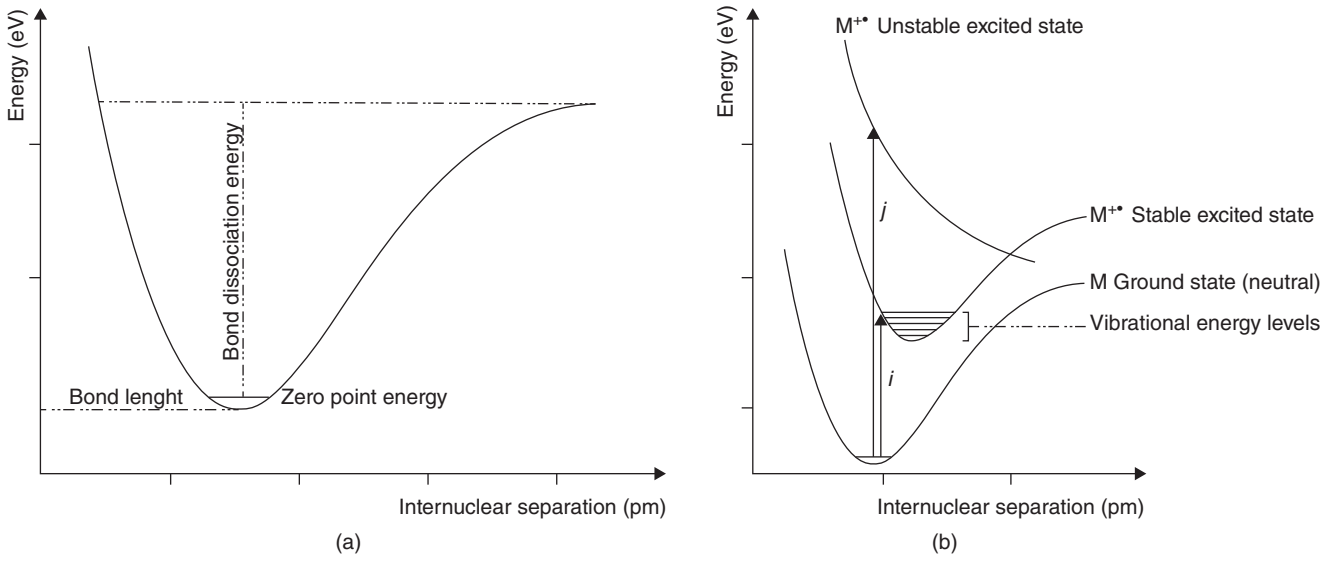

FIGURE 1.4 Ground electronic state of a neutral homodiatomic molecule (a). Vertical transitions depicting the ionization process in an EI source (b).

metastable and decompose in their flight to the detector. It is a process that is tightly related to the exact chemical structure of a molecule (Blanksby & Ellison, 2003).

1.2.1.3 Ion Transmission Ion transmission refers to the process of moving ions from one section to another within the mass spectrometer, for example, from the source through the analyzer and furthest to the detector. This process is not always necessarily accompanied by an *m*/*z* separation. In fact, in an EI source when transferring the ions produced into the analyzer, the goal is to do so with highest efficiency and lowest *m*/*z* spreading. Two complementary and simultaneous devices are applied (Figure 1.5). First, as the ions are being produced, a potential difference of the same sign is applied to the ion repeller, which is a plate placed before and perpendicular to the electron flux. This ion repeller pushes the ions toward the mass analyzer.

Second, three parallel (exact design changes depending on manufacturer) electrostatic lenses of equal sign are placed opposite and on-axis to the ion repeller, between the e^- flux and the mass analyzer. A potential difference of opposite sign to the ion repeller is applied in order to extract the ions out of the source, followed by a lower potential difference in order to focus the ions to finally reaccelerate them as they are sent into the mass analyzer, where separation according to their *m*/*z* takes place. Typical fragmentation characteristics under EI conditions are briefly discussed in Section 3.3.

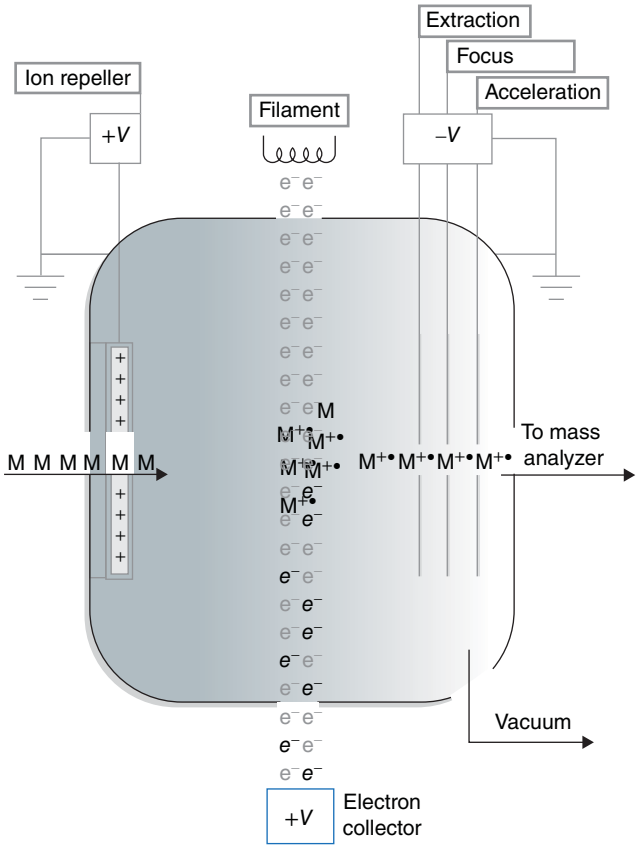

FIGURE 1.5 Devices for ion transmission from the EI ion source to the mass analyzer.

1.2.1.4 Analytical Applications of Electron Ionization EI is probably the most widely applied ionization technique in MS. It is extensively used in GC–MS, where it provides good sensitivity for most compounds and structure-informative fragmentation in highly reproducible mass spectra. Besides, after basic tuning of the ion source, which can be performed automatically under software control, there are essentially no experimental parameters to set or optimize. In terms of qualitative analysis, interpretation of the EI mass spectra can be performed based on a solid understanding of the fragmentation behavior of $M^{+\bullet}$ (Section 3.3) (McLafferty & Tureček, 1993; Smith, 2004). In addition, elaborate and searchable mass spectral libraries have been compiled to assist in the identification of compounds (Atwater et al., 1985; Stein & Scott, 1994; Ausloos et al., 1999; Koo et al., 2013). The results of these library searching routines can be quite powerful. If a mass spectrum of the unknown compound is present in the library, expert comparison of library and experimental mass spectra can lead to compound identification. If the compound is not present in the library, the computer library search often provides insight about the presence of substructures or other structural features of the unknown compound, which facilitates further spectrum interpretation. Although many researchers take the result of the library search for granted, a thorough and critical evaluation of the agreement between experimental and library spectrum is recommended. In addition, GC–MS with EI is also frequently used in quantitative analysis using either extracted-ion chromatograms (Section 1.3.1.1) or selected-ion monitoring (Section 1.5.2) before peak area determination. More recently, gas chromatography tandem mass spectrometry (GC–MS–MS) in selected-reaction monitoring (SRM) (Section 1.5.2) mode has become the method of choice in routine quantitative analysis of compounds present at very low levels in complex biological matrices.

As EI is limited to the analysis of volatile and thermostable analytes, analyte derivatization strategies have been developed to enhance the volatility and stability of more polar analytes. Derivatization obviously changes the fragmentation behavior of the analyte because the fragmentation may be directed from a different site in the molecule (Zaikin & Halket, 2009; Sparkman et al., 2011). Silylation and oximation reactions are most frequently carried out. Characteristic fragment ions derived from the derivatizing agent are readily seen, thereby improving analysis selectivity. For instance, the trimethylsilyl ether derivative ($(CH_3)_3SiOR$) of hydroxy group (OH) containing molecules show the trimethylsilyl group ion with *m*/*z* 73 ($[(CH_3)_3Si]^+$) and an ion with *m*/*z* 75 corresponding to protonated dimethylsilanone

($[(CH_3)_2SiO+H]^+$). When the target compound has several trimethylsilyl ether moieties, the formation of the pentamethyldisiloxane cation ($[(CH_3)_2SiOSi(CH_3)_3]^+$) with *m/z* 147 is observed (a commonly seen ion from GC column bleeding). These ions may undergo ion–neutral reactions with analyte molecules (M), one of these reactions is the adduct formation of an ion with *m/z* (M+73) (Carles et al., 2007).

After seeing the power of EI in GC–MS, the implementation of EI in LC–MS has been pursued as well. However, given the gas load of the mostly aqueous mobile-phase vapor admitted into the ion source and the MS vacuum system in LC–MS, it is more complicated to achieve the high-vacuum ion source conditions required for successful EI. The most successful approaches to EI in LC–MS (which were also commercialized) were the moving-belt interface (Arpino, 1989) and the particle-beam interface (Creaser & Stygall, 1993), both quite complex instrumental solutions. Unfortunately, these solutions did not provide the reliability, user-friendliness, and sensitivity required. More recently, the so-called direct-EI interface has been described, which provides nebulization of the effluent of a nano-LC column (flow rates < 100 nL min^{-1}), directly into the EI source (Cappiello et al., 2011).

1.2.2 Chemical Ionization

Chemical ionization (CI) is a soft ionization technique used to study chemical structure and reactivity. A CI source uses a reagent gas (G_R) inside a modified EI source to create conditions of high source pressure, such that G_R ions–molecule and molecule–e^- reactions can occur in high yield (Harrison, 1992; Munson, 2000). In fact, most instruments are equipped with a source that can be switched between EI and CI conditions. As seen so far, an EI source is an environment where neutral molecules (or atoms) and radicals, radical cations, cations, and electrons coexist. Intuitively, the presence of electrons in the source begs the question of whether or not positive ions are the only ions present in the source. As expected, negative-ion formation is an inherent process in EI and formation of radical anions is also observed (Bowie, 1984).

Thus, there can be a simultaneous presence of positive and negative ions inside an EI/CI source. Their transmission and detection are a matter of choice and depend on the voltage polarities chosen to carry out the experiments, for example, when analyzing negative ions except for the e^- collector voltage in Figure 1.5, all other voltages must be switched in polarity. CI creates conditions that favor the production of EE^+ and EE^-, and as a result, CI can be carried out in two different modes: positive mode as in positive-ion chemical ionization (PICI) and negative mode as in negative-ion chemical ionization (NICI) and electron-capture negative ionization (ECNI). Both modes can use the same source and often but not necessarily use the same G_R. Nevertheless, the function of the G_R serves a different purpose on each mode, and experimental conditions must be optimized for each type of analyte in relation to the mode of CI chosen. Ionization in CI happens without the transfer of large excess of energy from a G_R (and ions thereof) or from a secondary e^-; thus, the initially generated ions do not undergo extensive fragmentation. CI is a technique that offers both high sensitivity and selectivity. Nevertheless, it is not suitable to all kinds of molecules as the analytes must be volatile and thermostable and must present special structural features in order to be responsive to the technique.

1.2.2.1 Electron Ionization of the Reagent Gas, G_R

For particles of similar shape and at a given temperature, the mean free path between them is inversely proportional to the pressure. Usually, in EI the mean free path is ≥1 m, and caution must be taken as mean free paths of ≤0.5 m lead to ion–ion reactions, generating an atypical mass spectrum. As the G_R flows into the CI source, it establishes conditions of high pressure (1–100 Pa; 10^{-2}–1 mbar; while the pressure in the vacuum manifold is ≤10^{-3} Pa; 10^{-5} mbar) and its ionization by primary 70 eV electrons readily yields molecular ions ($G_R^{+\bullet}$). In many CI sources, higher electron energies (up to 400 eV) are applied in order to ensure that the electrons penetrate well the high-pressure environment of the ion source. Ensuing fragmentation of $G_R^{+\bullet}$ occurs by forming cations (G_{EE}^+), other radical cations ($G_{OE}^{+\bullet}$), neutral species (R, $R^\bullet$), and secondary electrons (e^-) (Eqs 1.2 and 1.3).

$$G_R + e^- \rightarrow G_R^{+\bullet} + 2e^- \quad (1.2)$$

$$G_R^{+\bullet} \rightarrow G_{EE}^+ + R^\bullet \quad (1.3a)$$

$$G_R^{+\bullet} \rightarrow G_{OE}^{+\bullet} + R \quad (1.3b)$$

Given a controlled flow of G_R into the source, it is the most abundant species and reacts (ion–molecule reactions) with the newly formed $G_R^{+\bullet}$, G_{EE}^+, $G_{OE}^{+\bullet}$ yielding reactive electrophilic cations that can undergo further reactions with analytes of interest. While EI is a unimolecular process, in CI bimolecular and even termolecular reactions generate a steady-state plasma inside the source as shown in Figure 1.6; methane is used as an example to illustrate the reactions observed.

When the sample is introduced into the source, it encounters a plasma of both positive and negative (low-energy electrons) reactive species. The most common reactions taking place involve proton transfer, electron capture, or adduct formation between the analyte of interest and charged species of the reactants. In this technique, the presence of the (de)protonated molecule is characteristic, which serves as a complementary tool to other types of MS methods. The ions generated in PICI, NICI, and ECNI happen via different mechanisms; nevertheless, all three can happen concurrently.

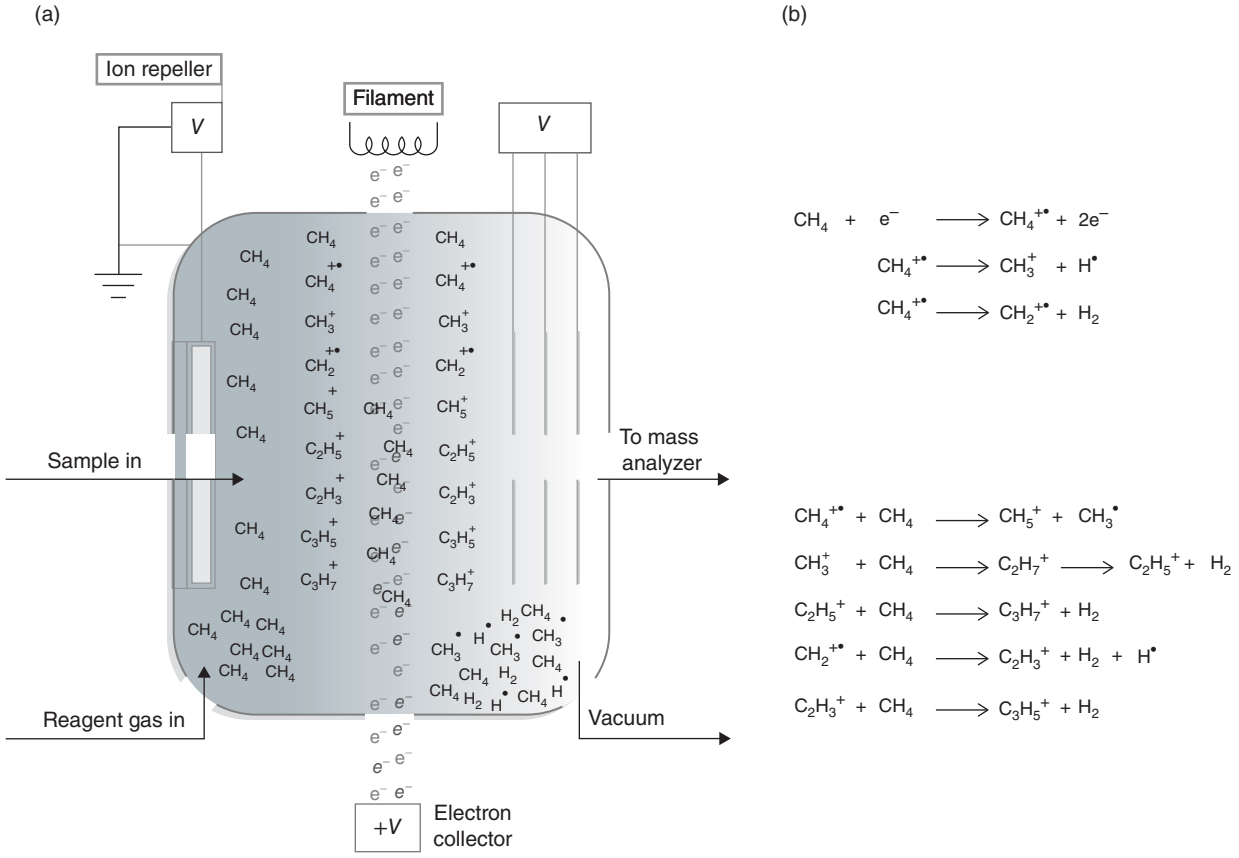

FIGURE 1.6 Ongoing processes inside a chemical ionization (CI) source during reagent gas ionization (methane) in a CI experiment (a). Main chemical reactions involved in the ionization of methane reagent gas in an EI source during a CI experiment (b).

1.2.2.2 Positive-Ion Chemical Ionization The main pathways that explain the experimental observations regarding ion formation in PICI between analyte molecules and G_R plasma are as follows: (i) proton transfer, (ii) electrophilic addition, (iii) anion abstraction, and (iv) charge exchange (CE).

Proton transfer Proton transfer is the most commonly observed reaction and serves as the basis for PICI measurements. These Brønsted–Lowry acid–base reactions afford protonated analyte molecules as long as their gas-phase basicity is greater than that of the reactive species present in the source. However, hydride (H^-) abstraction from the analyte molecules can also occur. The former case yields a cation $[M+H]^+$ with m/z (M+1), where M is the (monoisotopic) mass of the analyte molecule (Eq. 1.4a), whereas the latter case yields a cation $[M–H]^+$ with m/z (M−1) (Eq. 1.4b).

$$[G_R+H]^+ + M \rightarrow [M+H]^+ + G_R \quad (1.4a)$$

$$G_{EE}{}^+ + M \rightarrow [M–H]^+ + G_RH \quad (1.4b)$$

In addition to methane (Section 1.2.2.1), several other gases including propane, butane, isobutane, and ammonia can form cations that serve as G_R in Brønsted–Lowry acid–base reactions. If the reaction is exothermic, these cations will readily transfer protons to analyte molecules (M) forming $[M+H]^+$ cations. The exothermicity of the reaction is determined by the proton affinity (PA) difference between the reacting species (Table 1.1). In general, the more exothermic the reaction is, the more fragmentation is observed (more energy transferred to analyte molecule).

Careful choice of acid–base pairs allows control of the extent of the ionization and fragmentation process, thus either inducing or eliminating ionization and/or fragmentation. Eq. 1.5 shows the protonation and hydride abstraction reactions of an analyte molecule (M) when using methane as G_R.

$$[CH_5]^+ + M \rightarrow [M+H]^+ + CH_4 \quad (1.5a)$$

$$[C_2H_5]^+ + M \rightarrow [M–H]^+ + CH_3CH_3 \quad (1.5b)$$

TABLE 1.1 Proton affinities of compounds commonly used in GC–MS and LC–MS.

Compound	PA (kJ mol^{-1})	Compound	PA (kJ mol^{-1})
Methane (CH_4)	552	Methyl acetate (CH_3COOCH_3)	828
Ethyne ($HC{\equiv}CH$)	641	Ethenone ($H_2C{=}C{=}O$)	830
Ethene ($H_2C{=}CH_2$)	680	Diethyl ether ($C_2H_5OC_2H_5$)	838
Water (H_2O)	697	Ammonia (NH_3)	854
Hydrogen sulfide (H_2S)	712	Aniline ($C_6H_5NH_2$)	877
Formaldehyde ($H_2C{=}O$)	718	Methylamine (CH_3NH_2)	896
Propene ($CH_3CH{=}CH_2$)	752	Alanine ($(CH_3CHNH_2)COOH$)	899
Benzene (C_6H_6)	759	Ethyl amine ($CH_3CH_2NH_2$)	908
Methanol (CH_3OH)	761	Dimethylamine ($(CH_3)_2NH$)	923
Ethanol (C_2H_5OH)	788	Pyridine (C_5H_5N)	924
Acetonitrile ($CH_3C{\equiv}N$)	788	Dimethyl aniline ($C_6H_5N(CH_3)_2$)	935
Toluene ($C_6H_5CH_3$)	794	Trimethylamine ($(CH_3)_3N$)	942
Ethyl formate ($HCOOC_2H_5$)	808	Piperidine ($C_5H_{11}N$)	947
iso-Butene ($(CH_3)_2C{=}CH_2$)	820	Quinoline (C_9H_7N)	948
Acetone (CH_3COCH_3)	823	Triethylamine ($(C_2H_5)_3N$)	972

Source: Adapted from Lias, 1984 and Hunter, 1998. Reproduced with permission of the American Institute of Physics.

The methanium ion ($[CH_5]^+$) with *m/z* 17 is a good example of a G_R ionic species reacting in both protonation (Eq. 1.5a) and hydride abstraction reactions with analyte molecules (Eq. 1.5c).

$$[CH_5]^+ + M \rightarrow [M–H]^+ + CH_4 + H_2 \quad (1.5c)$$

Electrophilic addition Electrophilic addition (adduct formation, e.g., alkylation) is another type of acid–base reaction that occurs when analyte molecules have Lewis base character, for example, presence of heteroatoms with nonbonding electrons or π-electrons, allowing their reaction with electrophiles (even-electron cations, $G_{EE}{}^+$) present in the G_R plasma (Eq. 1.6).

$$G_{EE}{}^+ + M \rightarrow [M{+}G_{EE}]^+ \quad (1.6)$$

Some examples of adduct formation when using methane as G_R are shown in Eq. 1.7. Knowing the mass of the alkylating cation allows one to find the molecular mass of the target compound. For methane, these ions are found with *m/z* (M+15), (M+29), and (M+41).

$$[CH_3]^+ + M \rightarrow [M{+}CH_3]^+ \quad m/z \text{ (M+15)} \quad (1.7a)$$

$$[C_2H_5]^+ + M \rightarrow [M{+}C_2H_5]^+ \quad m/z \text{ (M+29)} \quad (1.7b)$$

$$[C_3H_5]^+ + M \rightarrow [M{+}C_3H_5]^+ \quad m/z \text{ (M+41)} \quad (1.7c)$$

Conditions within the source can be changed in order to promote or inhibit a given type of acid–base reaction from happening. This can be achieved by establishing physical conditions, for example, e^- energy and G_R pressure, in the source that will favor the formation of the G_R ions needed for either proton transfer or adduct formation. Table 1.2 shows the most common CI reagent gases used in MS, along with the adducts formed from analyte molecules–G_R plasma reactions.

Anion abstraction Anion abstraction happens when $G_{EE}{}^+$ ions react with sample molecules to form an analyte-derived cation and a neutral species as shown in Eq. 1.8. Proton abstraction is a good example (exothermic reaction with the nitrosonium cation (NO^+) for most alkanes) leading to $[M{-}H]^-$ ions with *m/z* (M−1). Alcohols (1° and 2°), aldehydes, and ketones undergo this kind of reaction. Tertiary alcohols undergo abstraction of hydroxy group (OH) leading to a stable tertiary carbocation $[M{-}OH]^+$ with *m/z* (M−17).

$$G_{EE}{}^+ + M \rightarrow [M–A]^+ + G_{EE}A \quad (1.8)$$

Hydride abstraction from alkanes when using cations such as $[C_2H_5]^+$ (Eq. 1.5b) and $[CF_3]^+$ is a good example as well; group electronegativity is useful in this respect (Wells, 1968). There is no reagent gas system exclusively developed for this mode of CI; the nitrosyl radical ($^{\bullet}NO$) or a mixture of nitrogen/nitrous oxide (N_2/NO_2) are reagent gases used to produce NO^+, which acts as hydrogen abstractor, and can also participate in adduct formation and charge-transfer reactions.

Charge exchange (CE) CE is the outcome of the interaction between a $G_R{}^{+\bullet}$ and a neutral analyte molecule. Ionization takes place when there is a transfer of charge to the analyte molecule producing an $M^{+\bullet}$ and a neutral G_R. The reaction

TABLE 1.2 Common reagent gases used in positive-ion CI and adducts formed thereof.

Reagent Gas (G_R)	G_{EE}^+ Plasma Ions	Adducts Formed	*m/z*
Methane (CH_4)	$[CH_3]^+$	$[M+CH_3]^+$	M+15
	$[CH_5]^+$	$[M+H]^+$	M+1
		$[M-H]^+$	M−1
	$[C_2H_3]^+$	$[M-H]^+$	M−1
	$[CH_2CH_3]^+$	$[M+C_2H_5]^+$	M+29
	$[CH_2CHCH_2]^+$	$[M+C_3H_5]^+$	M+41
Isobutane ($(CH_3)_2CHCH_3$)	$[(CH_3)_3C]^+$	$[M+(CH_3)_3C]^+$	M+57
	$[CH_3CHCH_3]^+$	$[M+H]^+$	M+1
		$[M+C_3H_7]^+$	M+43
	$[C_3H_3]^+$	$[M+C_3H_3]^+$	M+39
Ammonia (NH_3)	$[NH_4]^+$	$[M+H]^+$	M+1
		$[M+NH_4]^+$	M+18
	$[NH_4+NH_3]^+$	$[M+[NH_4+NH_3]]^+$	M+35

is observed when the recombination energy (exothermicity of the reaction $G_R^{+\bullet} + e^- \rightarrow G_R$) of G_R is higher than the IE of M (Eq. 1.9). The degree of fragmentation of $M^{+\bullet}$ depends on the exothermicity of the reaction. However, the molecular ions produced are usually of low internal energy. The presence of protonating species must be kept at a minimum in order to avoid formation of G_RH. Pure compounds are usually used as G_R for charge-exchange chemical ionization (CECI), nonetheless, mixtures with an inert buffer gas such as N_2 find application. Despite the fact that alkanes, for example, CH_4, and aromatic compounds, for example, benzene, chlorobenzene, can be used as G_R for CECI, aprotic solvents are preferred: rare gases, for example, Ne, Ar, Xe, methanedithione (S═C═S), sulfanylidenemethanone (S═C═O), nitrosyl ($^\bullet$NO).

$$G_R^{+\bullet} + M \rightarrow M^{+\bullet} + G_R \tag{1.9}$$

In addition to its routine application as an analytical tool, CI has also been used in mechanistic studies, such as the study of gas-phase ion–molecule reactions (organic chemistry in the high-vacuum gas phase), *regio-* and *stereo-*selectivity questions, conformational analysis, and the measurement of relative reaction rate constants.

1.2.2.3 Negative-Ion Chemical Ionization The study of reactions between negative ions of G_R and neutral sample molecules has not been carried out as thoroughly as it has been done for their positive counterparts. This mode of ionization happens in two different methods: NICI and ECNI. In the former case, it is the result from reactions of G_R anions present in the source and neutral analyte molecules (M). This occurs readily when stable anions of the G_R can be formed. ECNI, in contrast, is the process by which thermal electrons present in the source (e^-) react with neutral analyte molecules generating radical anions ($OE^{-\bullet}$) and anions (EE^-).

The main reactions in NICI can be grouped as (i) proton transfer, (ii) nucleophilic addition, (iii) nucleophilic displacement, and (iv) CE.

Proton transfer Proton transfer occurs when an anion (G_R^-) derived from a G_R or a G_R mixture reacts with a neutral analyte molecule containing a removable proton. This happens when the PA (or gas-phase basicity) of G_R^- is greater than the PA of the conjugate base of the analyte ($[M-H]^-$), according to Eq. 1.10.

$$G_R^- + M \rightarrow [M-H]^- + G_RH \tag{1.10}$$

Molecules with acidic H-atoms (removable) such as carboxylic acids and phenols are common examples of functional groups undergoing proton-transfer reactions. Therefore, the PA of typical anions can be used to predict the outcome of NICI proton-transfer reactions. Some examples of G_R^- are as follows: Cl^-, $[CN]^-$, $[O_2]^{-\bullet}$, F^-, $[CH_2CN]^-$, $[CH_3O]^-$, $O^{-\bullet}$, $[OH]^-$, H^-, $[NH_2]^-$, and $[C_5F_5]^-$ (Table 1.3).

There exist many gas mixtures to generate the anions of interest, for example, the use of fluorocarbons (trifluoromethane, CHF_3) and chlorofluorocarbons (CF_2Cl_2) to generate F^- and Cl^-, respectively, and the use of ammonia (NH_3) to generate $[NH_2]^-$ (Dougherty, 1981). Most of these anionic reactive species themselves are produced by associative electron-capture reactions, for example, formation of $[O_2]^{-\bullet}$. The reaction between methoxide ion ($[CH_3O]^-$, PA ≈ 1580 kJ mol^{-1}) and cyclopentadiene producing the cyclopentadiene anion ($[C_5H_5]^-$) (ΔPA ≈ −100 kJ mol^{-1}) serves as an example (Eq. 1.11).

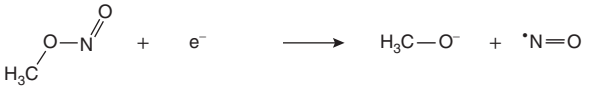

(1.11a)

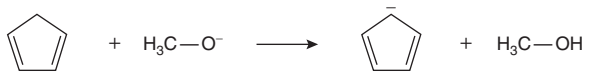

(1.11b)

Methyl nitrite (CH_3ONO) undergoes dissociative electron capture to produce the reactive species of interest CH_3O^- (Eq. 1.11a), which deprotonates cyclopentadiene producing the $[C_5H_5]^-$ (Eq. 1.11b). Superoxide ($O_2^{-\bullet}$, $PA \approx 1465\,kJ\,mol^{-1}$), formed by electron capture of nitrous oxide (NO_2) or a molecular oxygen/argon gas mixture, can behave as a basic species and deprotonates acidic compounds such as 4-nitrophenol producing the corresponding phenoxide ion ($PA_{calc} \approx 1350\,kJ\,mol^{-1}$) (Chandra & Uchimaru, 2002) and hydroperoxyl radical ($HOO^{\bullet}$), as illustrated in Eq. 1.12.

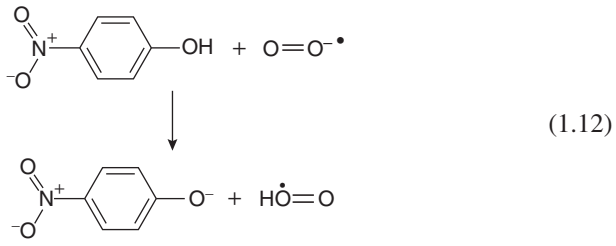

(1.12)

Hydroxide ions (HO^-, $PA \approx 1635\,kJ\,mol^{-1}$) are frequently used for their ability to produce NICI mass spectra of a diversity of functional groups: alcohols, ethers, neutral lipids, and hydrocarbons.

TABLE 1.3 Anions used for neutral analyte negative ionization in GC–MS and LC–MS.

Anion	PA ($kJ\,mol^{-1}$)
NH_2^- (amide)	1689
H^- (hydride)	1676
OH^- (hydroxide)	1636
$O^{-\bullet}$ (atomic oxygen radical anion)	1595
CH_3O^- (methoxide)	1583
$(CH_3)_2CHO^-$ (isopropoxide)	1565
$^-CH_2CN$ (cyanomethide)	1556
F^- (fluoride)	1554
$C_5H_5^-$ (cyclopentadiene anion)	1480
$O_2^{-\bullet}$ (molecular oxygen radical anion)	1465
CN^- (cyanide)	1462
Cl^- (chloride)	1395
$HCOO^-$ (formate)	1444*
CH_3COO^- (acetate)	1458*
CF_3COO^- (trifluoroacetate)	1350*

Source: Bruno & Svoronos, 2010; *Harrison, 1992. Reproduced with permission of American Chemical Society.

Nucleophilic addition Nucleophilic addition can occur when anions do not have very high proton affinities (e.g., $O_2^{-\bullet}$, $[CN]^-$ ($PA \approx 1460\,kJ\,mol^{-1}$), Cl^- ($PA \approx 1395\,kJ\,mol^{-1}$). Instead of undergoing acid–base reactions leading to deprotonated products, they form adducts by nucleophilic addition to analyte molecules (Eq. 1.11a).

$$G_R^- + M \rightarrow [M+G_R]^- \tag{1.13}$$

Examples of this reaction are hydrogen-bonded adducts formed by chloride ions (Cl^-) with analyte molecules containing functional groups with electrophilic H-atom, such as carboxylic acids, amides, aromatic amines, phenols, and organophosphorus pesticides. This leads to the production of $[M+Cl]^-$ ions with *m/z* (M+35) and *m/z* (M+37) in a ≈3:1 ratio of relative intensities. For instance, 4-nitrophenol reacts with Cl^- as shown in Eq. 1.14.

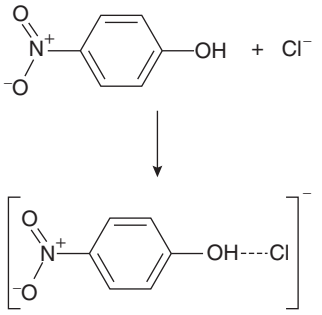

(1.14)

Nucleophilic addition is also observed with $O_2^{-\bullet}$ and compounds of low acidity such as aliphatic compounds forming the corresponding $[M+O_2]^{-\bullet}$ radical ion. Alcohols also undergo nucleophilic addition adduct formation. For instance, it was found that 11 different anionic species form adducts with neutral oligosaccharides (Jiang & Cole, 2005).

Nucleophilic displacement Nucleophilic displacement is a substitution reaction where an electrophilic center of an analyte molecule undergoes nucleophilic attack (e.g., S_N2). The leaving group thus produced can be a neutral radical or a new anionic species as illustrated in Eq. 1.15.

$$G_R^{-\bullet} + M \rightarrow [MG_R\text{–}H]^- + H^{\bullet} \tag{1.15a}$$

$$G_R^- + MA \rightarrow MG_R + A^- \tag{1.15b}$$

Many strongly basic anions such as atomic oxygen radical anion ($O^{-\bullet}$, $PA \approx 1595\,kJ\,mol^{-1}$) and HO^- usually react in proton-transfer reactions. Nonetheless, with certain analytes, they participate in gas-phase nucleophilic reactions. Both of these ions can be produced by using N_2O as G_R (e.g., N_2O, N_2O/CH_4). Examples of this mechanism are the gas-phase reactions of $O^{-\bullet}$ with phthalic acid alkyl esters (Stemmeler et al., 1994; Lépine et al., 1999) and the analysis of steroids with HO^- where both proton abstraction and nucleophilic displacement are observed (Roy et al., 1979).

Charge exchange (CE) CE occurs when a G_R (Lewis base) with lower electron affinity (EA) than that of the neutral analyte (Lewis acid) is allowed to react in the CI ion source and an electron transfer is effected as shown in Eq. 1.16. The degree of fragmentation depends on the exothermicity of the reaction. An important characteristic of this type of reaction is the possibility of obtaining single peak mass spectra, consisting of the anionized analyte molecule.

$$G_R{}^{-\bullet} + M \rightarrow M^{-\bullet} + G_R \tag{1.16}$$

As an example, the analysis of dibenzothiophene using $[O_2]^{-\bullet}$ as G_R delivered $M^{-\bullet}$, while the G_R was oxidized to molecular oxygen (O_2) (Hunt et al., 1976). Care must be taken to avoid the presence of competing species that would react with $M^{-\bullet}$, thereby lowering the sensitivity of the analysis. For instance, the presence of fluorine radicals ($F^{\bullet}$) would lead to the formation of fluoride ions (F^-) and neutral analyte M.

Despite the successes of NICI as an analytical tool, the most common technique used for the generation of negative ions is ECNI. Strictly speaking, these electron–molecule reactions are not chemical ionization processes. If at a given temperature there is an equilibrium between the generation and recombination of electrons, the electrons are said to be in thermal equilibrium. Thermal electrons have a kinetic energy $\leq$2 eV. Under these conditions, they can be captured by electronegative atoms present in analyte molecules, thereby forming radical anions ($OE^{-\bullet}$). The thermionic emission of electrons from heated filaments is the usual way of producing high-energy primary electrons in EI. The main source of secondary (thermal) electrons is the deceleration of primary electrons by collisional energy transfer with gases inside the source, such as G_R ionization as shown in Eq. 1.17.

$$2G_R + e^-_{70\,eV} \rightarrow G_R^* + G_R{}^{+\bullet} + 2e^-_{2\,eV} \tag{1.17}$$

Polyatomic gases are more efficient collisional energy sinks than diatomic and monoatomic gases, and therefore their rate of e^- thermalization is higher (e.g. $NH_3 > CO_2 > i\text{-}C_4H_{10} > CH_4 > N_2 > Ar$). After the reaction of the secondary electrons with the analyte molecules, the presence of a G_R (or a buffer gas) is essential for collisional stabilization of the newly formed excited radical anion $OE^{-\bullet}$. Otherwise, e^- detachment can happen and no analyte anion is observed.

Neutral analyte molecules undergo EC to form radical anions ($OE^{-\bullet}$). The ease, with which this process happens, depends on the EA of the neutral analyte and its ability to dissipate the excess internal energy after its formation (Eq. 1.18).

$$M + e^- \rightarrow M^{-\bullet} \tag{1.18}$$

Since charge density leads to instability, for example, HO^- is less stable than H_2O, charge dissipation must be effective. Therefore, analyte molecules must have electronic features that promote electron capture. Factors that contribute most prominently in the stabilization of a negative charge are as follows: orbital hybridization of the atom bearing the charge, for example, for carbanions the stability follows $sp > sp^2 > sp^3$, the presence of geminal or vicinal electronegative elements ($F > O > Cl > N > Br > I > S > C > P$) and/or electron-withdrawing functional groups or substituents ($—CF_3 > —CCl_3 > —CH_3$; $—CN \approx —CCH > —CHCH_2 \approx —C_6H_5$; $—OH > —NO_2 > —NH_2$), charge delocalization by resonance or aromaticity, and molecular polarizability whereby small atoms and molecules dissipate a charge less effectively than large ones, for example, the I-atom is more polarizable than an F-atom, thus I^- is a much better leaving group than F^- in substitution reactions. Usually, the most electronegative element present in the molecule determines its EA. For this reason, molecules with electronegative elements or groups, for example, nitro (NO_2), acyl (RCO), and cyano (CN), are attractive targets of ECNI. The main processes that explain the formation of negative species in ECNI are as follows: (i) associative electron capture, (ii) dissociative electron capture, and (iii) ion-pair formation reactions (Hiraoka, 2003; Stemmeler & Hites, 1988).

Associative electron capture Associative electron capture as shown in Eq. 1.18 gives the molecular radical anion $M^{-\bullet}$ after reaction of M with a low energy e^- (<2 eV). The molecular anion is formed without great excess energy, and additional collisional stabilization with (buffer) gases present in the source explains the high relative intensity of $M^{-\bullet}$ observed.

Dissociative electron capture Dissociative electron capture happens when electrons inside the ion source with a kinetic energy of up to $\approx$15 eV react with analyte molecules containing electronegative atoms or substituent groups that can form good leaving groups, for example, halogens, benzyl ($C_6H_5CH_2{}^-$), and methoxy (CH_3O^-), according to Eq. 1.19. The formation of a stable anion $[M–X]^-$ or X^- is the basis for this sensitive and selective type or CI analysis.

$$MX + e^- \rightarrow [M–X]^- + X^{\bullet} \tag{1.19a}$$

$$MX + e^- \rightarrow M^{\bullet} + X^- \tag{1.19b}$$

As expected, all these reactions are exothermic, and the outcome depends on the difference between the bond energy of the X group in the analyte and the EA of the analyte [M−X] and X fragments.

Ion-pair formation Ion-pair formation happens with electrons of $\approx$10–15 eV. The initially formed $OE^{-\bullet}$ has enough internal energy to dissociate into positive and negative ions

(Eq. 1.20). This process is not very common and does not find widespread use as an analytical method.

$$MX + e^- \rightarrow [M\text{–}X]^- + X^+ + e^- \quad (1.20a)$$

$$MX + e^- \rightarrow [M\text{–}X]^+ + X^- + e^- \quad (1.20b)$$

Attention must be given when choosing the buffer gases in such a way that they do not form stable negative ions or reactive species, in order to avoid competition reactions or reactions with neutral or charged analyte molecules, which inevitably lower the sensitivity of the analysis. Equally important is keeping matrix effects and impurities to a minimum. In addition, the vacuum pump speed must also be adequate to fulfill the pressure requirements of CI experiments.

1.2.2.4 Analytical Applications of Chemical Ionization

CI is not applied in combination with GC–MS as widely as is EI. In terms of analytical applications, the various modes of performing CI have different application areas. PICI is mainly used to determine or confirm the mass of the intact analyte molecule, for example, in cases where $M^{+\bullet}$ is not observed or is present with a very low relative intensity under EI conditions. In this context, PICI may become more important in GC–MS in the future, given the increasing use of SRM in tandem-quadrupole (TQ) instruments. The introduction of atmospheric-pressure chemical ionization (Section 1.2.5) for GC–MS is also highly interesting (van Bavel et al., 2015; Li et al., 2015). Different CI reactions can be achieved under those conditions, which are largely dependent on the reagent gas used and the instrumental parameters for attaining the sought-after results.

GC–MS with ECNI has found a wide range of applications in targeted quantitative analysis, for instance in forensic toxicology and pharmacology for the analysis of polar compounds. For such applications, pentafluoropropyl or pentafluorobenzyl ester derivatives are produced. As such, GC–ECNI-MS is routinely applied in forensic toxicology to determine illicit drugs, for instance for the presence of tetrahydrocannabinol (THC) in hair (Foltz, 1992; Moore et al., 2006). Enantioselective analysis of amphetamines has been reported after derivatization with (*S*)-(−)-*N*-(heptafluorobutanoyl)prolyl chloride (HFBPC) (Lim et al., 1993). HFBPC and its related compounds are very efficient chiral derivatizing reagent of amino groups (Leis & Windischhofer, 2012). GC–ECNI-MS also plays an important role in the analysis of environmental pollutants such as polybrominated compounds of both synthetic (polybrominated diphenyl ethers as fire retardants) and natural (polybrominated hexahydroxanthene derivatives) origins. In such cases, bromide ions (Br^-) are produced during dissociative ECNI (Eq. 1.19b). The high selectivity of the analysis lies in the production of ions with *m*/*z* 79 and 81 ($^{79}Br^-$ and $^{81}Br^-$ with ≈1:1 relative intensity) (Rosenfelder & Vetter, 2009).

Another possibility of dissociative electron capture leads to retention of charge by the analyte molecule, to effectively produce $[M-H]^-$ of the underivatized analyte, in combination with the production of a neutral radical ($X^\bullet$) leaving group (Eq. 1.19a). This behavior is applied in the GC–ECNI-MS analysis of fatty acids (RCOOH) such as arachidonic acid analogs after derivatization to their pentafluorobenzyl esters. In this case, the dissociative ECNI process leads to an ion corresponding to the deprotonated acid with *m*/*z* (M−1) and pentafluorobenzyl radical, as shown in Eq. 1.21 (Hadley et al., 1988).

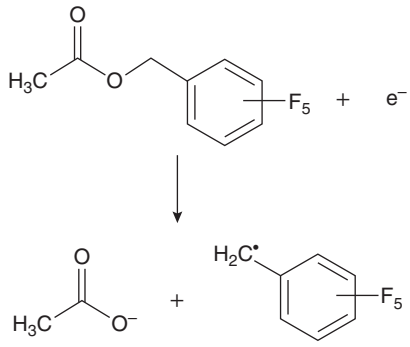

(1.21)

When comparing modes of ionization in CI, sensitivity is a parameter often employed to quantitatively gauge them. Inherently, neither NICI nor PICI is a more sensitive technique than the other. What determines the sensitivity is the number of extractable and detectable analyte ions present in the source at any time. For that reason and when possible, the relative second-order reaction rates in ECNI versus proton transfer and adduct formation in PICI are used to determine the sensitivity of a particular method. Generally speaking, electron-capture rate constants can be up to 1000 times larger or smaller than proton transfer, for example, methanol gas-phase H/D-exchange rate constant is $\approx 10^{-11}$ cm^3 molecule^{-1} s^{-1}, Green & Lebrilla, 1997). Therefore, CI experiments must be carefully planned to use G_R-analyte partners that will offer optimum sensitivity and selectivity.

1.2.3 Atmospheric-Pressure Ionization

GC enjoys the advantage of being able to deliver the analyte molecules inside the source in the gas phase, and that makes it suitable when using an EI source. Notwithstanding the technological challenges, precedents exist shortly after its development of GC coupling to MS (Holmes & Morrell, 1957). LC coupling to MS presents a greater challenge: analytes elute out of the LC column dissolved in liquid solvents of varying volumes and polarities (volatilities). The *conditio sine qua non* for MS is to have ions under vacuum and in the gas phase. Therefore, in order to couple LC to MS, devising a way to desolvate sample molecules, ionize, and transmit them to the high-vacuum environment of

the mass analyzer was indispensable. Atmospheric-pressure ionization (API) sources were developed to achieve that task, and three kinds of API are routinely used: electrospray ionization (ESI), atmospheric-pressure chemical ionization (APCI), and atmospheric-pressure photoionization (APPI). API techniques provide soft-ionization processes where the post-ionization energy of analyte molecules is not large enough to cause extensive fragmentation (if any), with an ion related to the intact molecule (as a cationized or anionized molecule) usually present. Equally important, API techniques offer an alternative ionization way apt for polar, low volatility (high molecular mass), and thermolabile compounds. Figure 1.7 is an approximate chart showing the molecular mass and polarity ranges of application for the most common ionization techniques in MS.

The three techniques accomplish the same task in different but related ways, the main difference being the process of analyte ionization itself. Desolvation and ion transmission share the same electromechanical principles in all three techniques: sample nebulization in an atmospheric-pressure chamber, inert gasses and thermal energy for desolvation, and reduced pressure. The source is also designed to keep neutral molecules from reaching the detector (lower background noise).

Since the analyte is dissolved in the mobile phase, one must make sure that prior to mass analysis the removal of unwanted material is as complete as possible, for example, remnants of solvents, buffers, and additives used to guarantee the ionization of neutral compounds while avoiding signal suppression by interfering chemicals. Therefore, the use of volatile solvents and additives is indicated. In this respect, gradient elution must be carefully planned not to adversely affect the mass spectrum. A flow reduction of the eluting mobile phase leads to more efficient analyte desolvation and analyte ionization. Several techniques exist to reduce the flow rate to the ESI source such as pre-source flow split (for concentrated samples as well) or the use of nL min^{-1} flow rates with LC columns of 10–100 μm internal diameter (Chervet et al., 1996).

In an API source, the coupling to an LC system column effluent or any other liquid flow is done via the sample inlet, where the liquid is nebulized into a fine aerosol of small droplets. The nebulization process in ESI (Section 1.2.4.1) differs from the one used for APCI and APPI (Section 1.2.5.1). In the course of droplet solvent evaporation mediated by heated desolvation gas, for example, nitrogen (N_2), analyte ionization is achieved by different processes in ESI (Section 1.2.4.2), APCI (Section 1.2.5.2), and APPI

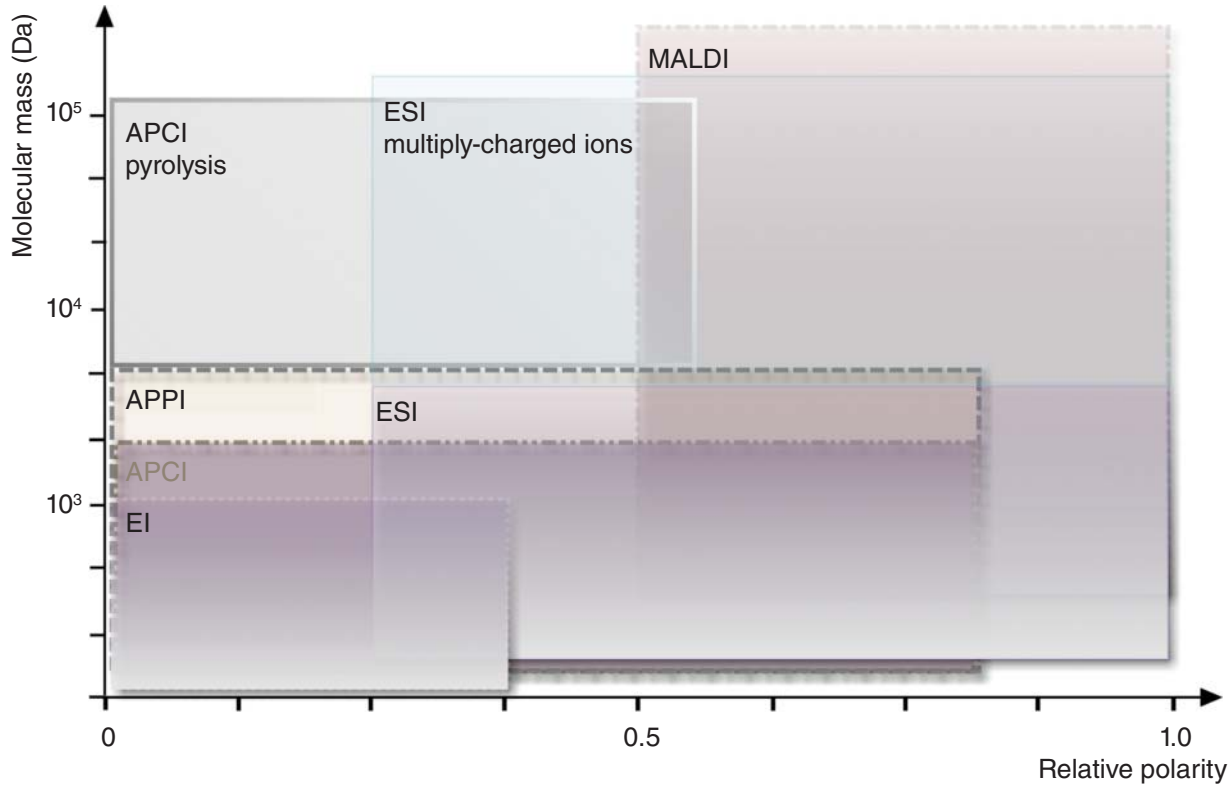

FIGURE 1.7 Approximate range of molecular mass and polarity for the most common ionization sources in MS.

(Section 1.2.5.3). The resulting mixture (containing analyte ions) is passed through the ion-sampling orifice into the first vacuum chamber of the differentially pumped interface between the API source and the mass analyzer. Before analyte ion transmission to a high-vacuum region, where mass analysis is performed, two or three stages of vacuum pumping are applied to remove as much mobile-phase vapors and N_2 as possible. A schematic diagram of an API source with an ESI inlet is shown in Figure 1.8. The API source parts are discussed in more detail, and inlet components are discussed separately for ESI (Section 1.2.4.1), APCI, and APPI (Section 1.2.5.1). Liquid nebulization at the sample inlet (electrospray needle or heated nebulizer) results in a fine aerosol of very small droplets. These droplets are then stripped of their solvent. In APCI and APPI, this is done within a heated nebulizer (Section 1.2.5.1), whereas in ESI, this is done in the API source. In order to achieve electrospray nebulization in ESI, a voltage difference (1–5 kV) is established between the electrospray needle and the ion-sampling orifice (Section 1.2.4.1). At higher flow rates ($>10\,\mu L\,min^{-1}$), N_2 gas is used to assist and support the nebulization process (pneumatically assisted ESI). This voltage difference can be applied in two different ways: in some ESI sources, the ESI needle is grounded and the voltage is applied to the ion-sampling orifice region, whereas in ESI sources from most instrument manufacturers, the voltage is applied to the ESI needle. The ions generated are transmitted through the vacuum interface toward the mass analyzer by means of voltages applied at different points in the source: ion-sampling orifice, skimmer, and RF-only multipole ion guide.

When flow rates are in excess of $1\,\mu L\,min^{-1}$, solvent evaporation in ESI must be seconded by the application of heat. Typically, this is done using N_2 as heated desolvation gas. Depending on the instrument design, heat exchange between the plume and the heated-nitrogen flow is implemented in different ways, that is, concurrent flow, counter-current flow, and orthogonal flow (or just off-axis) to the direction of liquid introduction. The solvent evaporation and ionization process, discussed in more detail in Section 1.2.4.2, results in a mixture of analyte ions, N_2 gas, solvent vapors, and neutral analyte molecules in the API source. A small part of this mixture is sampled into the first vacuum chamber aided by a voltage applied to the ion-sampling orifice. The remainder of the mixture leaves the API source region via an exhaust connected to a fume hood at atmospheric pressure.

An important practical problem in operating an API source with a wide variety of samples is the contamination of the ion-sampling orifice area by nonvolatile materials present in the liquid flow. This may seriously compromise the performance of the ESI source. The most important design feature to reduce ion-sampling orifice contamination is the orthogonal sample introduction (Hiraoka et al., 1995). In addition, several different designs are available making use of counter-current dry N_2 desolvation gas flow (Bruins et al., 1987). This is done in order to push unwanted materials away from the area of the ion-sampling orifice (Cole, 2010).

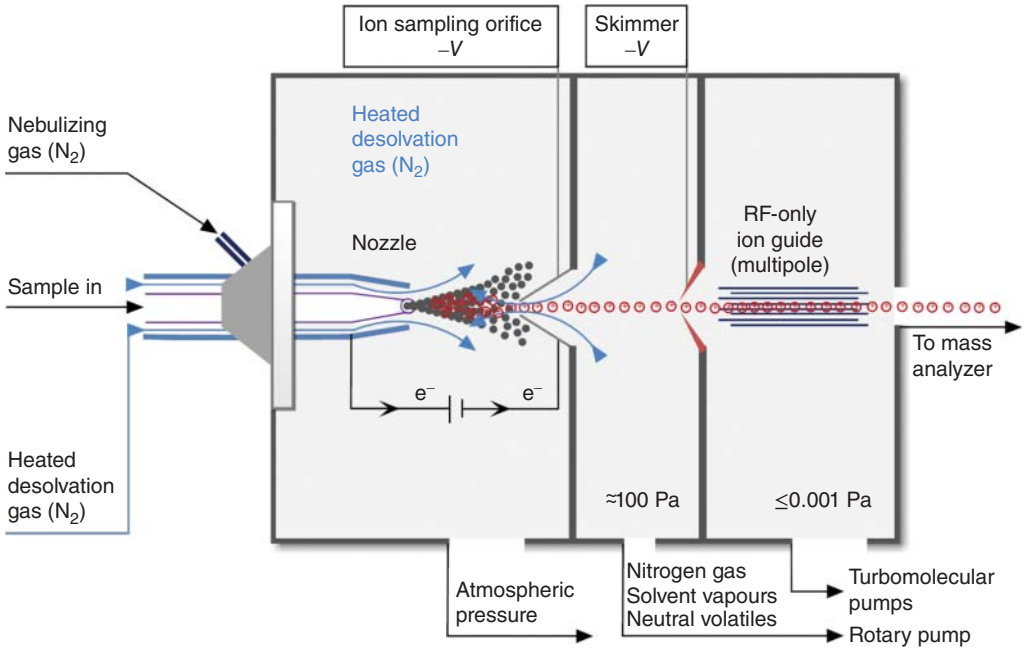

FIGURE 1.8 Schematic representation of an atmospheric-pressure ionization (API) source with an electrospray ionization (ESI) inlet.

The geometry of the ion-sampling orifice depends on the instrument at hand. In one of the original ESI source designs by Fenn (Whitehouse et al., 1985) and still in use today, a glass capillary with metallized inlet and outlet ends is used as ion-sampling orifice. It allows having different voltages at the inlet and outlet ends of the capillary, electrically decouples the API source region from the vacuum interface, and thereby enables the application of the high voltage to the ion-sampling orifice region rather than to the ESI needle. This also facilitates the coupling of capillary electrophoresis to MS. Other ion-sampling orifice designs include a heated stainless steel capillary and an orifice in a flat plate or a cone.

At the low-pressure (typically 100 Pa; 1 mbar) side of the ion-sampling orifice, expansion of the gas mixture occurs. Since the analyte ions usually have a higher mass than the N_2 and solvent molecules, they are preferentially found in the core of the expansion. Then, the core of the expansion is sampled by a skimmer into the second vacuum stage. Electrostatic or quadrupole lenses are applied between ion-sampling orifice and skimmer, that is, at the high-pressure side of the skimmer, in some API source designs to achieve focusing of the ions in order to enhance ion transmission in this region of the API source. The ions present at the low-pressure side of the skimmer are transmitted and focused through the vacuum chamber by means of RF-only multipole(s), which may be a quadrupole, a hexapole, or an octapole.

Source contribution to overall experimental performance will depend on the ionization and ion transmission efficiencies. Significant developments are made in trying to improve ion transmission from the vacuum interface to the mass analyzer. In some instrument designs, the ion optics described earlier (and even the skimmer) have recently been replaced with two-stage ion funnels, which consist of a series of parallel electrode plates orthogonally placed to the direction of ion transmission (Giles et al., 2004; Kelly et al., 2010). RF voltages and/or DC transient voltages are applied to guide the ions through them while speeding them up. In principle, any type of mass analyzer can be used, nevertheless some devices require additional instrumentation, for example, ion acceleration for time-of-flight instrument and pulsed ion-gating for ion-trap instruments.

1.2.4 Electrospray Ionization

1.2.4.1 Electrospray Nebulization Nowadays, ESI is the most widely used technique in MS for the ionization of liquid samples. Even though ESI has been successfully used as an ionization technique in MS for more than 30 years (Yamashita & Fenn, 1984a,1984b; Whitehouse et al., 1985), electrospray-related phenomena had already been recorded over 400 years ago by Gilbert (1600) who noted: "in the presence of a charged piece of amber, a drop of water deformed into a cone." Another more colorful example is the observation by Nollet (1754), who was the first to perform electrostatic spraying. While experimenting with human blood and electricity, he concluded that "a person, electrified by connection to a high-voltage generator, would not bleed normally if he were to cut himself; blood would spray from the wound". Electrospraying is a technique that exploits the electrohydrodynamic behavior of a liquid meniscus at the tip of a conductive hollow emitter, for example, a metallic or a contact electrode silica capillary, and under the influence of electrical shear stress (directly proportional to the voltage applied). This is done to electrostatically charge an electrically conductive liquid flowing through the emitter in order to atomize it, generating a spray containing charged self-dispersive microdroplets in a very fine aerosol. Electrospraying finds application in a wide variety of disciplines: aerosol sciences, coating processes[1], electronics, energy generation, food technology, fuel delivery, mass spectrometry, medical sciences, meteorology, mining, nuclear fission, just to mention a few. In ESI-MS, electrospraying or electrospray nebulization is achieved by placing the ESI emitter or ESI needle (electrode) under high voltage (1–5 kV) relative to the ion-sampling orifice (counter-electrode) (Figure 1.9a). In this way, a special electrolytic cell, where part of the ion transport is done in the gas phase, establishes a liquid–gas redox reaction (anode–cathode, respectively), with the flow of electrons as indicated (Kebarle & Verkerk, 2009). Accumulation of charge is effected at each electrode with the tip of the emitter been positively charged (in positive-ion mode). Heated nitrogen gas is supplied to the aerosol to assist in solvent evaporation and declustering of ion-solvent and ion-additive clusters that might have formed in the flowing liquid. The arrangement illustrated in Figures 1.9a is for the study of positive ions, but the sign is a matter of choice and negative-ion ESI is widely performed as well.

The action of the electric field in the solution makes (part of) the present negative ions undergo electrophoretic movement away from the counter-electrode, while the positive ions move toward it. The removal of negative charges from the flowing liquid causes a build-up of positive charge on the meniscus surface at the emitter tip (Figure 1.9b) (Bruins, 1998). Because of the potential difference applied, the liquid at the tip of the emitter is elongated into an elliptically shaped meniscus, where for every point of the surface there is equilibrium between the two main forces acting upon it: the cohesive surface tension that tends to hold the liquid back, and the electrostatic attraction from the counter-electrode that tends to draw the liquid out of the emitter. When the applied electric field is strong enough ($GV\,m^{-1}$) to overcome the (solvent-dependent) meniscus surface tension, the elliptically shaped meniscus suddenly elongates into a regular axisymmetric cone shape named Taylor cone (Taylor, 1964).

[1]Dole ran into electrospray during a visit to a car manufacturer where he saw car painting done with electrospraying (Dole et al., 1968; Mack et al., 1970).

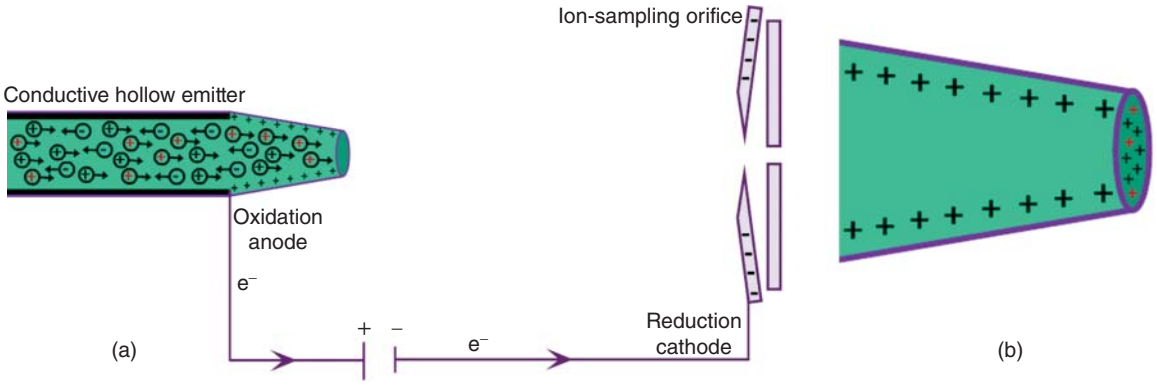

FIGURE 1.9 (a) Electrospray setup in a positive-ion ESI-MS experiment. (b) Positively charged meniscus formation at the electrospray emitter tip.

Depending on the experimental conditions, the Taylor cone can be linear, concave, or convex (Wilm, 2011). The meniscus adopts this shape because a cone can hold more charge than a sphere. The cone surface area depends on the flow rate of the liquid passing through the emitter. For a given experimental setup, there is a minimum flow rate below which formation of Taylor cone does not occur. Under controlled flow rate conditions, the threshold electric potential (V) needed for the formation of Taylor cone is directly proportional to $\sqrt{\gamma R}\ln(4d/R)$ (γ, the meniscus surface tension, R, the emitter tip inner radius, d, the distance between the emitter tip and the counter-electrode in Figure 1.9a) (Smith, 1986). The applied voltage accelerates the charges at the meniscus surface toward the apex of Taylor cone where the electric field is highest. When this electric field is strong enough, that is, the applied electric potential exceeds a certain threshold, the apex of Taylor cone becomes unstable and droplets of controllable and narrow size distribution (approximately monodisperse) begin to leave the cone apex forming a fine jet of charged droplets. Due to the electrostatic repulsion among the newly formed charged droplets and the V applied at the ion-sampling orifice, this jet is then radially dispersed into the so-called (spray) plume, containing a fine aerosol of charged droplets (Figure 1.10).

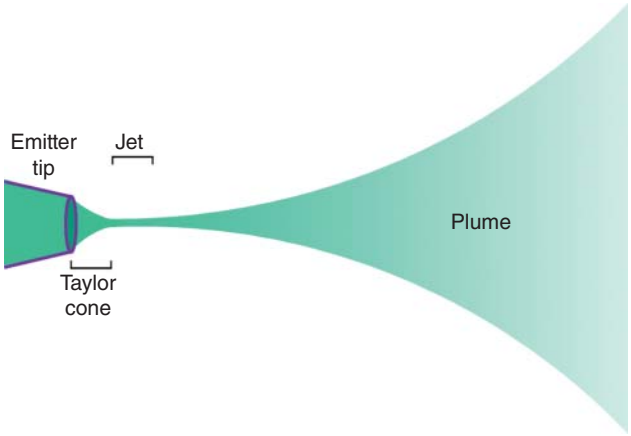

FIGURE 1.10 Taylor cone formation and charged aerosol generation in an ESI experiment.

The liquid flow rate is an important experimental parameter in ESI-MS. Conventional ESI sources (e.g., Whitehouse et al., 1985) are limited to flow rates up to $10\,\mu L\,min^{-1}$. Since ESI-MS was specifically developed as an ionization technique for LC–MS, the possibility to operate the source at higher flow rates was thoroughly investigated. A spraying process by means of a surrounding high-speed N_2 gas flow (nebulizer gas) (Bruins et al., 1987) was introduced as ionspray. This term has become a registered trademark, and the more general term of pneumatically assisted ESI was adopted. As pneumatically assisted ESI is the most widely applied ionization method, in most cases it is simply called ESI. Other alternative spraying modifications that have not found wide (commercial) application include sonic spray (no use of electric field) (Hirabayashi et al., 1994, 1995), electrosonic spray (Schmid et al., 2011), and ultrasonic nebulizer ES (Banks Jr., et al., 1994).

An important development in the field was the introduction of nano-electrospray ionization (nano-ESI), which is extensively used today for applications where sample availability is limited, especially in the field of proteomics. Nano-ESI is a more efficient way of generating gas-phase ions than conventional and pneumatically assisted ESI. This is achieved by the use of low flow rates ($<100\,nL\,min^{-1}$), which requires narrower ESI needle capillaries, or capillaries with a narrower tip diameter (1–5 µm internal diameter). Borosilicate glass capillary emitters with electrically conductive coatings such as a sputtered gold film are used as nano-ESI needles. The low flow rate reduces the energy needed for droplet liquid evaporation, and no pneumatic assistance is needed. Therefore, the distance between the emitter tip and the counter-electrode can be shorter. As a result, a lower spraying voltage (0.5–1.5 kV) can be applied, permitting the use of very polar solvents. Once the voltage is applied

the test solution flows by capillarity, refilling the emitter tip as droplets leave the Taylor cone apex. The flow rate and the droplet size depend on the diameter of the emitter tip. The aerosol thus formed contains nanodroplets (<200 nm in diameter), that is, 100–1000 times smaller in volume than conventional microdroplets (1–2 μm in diameter) seen in ESI experiments (Wilm & Mann, 1994; Wilm & Mann, 1996). In effect, more efficient analyte ionization is achieved and the loss of generated ions at the ion-sampling orifice is greatly reduced. The smaller droplets with higher surface-to-volume ratios lead to less discrimination effects where hydrophobic analytes are favored over hydrophilic analytes.

Variations in the way analyte ions are produced have also given way to newer ESI techniques such as fused droplet and extractive ESI. A more recent development is desorption techniques combined with electrospraying techniques. Sample molecules desorbed from a solid or liquid surface are made to ionize with ESI, for example, desorption ESI (DESI) and electrospray laser ionization (ELDI). In some cases, the use of an emitter can be avoided altogether, for example, direct electrospray probe (DEP), probe ESI (PESI), and paper spray (Section1.2.6).

1.2.4.2 Ionization Mechanisms in ESI What exactly happens to the charged droplets in their flight from the Taylor cone apex to the counter-electrode is still a matter of debate (Figure 1.11). Due to desolvation of the droplets with heated gas (usually N_2), they shrink in size as solvent evaporation occurs. Provided that charges are not shed from the droplet as the solvent evaporates, there is a decrease in droplet radius with a concomitant increase in charge density. This causes the uniformly distributed like charges (Q) on the droplet surface to be closer together, resulting in an increase in electrostatic repulsion. A stability limit (Rayleigh limit) is reached when the charge of the droplet (Q_R) and its radius (R) satisfy Rayleigh equation (Eq. 1.22), where ε_o is the vacuum permittivity (Rayleigh, 1882):

$$Q_R = 8\pi(\varepsilon_o \gamma R^3)^{1/2} \tag{1.22}$$

At $Q > Q_R$, the electrostatic repulsion is greater than the surface tension of the droplet. Then, the droplet breaks up in turn jetting out several smaller charged droplets, which have a much higher charge-to-mass ratio (Grimm & Beauchamp, 2002). This phenomenon is known as coulombic fission (explosion) and it is partly responsible for the formation of the spray plume. Evaporation of solvent continues and ultimately from ionized analyte–solvent nanodroplets free gas-phase ions are produced and accelerated toward the ion-sampling orifice counter-electrode.

Even though the exact mechanism of ESI is a complex physicochemical process where many variables play a role, for example, analyte solubility and surface activity, solvent polarity, and surface tension, there are two generally accepted models to explain the ionization process: the charge residue model (CRM; Dole et al., 1968; Mack et al., 1970) and the ion evaporation model (IEM; Iribarne & Thomson, 1976).

In the CRM after enough solvent evaporation-coulombic fission events, minute charged droplets (≈1 nm radius), each containing one analyte ion undergoes solvent evaporation until a solvent-free (gas-phase) analyte ion is obtained, thus retaining the droplet residual charge. Refinement of the model and experimental evidence have been put forward supporting the CRM model (Schmelzeisen-Redeker et al., 1989), for instance ionization of large macromolecules like proteins involves CRM (Winger et al., 1993).

In contrast, in the IEM, the liquid-phase analyte ions evaporate out of the droplets. As they leave the droplet, they remove a charge or several ones from it. After enough solvent evaporation-coulombic fission events, when a droplet has reached a radius of ≈10 nm, the electric field on the surface of the droplet is strong enough to make solvated charged analyte ions leave the charged droplets. Further desolvation results in a gas-phase ion. Experimental evidence exists supporting the IEM for small inorganic and organic ions (Kebarle & Verkerk, 2009). A modification of the IEM stipulates that the charge resides on the surface of the droplet, and the analyte

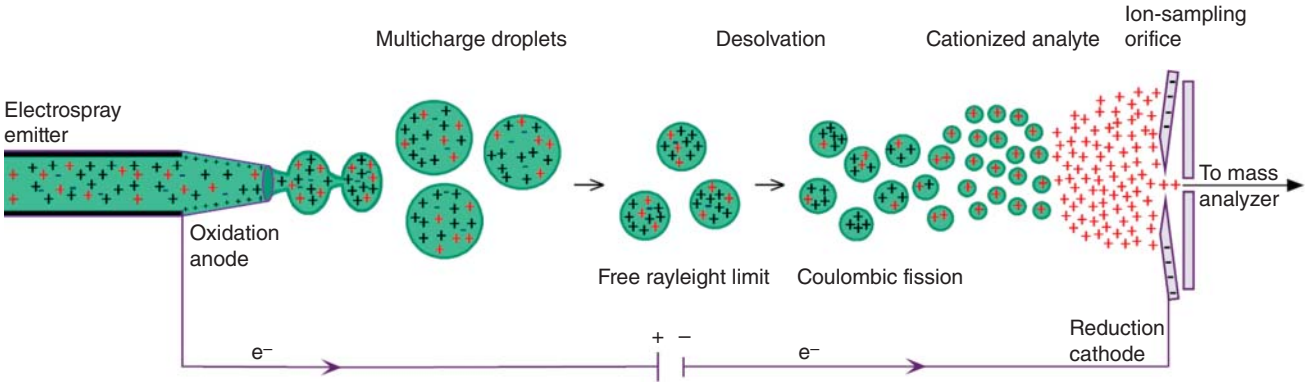

FIGURE 1.11 Analyte ion formation illustrating evaporation-coulombic fission events in positive-ion ESI-MS.

remains neutral inside it while in constant Brownian motion (Wong et al., 1988; Fenn, 1993; Nguyen & Fenn, 2007). After enough solvent evaporation-coulombic fission events, the surface charge density increases, for example, protons (H^+) in positive ESI. Because of the steric proximity of the surface protons to one or several electron-rich functional groups of the analyte, the analyte gets protonated. In this way, an analyte ion is produced, which finds itself in close proximity to the surface of the droplet. The newly formed ions or ionic complexes of analyte molecules then escape the droplet, carrying with them one or more charges. The ease with which an analyte ion leaves the droplet is reflected in the signal intensities of the mass spectrum. In general, the smaller the droplet from where the charged analyte escapes is, the more charges it will have. Many factors intervene such as shape, size, and fugacity of the analytes, ionic strength, and viscosity of the solvent. In fact, if other ionic species have more affinity for the droplet surface than the analyte molecules, ionization suppression is readily observed. The production of multiply-charged ions in ESI has been of tremendous importance for the analysis of macromolecules of both natural and synthetic origins (Fenn et al., 1989).

Usually in ESI, the type of reaction charging the analytes is a Brønsted–Lowry acid–base reaction. In positive ESI, ionization involves a protonation reaction resulting in $[M+H]^+$ with m/z (M+1), for example, an amine to an ammonium ion with m/z (M+1) (Eq. 1.23a). Multiple protonation reaction can occur as well, leading to $[M+nH]^{n+}$ with m/z ((M+n)/n) (Eq. 1.23b). However, Lewis acid–base reactions also occur leading to adduct formation such as $[M+Na]^+$ with m/z (M+23), (Eq. 1.23c). Doubly-charged ions can also be seen in positive ESI, for example, $[M+H+Na]^{2+}$ with m/z ((M+24)/2) (Section 2.2.8).

$$RNH_2 + H^+ \rightarrow [RNH_3]^+ \qquad m/z \text{ (M+1)} \tag{1.23a}$$

$$R(NH_2)_n + nH^+ \rightarrow [R(NH_3)_n]^{n+} \qquad m/z \text{ (M+}n\text{)}/n \tag{1.23b}$$

$$C_n(H_2O)_n + Na^+ \rightarrow [C_n(H_2O)_n{+}Na]^+ \qquad m/z \text{ (M+23)} \tag{1.23c}$$

In the negative mode, deprotonation reactions are common, leading to deprotonated molecules $[M-H]^-$ with m/z (M−1), for example, a carboxylic acid to a carboxylate ion (Eqs 1.24a and 1.24b). In addition, adduct formation occurs with anions such as chloride (Cl^-), acetate (CH_3COO^-), or formate ($HCOO^-$) leading to ions with m/z (M+X), for example, where $X = 35$ for Cl^-, $X = 59$ for CH_3COO^-, or $X = 45$ for $HCOO^-$ (Eq. 1.24c). Production of multiply-charged (multiple deprotonation) negative ions also occur, for example, $[M-2H]^{2-}$ with m/z ((M−2)/2).

$$RCOOH + B \rightarrow RCOO^- + [BH]^+ \qquad m/z \text{ (M–1)} \tag{1.24a}$$

$$RCOOH + B^- \rightarrow RCOO^- + BH \qquad m/z \text{ (M–1)} \tag{1.24b}$$

$$C_n(H_2O)_n + Cl^- \rightarrow [C_n(H_2O)_n{+}Cl]^- \qquad m/z \text{ (M+35)} \tag{1.24c}$$

The contribution of ESI to the overall sensitivity of the analysis is a direct result of the efficiency of the two main events carried out in the source: ionization and ion transmission (Page et al., 2007).

The ionization efficiency in ESI measures the production of gas-phase ions from analyte molecules present in the solution. This is a multifaceted problem that depends on interface design (sample introduction), analyte properties, solvent composition, and flow rate. Analyte properties and solvent composition must be carefully evaluated in order to promote ion formation of the desired charge, while having the environment needed to perform the ESI. The flow is a twofold limiting factor: there is a minimum flow required for a stable LC performance and ESI operation, and ionization efficiency increases as the flow rate through the emitter decreases. This seems contradictory because for a given set of conditions, the total Taylor cone-jet ESI current is proportional to the square root of the flow rate (Fernández de la Mora & Loscertales, 1994). The explanation lies in the fact that as the flow rate decreases the size of the droplet in the Taylor cone diminishes and less evaporation-coulombic fission events are needed before having free gas-phase analyte ions. Also, as the droplet size decreases, there is an increase in charge density (provided charges are not shed while solvent evaporation happens), thus there is more charge available per analyte molecule.

Another factor that affects overall sensitivity is the ion transmission efficiency between the atmospheric-pressure regions of the source where ionization is done and the mass analyzer high vacuum. The ion-sampling orifice functions as a conductance limit allowing only a small fraction of analyte ions to go through. As the plume is formed, dispersion of the sample is done over an area much larger that the ion-sampling orifice. Therefore, sampling of ions is done only over a small fraction (10^{-3}–10^{-5}) of all the ions actually produced. Reducing the distance between the emitter and the ion-sampling orifice does increase the overall efficiency. However, as this distance gets smaller, droplet solvent evaporation time is reduced and solvent stripping might not be that effective. This hampers gas-phase analyte ion production, and the ion transmission efficiency is reduced. Alternatively, in order to sample a larger area of the plume spray, the size of the ion-sampling orifice can be increased. Unfortunately, this causes strain on the vacuum needs as well as turbulent flows through the ion-sampling orifice. Care must be taken to prevent that overall ion transmission efficiency is not lowered. Several examples of systems developed to improve ion transmission exemplify well the scope of the problem (Ibrahim et al., 2006).

Careful observation must be done to realize the impact that each source parameter has upon the strength of the signal observed (sensitivity) in the mass spectrum. Four key parameters are as follows: LC effluent and emitter flow rates, source temperature, desolvation gas flow, and distance between the emitter tip and the ion-sampling orifice (Figure 1.8).

1.2.4.3 Analytical Applications of ESI The introduction of ESI and especially the observation of multiply-charged ions for proteins and other biomacromolecules (Fenn et al., 1989; Covey et al., 1988; Mann et al., 1989) have significantly transformed the analytical application of MS. Although some ionization techniques introduced in the 1980s, for example, fast-atom bombardment and thermospray ionization, enabled the MS analysis of increasingly polar molecules and also allowed the MS analysis of larger biomolecules, it was the introduction of both ESI and matrix-assisted laser desorption ionization (MALDI) (Tanaka et al., 1988; Karas & Hillenkamp, 1988) that really opened MS analysis for biochemical and biotechnological applications.

With respect to ESI, the ability to generate multiply-charged ions for biomacromolecules with high efficiency enabled the accurate determination of the molecular weight of proteins, oligonucleotides, and other biomacromolecules. Compared to the established method at the time, that is, two-dimensional (2D) gel electrophoresis, ESI-MS provides an easier, faster, and more accurate molecular weight determination (Section 2.8) (Smith et al., 1990; Smith et al., 1991). In fact, the introduction of ESI-MS can be considered one of the most important enabling technologies for current proteomic workflows and research.

In addition, the ESI technology has been developed into a highly robust, sensitive, and more user-friendly interface for LC–MS (compared to previous interface designs). In this respect, ESI-MS is applied not only for the LC–MS analysis of biological and synthetic macromolecules but also in applications concerning small-molecule analysis. Over 90% of all LC–MS methods comprising many areas of application are performed using ESI as the ionization technique. This is also reflected in the data collected in this book: ESI was used as an ionization technique for more than 95% of the drugs and pesticides whose fragmentation characteristics are discussed in Chapter 4. Several alternative ionization techniques have been introduced and developed over the past 20 years, yet none of them challenges the position of ESI as the leading ionization and interface strategy in LC–MS.

1.2.5 Atmospheric-Pressure Chemical Ionization and Photoionization

APCI and APPI are ionization techniques that can be considered as alternatives to ESI in LC–MS. In contrast to ESI, where solvent evaporation and ion formation are tightly coupled, the two processes happen separately in APCI. This enables the use of low-polarity solvents that would not favor analyte ionization in ESI because of insufficient conductivity. Another important difference with ESI is the higher flow rates used ($\approx$1 mL min^{-1}). In general, APCI and APPI are less affected by chemical interferences and enjoy high ionization efficiency. APCI has also been used for the analysis of flames and for environmental air pollution control. Commercial systems based on APCI have long been available in combination with both ion-mobility spectrometry (IMS) (Karasek, 1974) and mass spectrometry (Horning et al., 1973; Carroll et al., 1974; Carroll et al., 1981). As primary source of ionizing electrons, either a radioactive ^{63}Ni foil (Carroll et al., 1974; Carroll et al., 1981) or a corona discharge needle was applied (Shahin, 1966; Carroll et al., 1975). The actual commercial breakthrough of APCI for LC–MS can be attributed to the high-speed quantitative analysis of the drug phenylbutazone and three of its metabolites in plasma and urine using a prototype heated pneumatic nebulizer (Covey et al., 1986) and the (almost) simultaneous introduction of ionspray ionization mass spectrometry (Bruins et al., 1987). As a result, a commercially available API tandem mass spectrometry system was successfully introduced for LC–MS. The present discussion focuses on instrumentation, ionization, and application of APCI and APPI for LC–MS.

1.2.5.1 Instrumentation: The Heated Nebulizer The hardware of APCI for LC–MS is almost identical to the hardware used in ESI, that is, the same atmospheric-pressure ion source and atmospheric-pressure-to-vacuum interface are used (Section 1.2.3). However, there are two important changes to the hardware: (1) the ESI inlet device is replaced by a heated nebulizer, and (2) a corona discharge needle is installed in between the heated nebulizer and the ion-sampling orifice, off-axis and perpendicular to the incoming nebulized solvent flow (Figure 1.12).

The APCI heated nebulizer is a concentric pneumatic nebulizer attached to a heated quartz or stainless steel tube (300–600 °C). A high-flow stream of nitrogen (N_2) is used as nebulizer gas. The liquid flow (typically 1 mL min^{-1}), for example, the LC column effluent, is nebulized into a fine aerosol of small droplets, which is passed through the heated vaporization region where droplet desolvation by evaporation occurs. The droplet evaporation leads to a soft desolvation of analyte molecules from the liquid stream. In this way, analyte molecules are transferred from the liquid phase to the gas phase and made amenable to gas-phase ionization at atmospheric pressure. Optimization of the temperature regimes in the heated nebulizer, leading to a first high-temperature zone (up to 800 °C) and a second low-temperature zone, has been described. This reduces thermal degradation and memory effects in the heated nebulizer and results in an overall improvement in performance (Covey et al., 2001).

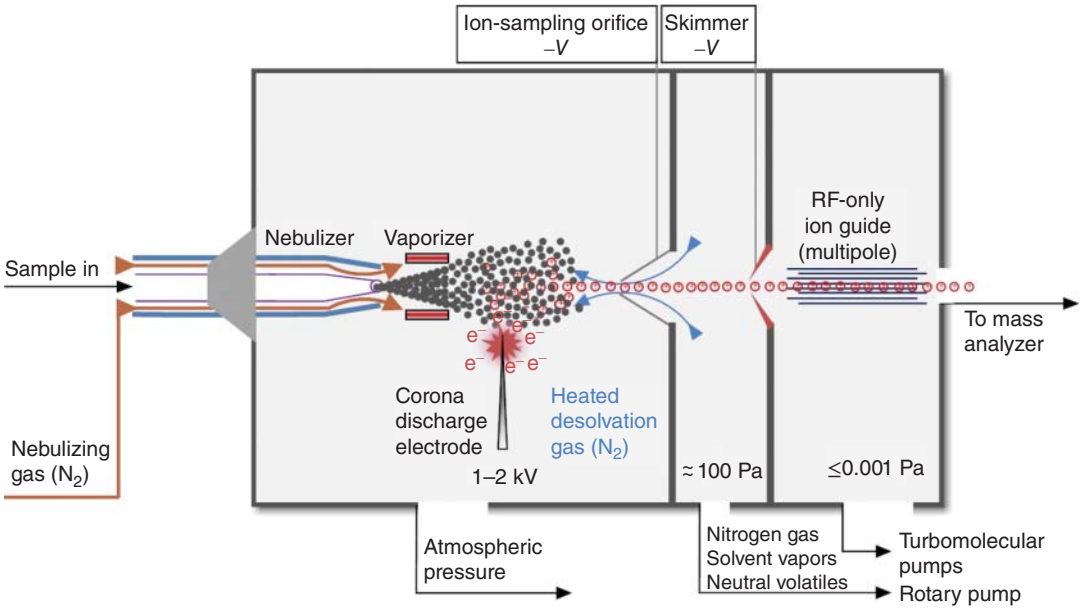

FIGURE 1.12 Schematic representation of an atmospheric-pressure ionization (API) source with an atmospheric-pressure chemical ionization (APCI) inlet.

Corona discharge is a pulsed atmospheric phenomenon (Saint Elmo's fire) that has been known for a long time. It resembles lightning in terms of an electrical discharge, in that it is an arc of very short duration and high power density. This produces visible plasma between a grounded object and a strong electric field in the atmosphere, such as those seen in thunderstorms created by volcanic eruptions. Thus, the presence of ionizable gases in the surroundings is a prerequisite. These arcs can happen between two electrodes, and furthermore they can be controlled in time and space. They are called transient discharges when they are in the nanosecond timescale (sparks are microsecond). In an APCI source, one uses an asymmetric electrode pair, where an electrode (corona discharge anode) having a strong curvature (e.g., sharp needle) is placed between the vaporizer and the ion-sampling orifice (cathode) (Figure 1.12). The corona discharge electrode is applied a voltage of 1–2 kV, thereby creating a high field region, which generates a transient discharge that spreads out toward the ion-sampling orifice. Notwithstanding the fact that it is a complex physicochemical process, corona discharge generators are technologically very reliable (van Veldhuizen & Rutgers, 2001).

The corona discharge acts as a source of primary electrons, and depending on the voltage applied to the needle (anode), the electrons produced will acquire several electronvolts of energy that are indispensable for the ionization of the reagent gas present in the APCI source. A corona discharge can be operated in either positive or negative mode, changing on whether the needle electrode is connected to the positive or the negative pole of the power supply, respectively.

In APPI-MS, the hardware is almost identical to that of APCI. However, no corona discharge is needed. The heated nebulizer is combined with a krypton (Kr) discharge lamp that replaces the corona discharge electrode. This lamp can

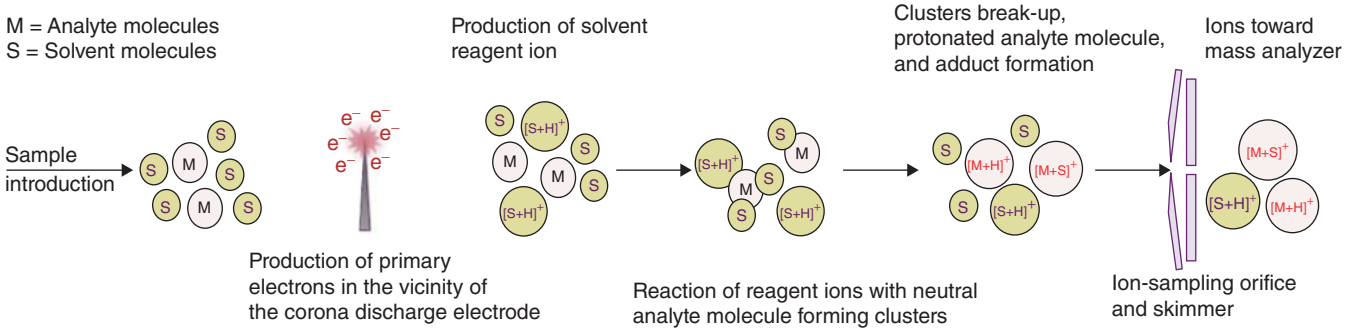

FIGURE 1.13 Schematic representation of the solute ionization process in positive-ion APCI-MS.

produce photons of 10.03 and 10.64 eV in a 4:1 ratio (Short et al., 2007), which interact with the vapors of the nebulized eluting solvent from the LC, thereby initiating the ionization process.

Several related API devices have been reported, including sonic spray (Hirabayashi et al., 1994) and laser spray ionization (Hiraoka et al., 1998). Combined ESI–APCI sources have become commercially available as well. They were especially developed for high-throughput characterization of combinatorial libraries (Gallagher et al., 2003). Several designs are available, featuring either scan-wise switching between ESI and APCI or simultaneous operation of ESI and APCI. In these combined ESI–APCI devices, the heated nebulizer is not used; analyte introduction is performed by pneumatically assisted ESI. Similarly, dual APCI/APPI and ESI/APPI have been described again in order to extend the applicability range of LC–MS in screening of combinatorial libraries and other studies in early drug discovery (Cai et al., 2005).

1.2.5.2 Ionization Mechanisms in APCI Like in conventional CI (Section 1.2.2), the ionization process in APCI is initiated by electron ionization, in this case by electrons from the corona discharge. The sequence of events is assumed to start with the ionization of the nitrogen bath gas (Huertas & Fontan, 1975; Carroll et al., 1981), according to Eq. 1.25.

$$N_2 + e^- \rightarrow [N_2]^{+\bullet} + 2e^- \tag{1.25}$$

In the presence of traces of water, the nitrogen molecular ion ($[N_2]^{+\bullet}$) enters a series of ion–molecule reactions, resulting in protonated water clusters, according to Eq. 1.26.

$$[N_2]^{+\bullet} + H_2O \rightarrow [H_2O]^{+\bullet} + N_2 \tag{1.26a}$$

$$[H_2O]^{+\bullet} + H_2O \rightarrow [H_3O]^+ + HO^{\bullet} \tag{1.26b}$$

$$[H_3O]^+ + nH_2O \rightarrow [H_3O(H_2O)_n]^+ \tag{1.26c}$$

The charge-exchange reaction (Eq. 1.26a) is likely to occur because the ionization energy of water (≈12.6 eV) is lower than that of nitrogen (≈15.6 eV). When an APCI-MS system is run with pure water as mobile phase, a series of protonated water clusters ($[H_3O(H_2O)_n]^+$) or solvated protons ($[(H_2O)_n{+}H]^+$) can be observed, with the ion with $n = 4$ is especially abundant due to the magic numbers determining the stability of such clusters (Tsuchiya et al., 1989).

In LC–MS applications, APCI is mostly performed in combination with reversed-phase LC (RPLC), featuring mixtures of water, an organic solvent, mostly acetonitrile (CH_3CN) or methanol (CH_3OH), and an ammonium-based buffer as the most frequently used mobile-phase constituents. This determines the gas/vapor mixture present in the APCI source. As a result, proton-transfer ion–molecule reactions can take place between the protonated water clusters and the mobile-phase constituents. The protonated water clusters transfer the proton to any species in the gas mixture with a higher PA (Table 1.1). In a CH_3CN–water mobile phase, as an example, this leads to the formation of mixed protonated CH_3CN–water clusters (with $m = 1$–3, and $p = 0$–1), according to Eq. 1.27.

$$[H_3O(H_2O)_n]^+ + CH_3CN \rightarrow [(CH_3CN)_m(H_2O)_p{+}H]^+ \tag{1.27}$$

The PA of these cluster ions resembles more the PA of CH_3CN than that of water. If an ammonium-based buffer is present in the mobile phase, the final reagent gas conditions are determined by ammonium-related ions (Eq. 1.28).

$$[H_3O(H_2O)_n]^+ + CH_3CN + [NH_4]^+ \rightarrow [(CH_3CN)_m{+}NH_4]^+ \tag{1.28a}$$

$$[H_3O(H_2O)_n]^+ + CH_3CN + [NH_4]^+ \rightarrow [(CH_3CN)_m(H_2O)_p{+}NH_4]^+ \tag{1.28b}$$

The size of any of these ion clusters depends on the experimental conditions ($m = 1$–2 is a common feature); the numbers given reflect the situation commonly observed in APCI for LC–MS. The ionization process can be described as a solvent-mediated CI process. It may be concluded that the PA of the APCI reagent gas in LC–MS is determined by the PA of the mobile-phase constituent with the highest PA.

Eventually, the protonated solvent cluster ions ($[S{+}H]^+$) enter into a proton-transfer ion–molecule reactions with the analyte molecules M, according to Eq. 1.29.

$$M + [S{+}H]^+ \rightarrow [M{+}H]^+ + S \tag{1.29}$$

This reaction proceeds to the protonated analyte molecule ($[M{+}H]^+$) as long as the PA of the analyte exceeds that of the protonated solvent cluster (Table 1.1). Initially, the analyte-related ions may be formed in clusters with water or/and solvent ions as well. Subsequent declustering is achieved by collision-induced processes in the vacuum interface.

The change of the APCI reagent gas as a function of the mobile-phase composition can be advantageous or disadvantageous. In principle, it introduces selectivity in the ionization process because analyte molecules with PAs lower than the PA of the cluster ions in the reagent gas are not ionized by proton-transfer CI. Thus, sample constituents with low PA are not ionized. On the other hand, in multiresidue analysis, the PAs of the target analytes may be greatly different. When the presence of an ammonium-based buffer is necessary in LC for those analytes in the mixture that show protolytic properties, the high PA of the reagent gas may exclude target analytes from being ionized. The ammonium-containing reagent gas predominantly ionizes

analyte molecules containing N-atoms, whereas compounds without an N-atom are excluded (Table 1.1). This is an issue deserving attention, especially in untargeted screening for unknowns, for example, in toxicology, in environmental and food safety analysis, and in impurity profiling of drugs (Chapter 5).

In addition to proton-transfer CI, electrophilic addition or adduct formation can take place, which is frequently observed with ammonium-containing mobile phases (Eq. 1.30).

$$M + [S{+}NH_4]^+ \rightarrow [M{+}NH_4]^+ + S \quad (1.30)$$

The formation of an ammoniated analyte molecule, $[M{+}NH_4]^+$, can be observed as long as the PA of the analyte is within $\approx\pm 30\,kJ\,mol^{-1}$ of the PA of NH_3. As a result, adduct-ion formation broadens the applicability range of APCI-MS with a particular mobile-phase composition because analyte molecules with PA slightly lower than that of the protonated solvent cluster can be ionized. It must be pointed out that the above discussion is based on the thermodynamics of the proton-transfer reactions and electrophilic addition reactions. Several (mostly collision-induced) processes take place in between the actual ionization event and the moment the analyte ions enter the mass analyzer. As a result of declustering processes due to collisions in the API source or the vacuum interface, $[M{+}NH_4]^+$ may be dissociated and $[M{+}H]^+$ is observed instead.

Other reaction types, described for positive-ion CI, such as CECI (Section 1.2.2.2), do not readily occur under RPLC conditions. Due to the aqueous solvent conditions, solvent molecular ions that could enter into charge-exchange reactions are not available because they would have had already reacted with solvent constituents, especially water. Charge-exchange reactions may occur under normal-phase LC (NPLC) conditions, but this has not been thoroughly investigated.

In summary, protonated solvent clusters are generated by ion–molecule reactions initiated by the corona discharge. These cluster ions act as reagent gas ions in the solvent-mediated APCI. The reagent gas properties are determined by the mobile-phase constituent with the highest PA. Analyte ionization results from proton-transfer reactions or electrophilic addition reactions (Figure 1.13). The high-pressure conditions in the API source give way to a high collision frequency between the ions, neutrals, and reagents, explaining the high ionization efficiency in APCI. Since collisions are not very energetic, little or no fragmentation of the ionized analyte molecule is produced.

In negative-ion mode, a similar treatment holds. Reactions leading to analyte anion formation share mechanistic similarities with NICI and ECNI observed in conventional CI (Section 1.2.2.3). Proton transfer begins with an ionization reaction leading to superoxide ($[O_2]^{-\bullet}$) as an important initial ionic species. Ion–molecule reactions of $[O_2]^{-\bullet}$ with the mobile-phase constituents of RPLC predominantly lead to deprotonated solvent molecules (Eq. 1.31).

$$O_2 + e^- \rightarrow [O_2]^{-\bullet} \quad (1.31a)$$

$$S + [O_2]^{-\bullet} \rightarrow [S{-}H]^- + HOO^{\bullet} \quad (1.31b)$$

Alternatively, a direct reaction of a solvent molecule with a primary electron leads to the production of a base, which in turn deprotonates neutral analyte molecules (Eq. 1.32).

$$S + e^- \rightarrow [S{-}X]^{\bullet} + X^- \quad (1.32a)$$

$$M + X^- \rightarrow [M{-}H]^- + XH \quad (1.32b)$$

Although one could envisage the methoxide (CH_3O^-) or the cyanomethide anion ($^-CH_2CN$), the reagent gas in negative-ion conditions in practice is determined by the buffer constituents, that is, by deprotonated acids such as formate ($HCOO^-$) and acetate (CH_3COO^-) anions. Thus, proton-transfer reactions between the deprotonated solvent ($[S{-}H]^-$) and the analyte molecule M are observed, according to Eq. 1.33.

$$M + [S{-}H]^- \rightarrow [M{-}H]^- + S \quad (1.33)$$

The reaction is determined by the relative gas-phase acidities ΔH_{acid} of the analyte and the reagent gas molecules (Section 1.2.2.3). The proton-transfer or proton-abstraction reaction proceeds if the ΔH_{acid} of the solvent-related anion exceeds that of the analyte molecule. This limits the applicability of negative-ion APCI to compounds with acidic H-atoms, that is, carboxylic acids, phenols, and compounds exhibiting tautomeric equilibria (amide–iminol or alike). Again, adduct formation, for example, attachment of $HCOO^-$ or CH_3COO^-, can take place according to Eq. 1.34.

$$M + HCOO^- \rightarrow [M{+}HCOO]^- \quad (1.34)$$

For many polar molecules, the latter reaction is thermodynamically favorable, leading to the generation of $[M{+}HCOO]^-$ or $[M{+}CH_3COO]^-$ in mobile phases containing formic and acetic acid, respectively, as observed for corticosteroids (Section 4.6.6).

ECNI is an important ionization technique in GC–MS (Section 1.2.2). For APCI in LC–MS, the applicability of ECNI seems limited. It has been demonstrated that low-energy thermal electrons, generated in the initial step of the APCI process, can be captured by compounds with favorable electron affinities. Pentafluorobenzyl derivatives of steroids and prostaglandins could be detected with 25–100 times improved detection limits compared to conventional negative-ion APCI (e.g., Singh et al., 2000; Mesaros et al., 2010).

Charge exchange, although not very common, can happen according to Eq. 1.35.

$$X^{-\bullet} + M \rightarrow M^{-\bullet} + X \quad (1.35)$$

Superoxide ($[O_2]^{-\bullet}$) can be the radical anion initially formed. Nitroaromatics undergo charge exchange most likely with mobile-phase solvent-based radical anions, for example, methanol ($[CH_3OH]^{-\bullet}$). An example of this is the analysis of 1,3,5-trinitrotoluene (TNT), which shows both $M^{-\bullet}$ with *m/z* 227 and $[M-H]^-$ with *m/z* 226. In addition, two main fragment ions were observed with *m/z* 210 and 197 after the loss from $M^{+\bullet}$ of either the hydroxyl ($^{\bullet}OH$) or the nitrosyl ($^{\bullet}NO$) radical, respectively (Holmgren et al., 2005).

With some analytes, apparent fragmentation occurs under APCI-MS conditions. In most cases, these fragment ions are due to the ionization by APCI of thermal degradation products generated in the heated nebulizer. An interesting example of this process is the thermally induced reduction of an aromatic nitro group ($-NO_2$) into an amine group ($-NH_2$), observed in the positive-ion APCI-MS analysis of aromatic nitro compounds (Karancsi & Slégel, 1999). A fragment due to the loss of 30 Da was observed. H/D-exchange experiments showed that this loss is not due to the loss of $^{\bullet}NO$, but rather due to the indicated reduction.

1.2.5.3 Ionization Mechanisms in APPI APPI was introduced as a new ionization technique for LC–MS in 2000 by two groups simultaneously (Robb et al., 2000; Syage et al., 2000). APPI-MS was considered a highly promising alternative to ESI-MS and APCI-MS. It has been extensively reviewed (Raffaelli & Saba, 2003; Bos et al., 2006; Robb & Blades, 2008; Marchi et al., 2009). Two different APPI source designs have become commercially available.

The initial concept of APPI is that the absorption of a photon ($h\nu$) from the krypton (Kr) lamp results in an electronically excited molecules ([M]*) with sufficient energy for the ejection of an electron to happen, with the formation of the analyte molecular ion ($M^{+\bullet}$) (Eq. 1.36).

$$M + h\nu \rightarrow [M]^* \rightarrow M^{+\bullet} + e^- \quad (1.36)$$

Ionization happens if the photon energy is larger than the first ionization energy of the target compound ($h\nu > IE_M$), and a single photon ionization occurs, forming a molecular ion $M^{+\bullet}$ (or $M^{-\bullet}$). The reason for using a Kr discharge lamp is because the energy of the photons produced (10.03 eV) is greater than the ionization energies (IE) of most organic compounds (7–10 eV) and lower than the IE for the most commonly used LC solvents, for example, methanol (IE = 10.8 eV), water (IE = 12.6 eV), and acetonitrile (IE = 12.2 eV) (Robb et al., 2000). Since argon (Ar) discharge lamps can emit photons with an energy of 11.7 eV, it generates ≈100-fold more solvent ions than when using Kr lamps, and the abundance of $M^{+\bullet}$ is higher as well. In general, Kr lamps give a better signal-to-noise ratio for a low solvent flow rate and Ar lamps do so for high solvent flow rates (Marchi et al., 2009).

In case $IE_M > h\nu$, [M]* may undergo de-excitation mainly via photodissociation (Eq. 1.37a), photon emission (Eq. 1.37b), or collisional quenching with gases present in the source (Eq. 1.37c).

$$M^* \rightarrow A + B \quad (1.37a)$$

$$M^* \rightarrow M + h\nu \quad (1.37b)$$

$$M^* + G \rightarrow M + G^* \quad (1.37c)$$

This direct-APPI approach is primarily promoted by one of the two initial research groups (Syage et al., 2000; Hanold et al., 2004). However, $M^{+\bullet}$ shows a high tendency to react with other compounds in the API source. As a result, the direct-APPI process is not very efficient. Alternatively, an easily ionizable compound, that is, a so-called dopant D, can be added to the mobile phase or to the nebulizing gas to enhance the response. Toluene, chlorobenzene, anisole, or acetone is frequently used as dopant (Robb et al., 2000; Kauppila et al., 2004a). In the presence of a dopant, the APPI process occurs via a charge-exchange reaction between the dopant molecular ion ($D^{+\bullet}$) and the analyte molecule M (Eq. 1.38). This reaction proceeds only when the EA of the analyte is higher than the EA of the dopant.

$$D + h\nu \rightarrow D^{+\bullet} \quad (1.38a)$$

$$D^{+\bullet} + M \rightarrow D + M^{+\bullet} \qquad EA_M > EA_D \quad (1.38b)$$

Unfortunately, although in both direct-APPI and dopant-APPI an analyte $M^{+\bullet}$ would be expected, a protonated molecule $[M+H]^+$ is observed for many analytes. This is due to ionization of the mobile-phase constituents by APPI. In the direct-APPI approach, the protonated molecule is formed due to a reaction of the analyte $M^{+\bullet}$ with a solvent molecule S (Eq. 1.39a):

$$M^{+\bullet} + S \rightarrow [M+H]^+ + [S-H]^{\bullet} \quad (1.39a)$$

The formation of $[M+H]^+$ is especially important in protic solvents, that is, under RPLC conditions. Similar processes are applicable in negative-ion APPI (Kauppila et al., 2004b). If the PA of the analyte is higher than the PA of the deprotonated dopant ion, solvent molecules can serve as intermediates between the dopant ion and the analyte M, leading to the formation of $[M+H]^+$ when the $PA_M > PA_S$ (Eqs 1.39b and 1.39c). In dopant-APPI, the formation of $[M+H]^+$ is attributed to internal proton rearrangement in the solvated dopant ion clusters (Robb & Blades, 2005).

$$D^{+\bullet} + nS \rightarrow [S_n+H]^+ + [D-H]^{\bullet} \qquad PA_S > PA_{[D-H]^{\bullet}} \quad (1.39b)$$

$$[S_n+H]^+ + M \rightarrow [M+H]^+ + nS \qquad PA_M > PA_S \quad (1.39c)$$

The prospect of being able to generate $M^{+\bullet}$ of analyte molecules under LC–MS conditions is that via fragmentation by collision-induced dissociation (CID) in MS–MS product-ion mass spectra can be obtained that show great resemblance to EI mass spectra, and thus may be searched against the large mass spectral libraries available (Section 1.2.1.4).

1.2.5.4 Analytical Applications of APCI and APPI Both APCI and APPI can be used as an alternative to ESI in LC–MS, especially in the analysis of the less polar analytes (Figure 1.7). APCI can be effectively used in the analysis of a wide variety of drugs in biological matrices. Compared to ESI, the ionization process of APCI is less prone to ionization suppression by matrix effects (Matuszewski et al., 2003; Matuszewski, 2006). Therefore, if similar sensitivity can be reached in quantitative bioanalysis, APCI should often be preferred over ESI in method development. Despite this, many researchers continue working with ESI, probably because they need to invest some effort in understanding the specific practical features of APCI. Perhaps the instrument manufacturers should invest more effort in optimizing the performance of their APCI devices.

Despite its initial promise, APPI did not become a major ionization technique in LC–MS. From a recent review (Marchi et al., 2009), a clear view can be obtained on the most important application areas of APPI, that is, especially for the analysis of steroids and polycyclic aromatic hydrocarbons and synthetic organic chemicals.

Over the years, a large number of comparative studies of the performance of APPI relative to APCI and ESI has been reported, for example, in the LC–MS analysis of flavonoids in plant extracts (Rauha et al., 2001), anabolic steroids for sports doping analysis (Leinonen et al., 2002), dinitropyrene and aminonitropyrene in biological matrices (Straube et al., 2004), cyclosporin A in rat plasma (Wang et al., 2005), lipids (Cai & Syage, 2006), chiral pharmaceuticals by NPLC (Cai et al., 2007), estrogens in water (Lien et al., 2009), hexabromocyclododecane enantiomers in environmental samples (Ross & Wong, 2010), several drugs in municipal wastewater (Garcia-Ac et al., 2011), environmental contaminants in water (Wang & Gardinali, 2012), and ergot alkaloids from endophyte-infected sleepy grass (*Achnatherum robustum*) (Jarmusch et al., 2016).

In general, considerable attention was paid at optimizing solvent composition to obtain optimum performance. For the quantitative analysis of flavonoids, negative-ion ESI gave the best results (Rauha et al., 2001). In negative-ion mode, flavonoids show less fragmentation than in positive-ion mode. Therefore, the negative-ion mode is preferred for quantitative analysis, while the positive-ion mode is more favorable for confirmation of identity or identification purposes. For the analysis of anabolic steroids, positive-ion ESI was found best for the purpose. Although in-source fragment ions involving the loss of water were observed with all three ionization methods tested, they were far more abundant in APCI and APPI (Leinonen et al., 2002).

Dinitropyrenes and their metabolites aminonitropyrenes and diaminopyrenes may be used as biomarkers for monitoring human exposure to diesel engine emissions. Dinitropyrene itself is not effectively ionized by ESI. Best results were obtained with APPI, where $[M-30]^{+\bullet}$ for dinitropyrene and $[M+H-30]^{+}$ for aminonitropyrene were observed, with similar detection limits in RPLC and NPLC (Straube et al., 2004).

For cyclosporin A, comparable results were obtained with all three ionization techniques (Wang et al., 2005).

For free fatty acids and their esters, monoacylglycerols, diacylglycerols, and triacylglycerols, APPI is two to four times more sensitive than APCI and much more sensitive than ESI, unless mobile-phase additives such as ammonium formate or sodium acetate are used in combination with ESI (Cai & Syage, 2006). The ability to use APPI under NPLC conditions can be useful in chiral separations. This was tested for several chiral drugs. In comparison with APCI, APPI generated higher peak area as well as lower baseline noise, that is, 2–500 times better signal-to-noise ratio (S/N) (Cai et al., 2007).

In the analysis of estrogens, that is, estrone, 17β-estradiol, estriol, 17α-ethinylestradiol, 4-nonylphenol, 4-*tert*-octylphenol, and bisphenol A, in sewage treatment plant effluent and in river water, the best performance was achieved for the dansylated derivatives in positive-ion ESI. For native compounds, negative-ion ESI outperformed APCI, APPI, and a combined APCI/APPI, all operated in negative-ion mode (Lien et al., 2009). In another study on native estrogens and other steroids, that is, testosterone, equilenin, progesterone, equilin, 17β-estradiol, 17α-ethynylestradiol, estrone, androsterone, mestranol, and estriol (Wang & Gardinali, 2012), negative-ion APPI using toluene as dopant was found to provide a better performance than ESI and APCI.

Anion-attachment APPI with 1,4-dibromobutane as dopant generated $[M+Br]^{-}$ for hexabromocyclododecane enantiomers. Compared to APPI and ESI, anion-attachment APPI shows better S/N and reduced matrix effects (Ross & Wong, 2010).

In the analysis of cyclophosphamide, methotrexate, bezafibrate, enalapril, and orlistat in wastewater samples, ESI provided better S/N than APCI and APPI (Garcia-Ac et al., 2011).

In the analysis of ergot alkaloids in extracts of the grass *Achnatherum robustum* infected with the *Epichloë* fungus, comparable results were obtained with ESI and APPI (Jarmusch et al., 2016). From these comparative studies, it may be concluded that all three ionization methods, ESI, APPI, and APCI, have their merits with specific analytes or samples.

1.2.6 Other Ionization Techniques

Apart from EI, CI, ESI, APCI, and APPI, there is a wide variety of other ionization techniques that are used or have been used in MS. Some of these techniques are briefly discussed in this section.

1.2.6.1 Energy-Sudden Desorption Ionization Techniques In two interesting review papers, it was concluded that many soft ionization techniques have some common features (Arpino & Guiochon, 1982; Vestal, 1983): they all need some kind of matrix component and the ionization is effected by a short-duration energy input, thus the term "energy-sudden" ionization methods was coined (Vestal, 1983). The ionization techniques discussed include field ionization and field desorption ionization (FDI), ^{252}Cf plasma desorption ionization (PDI), fast-atom bombardment (FAB), laser-desorption ionization (LDI), and thermospray ionization (TSI). Ionization techniques such as ESI and MALDI, which had not been introduced at the time, readily fit this model. The matrix involved can be a specific compound mixed with the analyte to achieve analyte ionization, that is, nitrocellulose in PDI; glycerol in FAB; or sinapinic acid (SA), 2,5-dihydroxybenzoic acid (DHB), or α-cyano-4-hydroxycinnamic acid (CHCA) in MALDI, while in TSI and ESI the matrix is the liquid phase from which droplets are generated. Important common processes in the ionization mechanism of these methods are the formation of analyte ions in the sample matrix prior to evaporation or desorption combined with rapid evaporation prior to ionization. The latter is achieved by very rapid heating or by sputtering with high-energy photons or particles. The energy deposited on the sample surface, which can also come from a strong electric field as in ESI, can provide preformed ions in the condensed phase with sufficient kinetic energy to leave the matrix and/or can cause (gas-phase) ionization reactions to occur near the interface of the solid or liquid and the vacuum (the so-called selvedge).

In general terms, a simplified view on the ionization process involves the formation of primary matrix ions because (clusters of) matrix molecules (S) undergo acid–base reaction (Eq. 1.40a).

$$\mathrm{S} + \text{energy} \rightarrow [\mathrm{S{+}H}]^+ + [\mathrm{S{-}H}]^- \qquad (1.40a)$$

This is followed by secondary ion formation from matrix ion–analyte reactions. The ions produced are usually protonated (Eq. 1.40b) or deprotonated analyte molecules (Eq. 1.40c) although radical cations or anions can also be observed.

$$[\mathrm{S{+}H}]^+ + \mathrm{M} \rightarrow \mathrm{S} + [\mathrm{M{+}H}]^+ \qquad (1.40b)$$

$$[\mathrm{S{-}H}]^- + \mathrm{M} \rightarrow \mathrm{S} + [\mathrm{M{-}H}]^- \qquad (1.40c)$$

In FDI, the sample is deposited on a thin FDI emitter (a few μm in diameter, activated to provide for carbon microneedles on the surface). The emitter is kept at a high potential (>5 kV) in the high-vacuum ion source and a current is passed through to achieve slow heating of the emitter. As a result, nonvolatile analytes can be desorbed and ionized by various mechanisms (Beckey, 1977; Schulten, 1982; Lattimer & Schulten, 1989). For nonpolar analytes, mainly $M^{+\bullet}$ (by electron tunneling from the sample molecules into the emitter) is observed, whereas for more polar analytes like glycosides, lipids and peptides $[M{+}H]^+$ and/or $[M{+}Na]^+$ are observed. Liquid injection field desorption ionization (LIFDI) is a more user-friendly alternative to FDI because it enables sample application to the emitter while keeping the system under vacuum (Linden, 2004).

In FAB and liquid secondary ion mass spectrometry (LSIMS), the analyte of interest is dissolved in an appropriate matrix solvent, such as glycerol, diethanolamine, or other polar solvents with low vapor pressure. The solution is applied as a thin film onto a metal target, which subsequently is exposed to a beam of high-energy particles, that is, Ar or Xe atoms or Cs^+ ions. Analyte ionization is achieved by three processes: (1) desorption of preformed ions by energy transfer upon particle impact, (2) desolvation of preformed ions in the splash droplets resulting from disruption of the liquid layer upon particle impact, and (3) gas-phase ion–molecule reactions in the selvedge (Barber et al., 1981; Bélanger & Paré, 1986; Fenselau & Cotter, 1987). In FAB mass spectra, mostly $[M{+}H]^+$, $[M{+}Na]^+$, and/or $[M{+}K]^+$ are detected in positive-ion mode and $[M{-}H]^-$ in negative-ion mode, often along with some fragment ions. Apart from the analyte-related ions, (abundant) background ions are observed, which are due to matrix cluster ions, for example, $[(\text{glycerol})_n{+}H]^+$ with $n = 1$–10. With the introduction of ESI and MALDI, FAB has become obsolete.

TSI was developed in the mid-1970s as an interface for LC–MS (Blakley et al., 1978; Blakley & Vestal, 1983; Arpino, 1990, 1992). During this development, the system evolved from highly complex hardware into an easy-to-use interface for LC–MS that has been successfully commercialized and applied in the 1980s and the early 1990s, until it started to lose territory in favor of ESI. Nowadays, TSI is obsolete as an LC–MS interface. The heated source block of a typical TSI-MS system contains a gas-tight cylindrical tube, which at one end has the vaporizer probe and at the other end has a connection to a rotary pump. It is equipped with a (liquid-nitrogen) cold trap to avoid pump-oil contamination by solvent vapors. A temperature sensor is placed downstream to monitor the temperature of the vapor jet. The ion source contains an off-axis ion-sampling cone that acts as the entrance slit to the mass analyzer and opposite to that of a repeller electrode. A filament behind an electron entrance

slit and/or a discharge electrode may be positioned upstream (Blakley & Vestal, 1983; Vestal & Fergusson, 1985).

The TSI hardware provides several ionization modes. Apart from electron-ionization initiated processes, where electrons from the filament or discharge electrode are the primary source of ionization, two liquid-based ionization modes are available. With ionic analytes and preformed ions in solution, ionization can be achieved by ion evaporation processes (Section 1.2.4.2). With neutral analytes, TSI buffer ionization is predominant: ionization takes place by either gas-phase ion–molecule reactions or rapid proton-transfer reactions at the selvedge. In the latter case, the addition of ammonium acetate or any other volatile buffer to the LC effluent is obligatory (Blakley et al., 1980; Vestal, 1983; Arpino, 1990; Katta et al., 1991).

1.2.6.2 Matrix-Assisted Laser Desorption Ionization MALDI was introduced in 1988 by two research groups simultaneously (Tanaka et al., 1988; Karas & Hillenkamp, 1988). MALDI was developed as a solution for the ionization of nonvolatile and high-molecular mass analytes. In a typical MALDI experiment, a mixture of the sample solution and an appropriate matrix solution is deposited onto a metal target (sample holder). Upon drying, co-crystallization of matrix and analyte molecules takes place. However, analysis of (nonvolatile) liquid matrices containing the analyte of interest is also possible when compounds are capable of absorbing UV and/or IR radiation. The matrix serves several purposes, that is, it is the mechanical support for the analyte, it reduces intermolecular hydrogen bonding and thereby results in isolated analyte molecules, while it also serves as energy-transfer agent between the excitation source and the analyte in question. The crystals on the target under vacuum are then bombarded by laser pulses delivering photons with an energy that matches the maximum absorption frequency of the matrix, for example, with 337 nm from an N_2 laser for the matrices mentioned earlier. A two-step ionization process is assumed to take place, where first the laser energy is absorbed by the matrix molecules, which are then desorbed and ionized by protonation. In the hot plume generated in this ablation step, proton transfer between matrix ions and analyte molecules leads to protonated analytes (Knochenmuss, 2006; Karas & Krüger, 2003). Gas-phase analyte ions are generated in the selvedge, according to Eq. 1.40. The ions produced tend to be stable and undergo little or no fragmentation, thus the protonated analyte is an important feature of the mass spectrum (Figure 1.14). The ions generated can be mass analyzed, which is mostly done using a time-of-flight mass spectrometer (Section 1.3.4).

MALDI is an important ionization technique for peptides and proteins. Unlike in ESI, where ion envelopes of multiply-charged ions are generated (Sections 1.2.4.3 and 2.8), in MALDI-MS mostly singly-charged $[M+H]^+$ ions are generated, together with less abundant doubly-charged $[M+2H]^{2+}$ and proton-bound dimeric $[2M+H]^+$ ions.

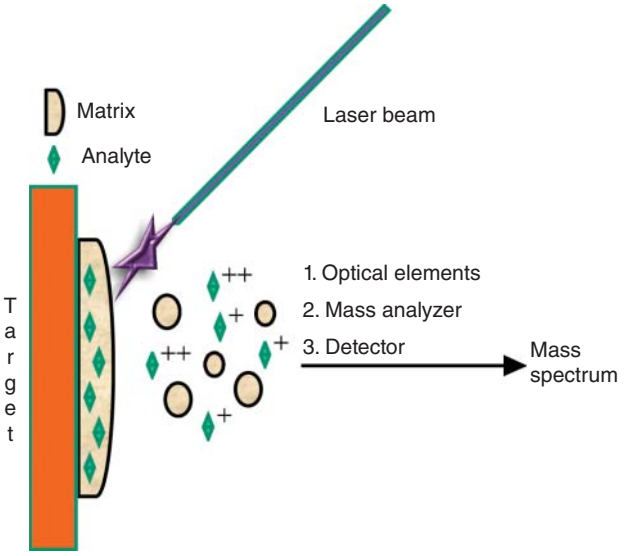

FIGURE 1.14 Schematic representation of analyte evaporation and ionization in a MALDI-MS experiment.

In addition to the analysis of peptides and proteins, MALDI is especially useful in the analysis of bio(macro) molecules such as oligosaccharides and glycans, oligonucleotides, and lipids, but it is also used for synthetic polymers, and in some cases even of small molecules such as drugs and antibiotics (Mann & Talbo, 1996; Karas, 1996). Moreover, MALDI-MS plays an important role in imaging mass spectrometry (Angel & Caprioli, 2013) and in the identification of bacteria and microbial fingerprinting (Clark et al., 2013), which are two emerging application areas of MS.

1.2.6.3 Atmospheric-Pressure Desorption Ionization Techniques In recent years, several atmospheric-pressure desorption ionization techniques have been introduced (Van Berkel et al., 2008; Huang et al., 2010). The first and most widely used technique is DESI. In DESI, the high-velocity spray of charged microdroplets from a (pneumatically assisted) electrospray needle is directed at a surface, which is mounted in front of the ion-sampling orifice of an API source. Surface constituents are released and ionized. These gas-phase ions are then introduced into the MS (Takáts et al., 2005). DESI-MS enables analyte ionization directly from solid surfaces. No extensive sample pretreatment or prior separation is performed. DESI-MS has been applied in the analysis of drugs in tablets, for example, for illicit drugs, or of natural products in plants. Chemical imaging of surfaces

such as thin-layer chromatography plates and tissue sections can also be performed.

Among the other atmospheric-pressure desorption ionization techniques available are atmospheric-pressure matrix-assisted laser desorption ionization (AP-MALDI) (Creaser & Ratcliffe, 2006), direct analysis in real time (DART) (Cody et al., 2005), and atmospheric-pressure solids analysis probe (ASAP) (McEwen et al., 2005).

1.3 MASS SPECTROMETER BUILDING BLOCKS

1.3.1 Introduction

Mass spectrometry involves the generation of gas-phase ions from analyte molecules, the subsequent separation or mass analysis of these ions according to their *m*/*z*-values, and their detection. The instrument must be equipped with computing capabilities for instrument setup, data acquisition, and (advanced) data processing (Figure 1.15). Prior to analyte ionization, sample introduction must be performed. This may involve the introduction of individual samples by means of a direct insertion technique. However, sample introduction via hyphenated chromatographic techniques, that is, GC or LC, is performed more frequently. In such a hyphenated setup, the mass spectrometer can be used as a detector to provide mass spectrometric information on the analytes eluting after a chromatographic separation. GC–MS and LC–MS are very powerful and widely used analytical tools in many areas of chemistry, pharmacy, biology, and plenty other fields.

In analytical chemistry, six basic types of mass analyzers are used, two that provide unit-mass resolution, that is, the quadrupole and the ion-trap mass spectrometers, and four that provide high-resolution accurate-mass (HRAM) analysis, that is, time-of-flight (TOF), sector, orbitrap and Fourier-transform ion cyclotron resonance (FT-ICR) mass spectrometers. Except for sector instruments where other definition applies, the resolution of a high-resolution mass spectrometer is measured from the FWHM for a given *m*/*z* value (Section 2.6). The value for resolution is calculated from the ratio of *m*/*z* and FWHM. Instruments providing unit-mass resolution show FWHM of ≈0.7 for singly-charged ions over the entire applicable *m*/*z* range.

In addition to mass spectrometric resolution, the achievable mass accuracy is another important figure of merit (Section 2.6). When proper calibration of the *m*/*z* axis is performed, a unit-mass resolution instrument can provide a mass accuracy of ±0.1 for singly-charged ions over the entire applicable *m*/*z* range. For high-resolution instruments, accurate-mass determination can be achieved, currently down to 1 ppm. For singly-charged ions with *m*/*z* <1000, this means that the error is in the third decimal place (e.g., >0.001). Internal mass calibration or frequent external calibration is required to routinely maintain the high mass accuracy of HRAM instruments.

An MS experiment generally requires high-vacuum conditions (pressure $\leq 10^{-3}$ Pa; $\leq 10^{-5}$ mbar) in both the mass analyzer and the ion detection system. Depending on the technique applied, analyte ionization may be performed either in high vacuum or at atmospheric pressure (Section 1.2). In the latter case, a vacuum interface is required to transfer ions from the API source into the high-vacuum mass analyzer region.

1.3.1.1 Basic Data Acquisition and Data Processing In its basic operation in GC–MS or LC–MS, the mass spectrometer can be set to continuously acquire mass spectra between a low *m*/*z* and a high *m*/*z* within a preset time period (≤1 s). This is the full-scan mode. However, since several types of mass spectrometers do not actually scan, the more general term full-spectrum mode is preferred over the term full-scan mode. The ionization technique applied and the resolution of the mass spectrometer utilized determine the information content of the mass spectrum. Initially, the mass spectra are acquired in continuous or profile mode, for example, with ≈10 data points per *m*/*z* value for a unit-mass resolution instrument, whereas far more data points per *m*/*z* are required in HRAM-MS to provide the appropriate resolution and mass accuracy. The data system digitally stores the information in

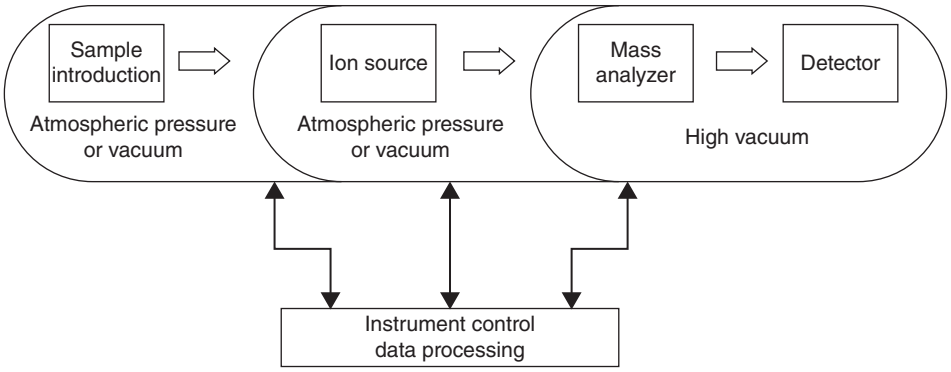

FIGURE 1.15 Flow chart of a typical MS experimental setup.

either the profile mode, that is, continuum spectra, possibly after data reduction like in apodization, in order to reduce the size of the data file (e.g., Scigelova et al., 2011), or the centroid mode, where only a weighted average of the mass peak is saved (Urban et al., 2014) (Figure 1.16). Centroiding procedures greatly reduce the data file size but may also reduce the information content of the initial raw data acquired. Post-acquisition data processing tools may require either profile or centroid data. Data acquisition modes for MS are further discussed in Section 1.5.

In the full-spectrum mode, a three-dimensional (3D) data array is acquired with time, m/z, and ion intensity (often expressed in counts) as the three axes. The data acquired can be visualized in different ways. The total-ion chromatogram (TIC) is a plot of the sum of the ion counts of the individual mass spectra as a function of time (or spectrum number). In a base-peak chromatogram (BPC), the ion count recorded for the most abundant ion in each spectrum, that is, irrespective of the m/z of that ion, is plotted as a function of time. BPCs are especially useful for peak searching in chromatograms with relatively high chemical background, such as in LC–MS. At any given time in the TIC or BPC, a mass spectrum can be obtained, which represents a slice of the data array of the ion counts as a function of m/z.

It is often useful to generate summed, averaged, and/or background subtracted mass spectra. The mass spectrum may be computer searched against a mass spectral library to assist in compound identification. The information from the TIC (Figure 1.17a) and the mass spectra can be combined in either a 3D representation, with time, m/z, and ion intensity/counts as the three axes x, y, and z, respectively (Figure 1.17b and c), or a contour plot, which basically is a 2D representation of the time against m/z where the ions detected are seen as spots; colors may be used to represent relative intensity/counts (Figure 1.17d). In an extracted-ion chromatogram (XIC), the counts for an ion with a particular m/z are plotted as a function of time. By default, a selection width or selection window of $m/z \pm 0.5$ is used to generate the XIC. However, with HRMS, a narrower selection window, for example, $m/z \pm 0.01$, may be used to achieve XIC with a greatly improved S/N.

Quadrupole, ion-trap, and sector mass analyzers can also acquire data in the selected-ion mode. In that case, the mass analyzer is programmed to select a particular m/z for transmission to the detector during a preset period (the so-called dwell time, typically 5–200 ms) and to subsequently jump to other preselected m/z values; after monitoring all the preselected m/z values, the same function is repeated, for example, during (part of) the chromatographic run-time. Compared to the full-spectrum mode, the selected-ion mode provides a longer measurement time for the selected ion (or ions), which results in enhanced S/N. The data can be displayed in terms of XICs. This acquisition mode is especially applied in targeted quantitative analysis. With instruments not capable of a selected-ion mode, that is, TOF and orbitrap mass analyzers, improved S/N and targeted quantitative analysis can be achieved post-acquisition in narrow-window XICs, as discussed earlier.

1.3.1.2 Ion Detection The ion detection device must be capable of converting the tiny electric current of the incoming ions into a measurable and usable signal. The actual detector employed depends on the type of mass analyzer. In general, ion detection systems must be backed by sufficiently fast electronics, including analog-to-digital converters (ADCs), to enable the high-speed data acquisition required in MS (de Hoffmann & Stroobant, 2007). Broadly speaking, ions are made to collide onto a special surface called the conversion dynode, made of a low IE material such as Pb, Be–Cu, which upon impact by the fast incoming ions emits electrons and possibly other secondary particles (Figure 1.18). These electrons are then converted into a usable current by a signal amplification system (e.g., an electron multiplier (EM)). The EM may be a device of either the continuous dynode type or the discrete dynode type (Allen, 1947). In an EM, the secondary particles from the conversion dynode hit the first dynode (EM entrance) and cause the emission of secondary electrons, which in turn do the same as they are directed toward the subsequent dynodes. Finally, the resulting current is detected over a collector plate and amplified by an electrometer. This repeated emission of secondary electrons creates a cascade effect with a typical current gain for an EM with an order of magnitude of 10^6–10^7. A conversion dynode, held at a high electric potential (5–20 kV), is positioned in front of the multiplier to increase the signal intensity of ions, especially in the high-mass region, as well as to enable the detection of negative ions. The EM is used for ion detection in quadrupole, ion-trap, and sector instruments.

In some instruments, a photomultiplier is used instead of an EM. In this system, a conversion dynode is used to generate electrons from the incoming ions by secondary emission. These secondary electrons in turn are directed toward a phosphorescent screen, which upon electronic excitation emits photons. These photons are sent to a photomultiplier, where typically signal amplification with an order of magnitude of 10^5 is achieved.

With TOF instruments, where the ion beam shows more spatial spreading, microchannel plate (MCP) detectors are applied. An MCP is an array of parallel miniature electron multipliers (Wiza, 1979). In order to generate a mass spectrum from the ion arrival events in TOF instruments, either a time-to-digital converter (TDC) or an ADC has to be used. TDCs provide excellent time resolution and low random noise, but do not discriminate in the intensity of the pulse. Therefore, high ion densities may lead to saturation effects, thus greatly limiting the dynamic range. In an ADC, the integrated circuit chip receives a time-dependent signal and typically generates a 10-bit digital output: both

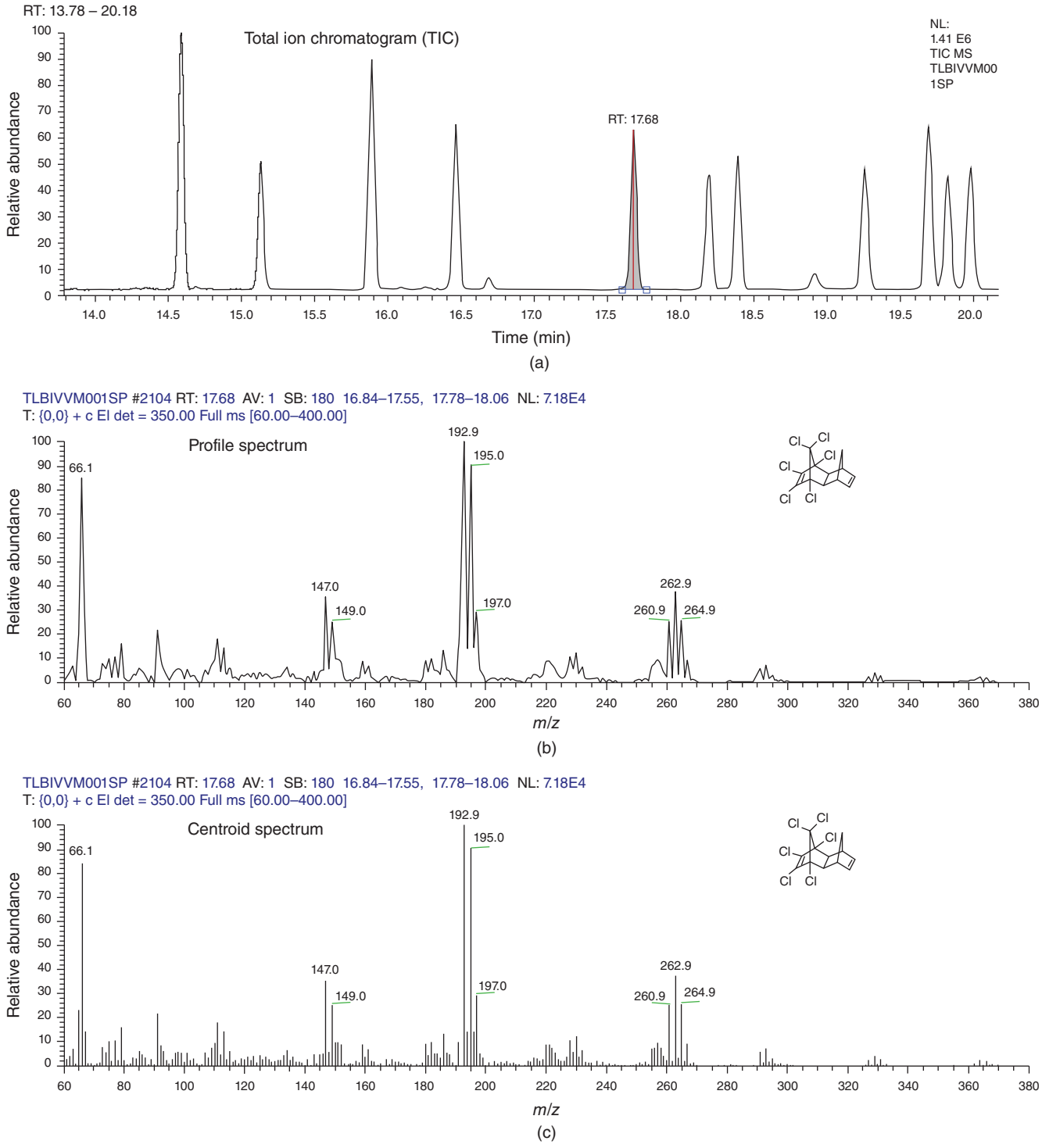

FIGURE 1.16 GC–MS analysis of a mixture of organochlorine insecticides. (a) Total-ion chromatogram (TIC), (b) profile or continuum mass spectrum for isodrin, and (c) centroid mass spectrum for isodrin.

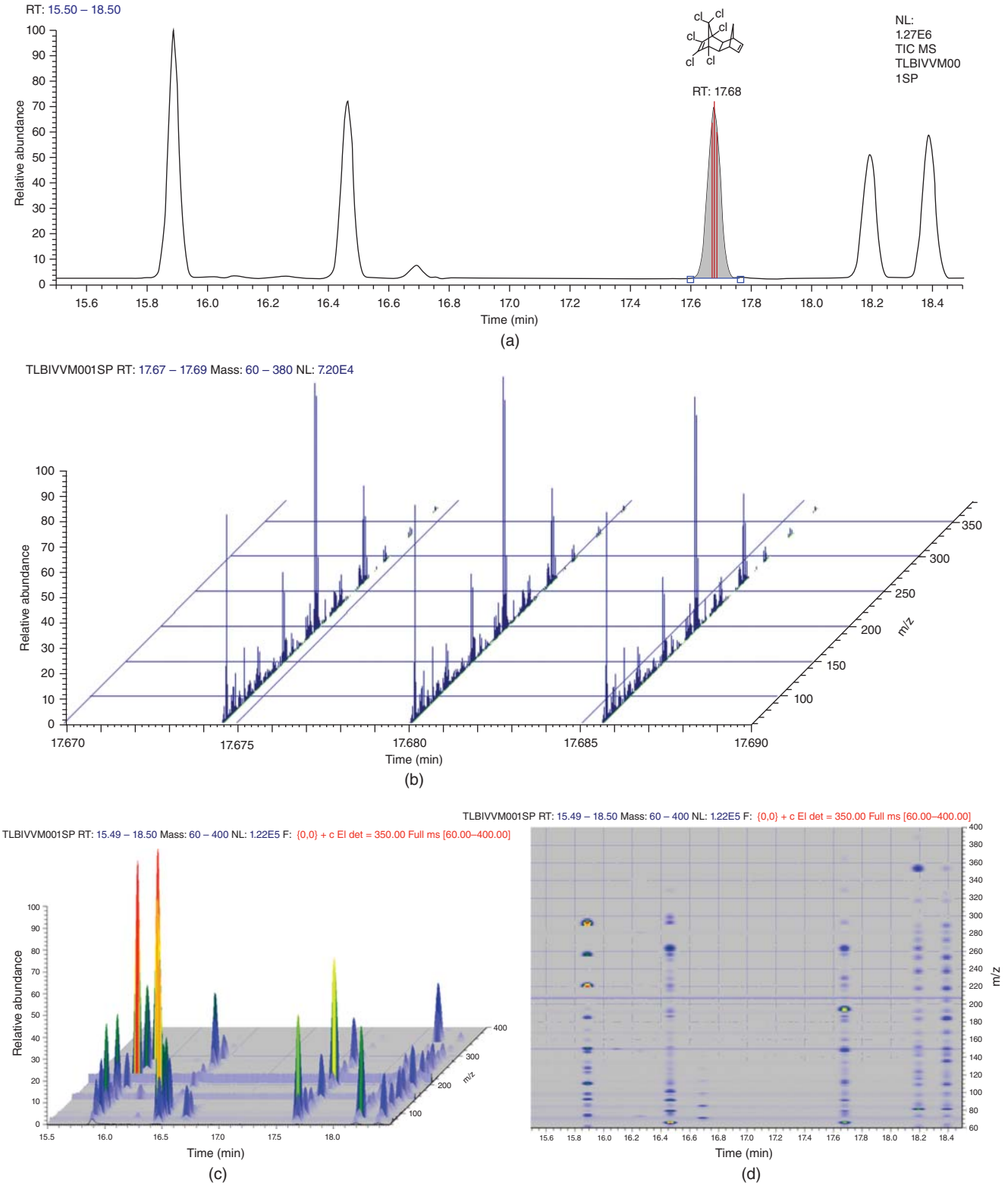

FIGURE 1.17 Different graphical representations of the chromatography–MS data. (a) Conventional 2D TIC, (b) zoom-in showing individual spectra as a function of time, (c) 3D TIC, and (d) contour plot of the 3D TIC shown in (c).

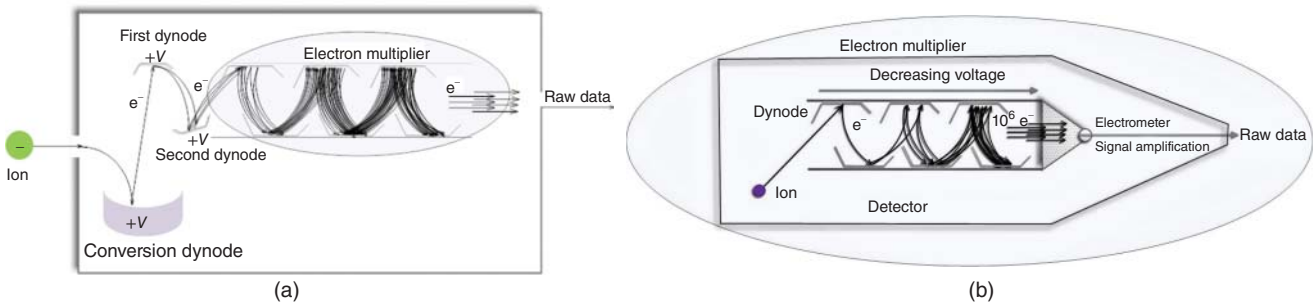

FIGURE 1.18 Schematic diagram of an electron multiplier for ion detection.

arrival time and the number of colliding ions are recorded. Currently applied ADCs can provide 1–4 GHz time resolution and discriminate 1024 different ion intensity levels. In FT-ICR-MS and orbitrap-MS systems, ion detection is based on the detection of high-frequency image currents of the coherently moving ions (Marshall et al., 1998). The signals of all ions with different m/z values are detected simultaneously. The time-domain signal is Fourier-transformed to the frequency-domain signal, which can be converted into mass spectra.

1.3.2 Quadrupole Mass Analyzer

The majority of mass spectrometers in use in laboratories around the world are based on quadrupole mass analyzer technology. A quadrupole mass analyzer consists of two pairs of rods of hyperbolic or circular cross section that are accurately positioned parallel to each other and in a radial array. Generally, stainless-steel or metal-coated ceramic rods are employed. Each pair of rods is charged by either a positive or a negative direct-current (DC) potential with a superimposed alternating-current (AC) radiofrequency potential (RF, MHz) as shown in Figure 1.19. The latter successively reinforces and overwhelms the DC field.

Ions coming from the source are introduced into the quadrupole field by means of a low accelerating potential. Due to the applied oscillating fields, the ions are sequentially attracted and repelled by the rod pairs, and they oscillate in the yz- and xz-planes as they traverse the quadrupole filter. The theoretical description of the trajectory the ions follow in the quadrupole electric field involves a large number of physical parameters. Solutions to these Mathieu differential equations can be simplified by defining the a and q terms, where a is proportional to the DC and q is proportional to the RF (the mass m is in the denominator). This allows the construction of a stability diagram (a–q diagram), which is useful in understanding the features of quadrupole mass analysis (Figure 1.20). A limited number of combinations of a and q, that is, of DC and RF, leads to stable trajectories for the ions in the hyperbolic space defined by the quadrupole field between the rods, allowing them to travel the length of the analyzer and reach the detector.

The quadrupole mass filter is operated with a fixed ratio of DC and RF; the ratio determines the resolution of the device. Now assume that the device is operated at unit-mass resolution. At a given DC/RF combination within the stable region of the stability diagram, the ions with only one m/z (actually $m/z \pm 0.35$ as FWHM at unit-mass resolution is 0.7) show a stable trajectory toward the end of the rods and are thus transmitted to the detector, while ions with unstable trajectories do not pass the mass filter because the amplitude of their oscillation becomes infinite. Consequently, they are

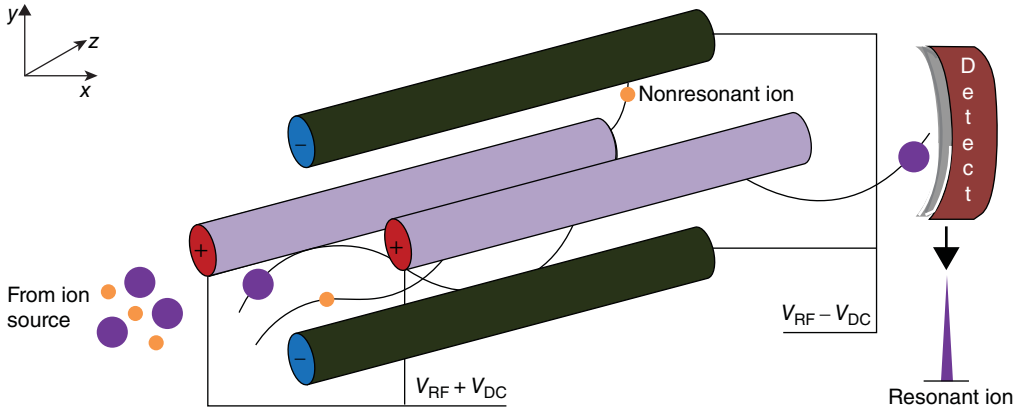

FIGURE 1.19 Schematic diagram of a quadrupole mass analyzer.

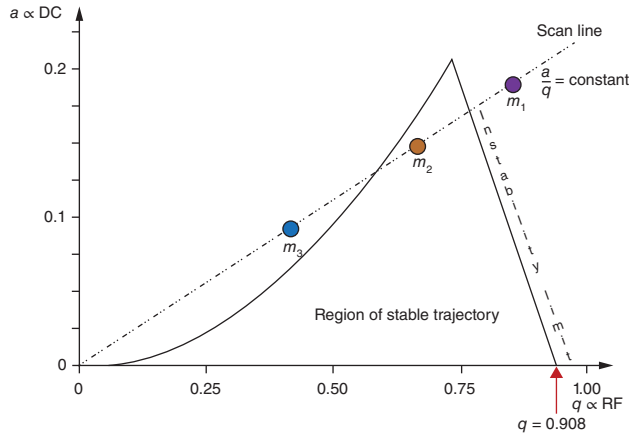

FIGURE 1.20 Stability diagram for a quadrupole mass filter.

discharged against the rods and/or lost in the vacuum system. Thus, the quadrupole mass analyzer can be considered as a variable band-pass filter (Miller & Denton, 1986). By ramping DC and RF voltages at a fixed ratio, that is, moving along the scan line in the stability diagram, ions of increasing *m*/*z* values are transmitted one after another to the ion detector, as they pass the instability limit ($q = 0.908$) (Figure 1.20).

Since the ramping of voltages can be done quite fast in modern electronics, scan speeds as high as 10,000 *m*/*z* s^{-1} can be achieved. In principle, the resolution of the quadrupole mass analyzer depends on the ratio of DC and RF, that is, the slope of the scan line in the stability diagram. However, operation at higher than unit-mass resolution generally greatly compromises the ion transmission and thereby the sensitivity (Tyler et al., 1996). Therefore, the quadrupole is generally operated at unit-mass resolution. Recently, it has been demonstrated that by improving the quadrupole design, the stability of the RF power supply and the temperature control enhanced mass resolution (FWHM of down to 0.2 instead of usual 0.7) on a quadrupole mass analyzer can be achieved without dramatic losses in signal intensity (Yang et al., 2002). This feature has not found wide application. Thus, in full-spectrum mode, the quadrupole mass analyzer provides at least unit-mass resolution and nominal monoisotopic mass determination and can be operated with great ease and versatility. It provides fast spectrum acquisition at limited costs, clearly justifying its popularity.

Apart from full-spectrum mode, featuring ramping of DC and RF at a fixed ratio, the quadrupole mass analyzer can be operated in three additional modes. It can be applied in selected-ion monitoring (SIM) mode, dwelling on selected *m*/*z* values for 10–200 ms, and capable of rapidly switching (within ≤5 ms) between different *m*/*z* values. In SIM mode, significantly improved S/N can be achieved, making the SIM mode of a quadrupole ideal for routine targeted quantitative analysis. Another important mode of operation is the RF-only mode. In this mode, the quadrupole can be used as an ion transport and focusing device. As such, RF-only quadrupoles have been used in vacuum interfaces of API-MS systems and as collision cells and/or ion-transport devices in MS–MS instruments (Section 1.4.2). Finally, it has been demonstrated that a quadrupole mass analyzer can be applied as linear ion trap. In this mode of operation, the quadrupole provides similar features as a conventional 3D ion trap (Section 1.4.3) (Hager, 2002; Schwartz et al., 2002; Douglas et al., 2005).

1.3.3 Ion-Trap Mass Analyzer

The introduction of the 3D ion trap has been an important development in quadrupole technology (March, 1997; Jonscher & Yates, 1997). Ion-trap MS is based on the same principles of quadrupole technology developed by Paul (Paul & Steinwedel, 1953; Paul & Raether, 1955; Paul, 1990). Two major advances, made by the group of Stafford, revived the interest in ion-trap technology: the development of the *m*/*z*-selective instability mode of operation and the use of He as damping gas (Stafford et al., 1984; Louris et al., 1987; Stafford, 2002). Additional improvements followed soon after.

A 3D quadrupole ion trap consists of a ring electrode with a hyperbolic geometry to which an RF voltage is applied and two end-cap electrodes resembling inverted hyperbolic saucers (Figure 1.21). The ring electrode is positioned symmetrically in between the two end-cap electrodes. The electrodes are electrically isolated by means of nonconducting

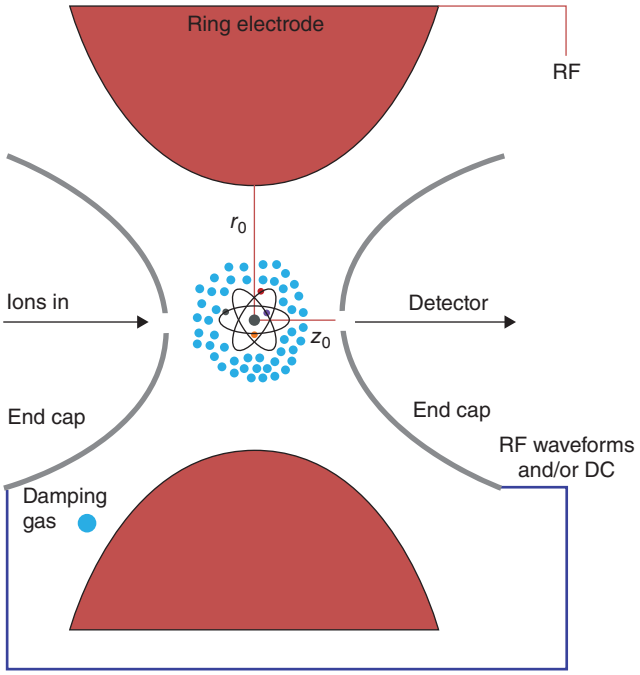

FIGURE 1.21 Schematic diagram of an ion-trap mass analyzer.

spacers. The internal volume of a typical 3D ion trap is ≈1 cm^3. Both end-cap electrodes contain holes: one of them for the introduction of ions from an external ion source into the trap and the other one for ion ejection from the trap toward an external EM. A He bath gas (≈0.2 Pa; ≈0.002 mbar) is used to stabilize the ion trajectories in the trap by acting as energy sink to help keep the ions in tight small orbits in the center of the trap. The overall effect is a dramatic improvement in resolution and reproducibility.

The basic mass analysis process consists of two steps, performed consecutively in time. First, a pulse of ions is injected and stored in the trap by the application of an appropriate low-RF voltage to the ring electrode. As a result, all ions above a low-m/z cutoff are stored in the trap. The ion injection pulse has a variable duration, depending on the ion current, because too high a number of ions in the ion trap, that is, in excess of $\approx 10^5$ ions, adversely influences mass resolution and accuracy due to space-charge effects. Automatic gain or ion charge control (software controlled) has been developed, which dynamically adjusts the duration of the ion injection pulse from the external ion source (March, 1997). Filling the ion trap by means of the ion injection pulse results in an accumulation of ions, which in practice leads to an enhanced full-spectrum sensitivity when compared to the linear quadrupole mass analyzer.

Once the ions are trapped, an m/z-selective instability scan is performed. The (fundamental) RF voltage applied to the ring electrode is ramped to consecutively eject from the trap and toward the external detector first the low-m/z ions, and likewise all other ions in order of increasing m/z values (resonant ion ejection at $q = 0.908$) (Jonscher & Yates, 1997). The resonant ion ejection may be supported by additional waveforms applied to the end-cap electrodes. Alternatively, a (resonant) supplementary RF can be applied to the end-cap electrodes to cause the ions to gain energy: the amplitude of the ion trajectory expands and the ions approach the end-cap electrodes until they are ejected from the trap at values of q lower than 0.908. The q value, where ions are ejected under these conditions, depends on the frequency of the supplementary RF potential. This operational mode is needed to achieve the ejection of ions with high-m/z values ($m/z \gtrsim 600$), but it is also important in the selection of precursor ions in an MS^n experiment (Section 1.4.3).

The achievable resolution depends on the scan speed. Ion ejection and subsequent detection can be achieved with unit-mass resolution or at enhanced resolution by slowing down the scan rate of the RF voltage on the ring electrode. In this respect, improvements have been made over time. Older ion traps provide peak widths (FWHM) of 0.2 at a scan speed of ≈300 $m/z\,s^{-1}$, unit-mass resolution (FWHM ≈ 0.7) at 5500 $m/z\,s^{-1}$, and degraded resolution (FWHM of 3.0 at 55,000 $m/z\,s^{-1}$), whereas more recently introduced systems provide better resolution at higher scan speeds, for example, FWHM of 0.1 at 4600 $m/z\,s^{-1}$ and of 0.58 at 52,000 $m/z\,s^{-1}$. An FWHM of 0.1 enables almost baseline resolution for a quadruply-charged ion (e.g., $[M+4H]^{4+}$) of a peptide.

More recently, 2D or linear ion traps (LITs) have been introduced as an alternative to 3D ion traps (Hager, 2002; Schwartz et al., 2002; Douglas et al., 2005). Similar to a quadrupole, the ions are confined radially by a 2D RF field. Ion ejection can be done either radially, as is done in a stand-alone LIT, or axially, as is done in quadrupole–linear ion-trap (Q–LIT) hybrid instruments (Section 1.4.4) and in LITs applied in orbitrap or FT-ICR hybrid instruments (Section 1.4.6). Because an LIT is less prone to space-charging effects, a higher number of ions can be accumulated and enhanced sensitivity (up to 60-fold) can be achieved. LITs are extensively used in hybrid MS–MS technology, but stand-alone versions of LITs have been introduced as well, thus competing against the 3D ion traps.

1.3.4 Time-of-Flight Mass Analyzer

A basic TOF mass spectrometer consists of a pulsed ion source, an accelerating grid, a field-free flight tube, and a detector (Guilhaus et al., 2000; Lacorte & Fernandez-Alba, 2006). In TOF-MS, owing to the applied accelerating potential, all ions begin their flight toward the detector at the same time and with the same initial kinetic energy. Because of their higher velocity, low-m/z ions will arrive to the detector before higher-m/z ions. Therefore, the time it takes an ion to reach the detector is related to its m/z (Figure 1.22).

Thus, if a particular ion with a given m/z is accelerated by a potential V, the flight time t to reach the detector placed at a distance d can be calculated from Eq. 1.41.

$$t = d\sqrt{\frac{m}{2zeV}} \tag{1.41}$$

Pulsing of the ion introduction into the flight tube is required to avoid the simultaneous arrival of ions of different

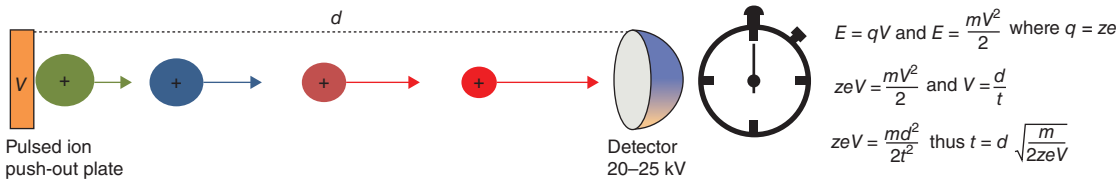

FIGURE 1.22 Principle of time-of-flight mass spectrometry.

m/*z* to the detector. The introduction of MALDI as a powerful ionization technique in the MS analysis of large biomolecules led to a revaluation of TOF-MS (Karas & Hillenkamp, 1988; Karas, 1996). The pulse rate of the laser used in MALDI (typically <1 kHz) makes the use of a TOF-MS instrument highly attractive. In addition, the *m*/*z* range of a TOF-MS instrument is unlimited in principle. Much higher pulse frequencies are applied (20–50 kHz) in combinations of TOF-MS with continuous ion sources (e.g., in ESI). As the data system cannot process such a high acquisition rate, mass spectra from multiple ionization events or pulses are accumulated. This leads to enhanced spectrum quality by averaging random noise. Acquisition rates as high as 100 spectra s^{-1} have been reported for LC–MS applications, although lower acquisition rates (1–10 spectra s^{-1}) are used more frequently.

The initial ion kinetic energy spread of the ions arising from their generation in the ion source is the most important limiting factor determining the achievable resolution in TOF-MS. With the progress in fast electronics, the speed of detection and acquisition electronics is no longer a limiting factor nowadays. In MALDI-TOF-MS, delayed extraction has been applied to reduce the ion kinetic energy spread of the ions (Vestal et al., 1995), whereas in ESI-TOF-MS, orthogonal acceleration has been a powerful tool (Guilhaus et al., 2000). Even more important in reducing the deteriorating effect of the ion kinetic energy spread on the resolution is the use of a reflectron (Doroshenko & Cotter, 1989; Guilhaus et al., 2000). A reflectron consists of a series of equally spaced grid or ring electrodes connected to a resistive network (Figure 1.23). It creates a homogeneous or curved retarding field that acts like an ion mirror. If two ions with equal *m*/*z* but slightly different kinetic energy enter the reflectron, the ion with the higher kinetic energy penetrates deeper into the field and thus has a slightly longer flight path than the ion with the somewhat lower kinetic energy. In effect, the two ions reach the detector more synchronously. It is important to keep in mind that while the arrival of the ions to the detector is nearly synchronous, the kinetic energy of the ions is the same as it was before they entered. Added value of the reflectron is that it effectively approximately doubles the flight distance *d*.

Significant progress has been made in TOF instrumentation, mainly directed at enhancing resolution and improving sensitivity and dynamic range. With a reflectron TOF in combination with orthogonal acceleration (with an ESI source), a mass resolution in excess of 15,000 (FWHM) can be readily achieved, enabling accurate-mass determination (<3 ppm) (Xie et al., 2012). Currently, commercial TOF-MS systems are available with a mass resolution in excess of 70,000 (FWHM).

1.3.5 Orbitrap Mass Analyzer

An orbitrap consists of three electrodes: a spindle-like central electrode (A) and two cup-shaped outer electrodes (B) facing each other (Figure 1.24). Ions are injected tangentially into the electric field present in the volume between the central and the outer electrodes. A radial electric field resulting from the voltage applied between the central and outer electrodes leads to circular movements of the ions around the central electrode. The electrostatic attraction of the ions to the inner electrode is balanced by their centrifugal forces. In addition, the axial electric field caused by the shape of the electrodes initiates harmonic axial oscillations of the ions along the central electrode. Thus, ions circle around the central electrode in rings, as they move back and forth along the axis of the central electrode. This oscillation is proportional to $(m/z)^{-1/2}$ and, furthermore, independent of the ion velocity. By sensing the ion oscillation frequency in a similar manner as done in FT-ICR-MS, the orbitrap can be used as a mass analyzer. The image current resulting from these axial oscillations is measured using the outer electrodes. The digitized time-domain image current is Fourier-transformed into the frequency domain. The *m*/*z* value of an ion is related to the frequency ω of the axial oscillations as $\omega = (k \times z/m)^{1/2}$. Thus, the frequency-domain spectrum can be converted into a mass spectrum (Hu et al., 2005; Makarov et al., 2006; Zubarev & Makarov, 2013).

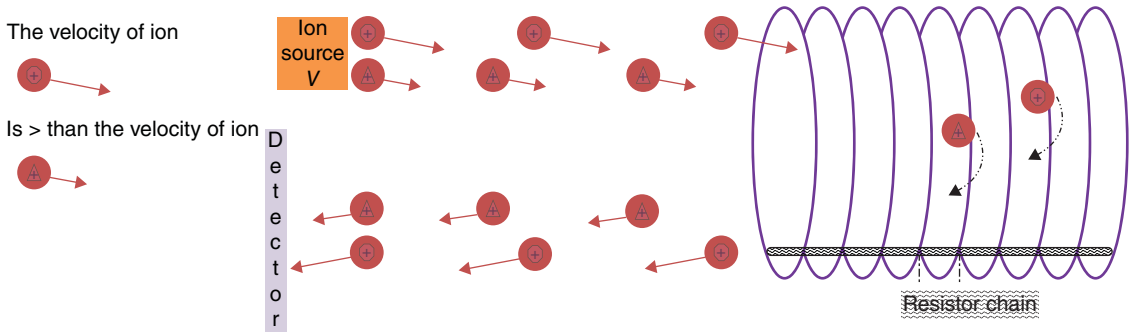

FIGURE 1.23 Operation principle of kinetic-energy focusing in a reflectron time-of-flight mass spectrometer.

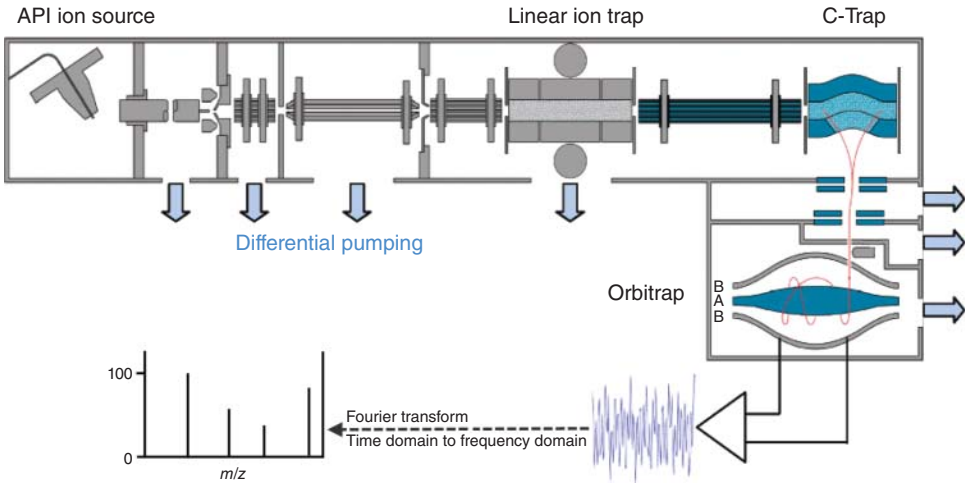

FIGURE 1.24 Schematic diagram on a linear-ion-trap–orbitrap hybrid instrument. (Source: Reprinted and adapted from (Makarov et al., 2006) with permission, ©2006, American Chemical Society.)

An important practical aspect is the adequate delivery of ions into the orbitrap. To this end, a curved high-pressure RF-only quadrupole, the so-called C-trap, is applied in combination with two flat electrodes. The C-trap is filled with N_2 bath gas ($\approx 10^{-2}$ Pa; $\approx$1 mbar) for collisional damping. After filling the C-trap with ions, the ion package is compressed by applying 200 V to the flat electrodes. Rapidly ramping the RF voltage at the C-trap rods (within 200 ns) in combination with high voltages on the flat electrodes accelerates a concise ion package via a dual electrostatic deflector and through three stages of differential pumping into the orbitrap (2×10^{-5} Pa; 2×10^{-10} mbar) (Makarov et al., 2006). A high-field compact orbitrap was introduced in 2011, providing enhanced performance characteristics (Michalski et al., 2011; Zubarev & Makarov, 2013).

An orbitrap mass spectrometer allows ultra-high-resolution measurements (in excess of 10^5, FWHM). The achievable mass resolution depends on the spectrum acquisition time. The initially introduced orbitrap systems needed $\approx$1.6 s to acquire a mass spectrum with a resolution of 100,000 (at m/z 200, FWHM). The more recently introduced high-field orbitrap instruments provide mass spectra with a resolution of 17,500 (FWHM) with 64 ms and a resolution of 140,000 with 512 ms spectrum acquisition time. At a resolution in excess of 100,000, a mass accuracy within 1 ppm can be achieved. Although a stand-alone version of the orbitrap has been produced (Geiger et al., 2010), far better analytical capabilities can be achieved with hybrid systems (Section 1.4.6).

1.3.6 Other Mass Analyzers

In addition to the four types of mass analyzers just discussed, brief attention should be paid to two other types of mass analyzers: the sector instrument and the FT-ICR-MS instrument. Perhaps any discussion on mass analyzers should start with sector instruments because historically they are at the basis of all MS developments. However, since sector instrument are no longer used in combination with ESI and APCI, their principles and operation are not very relevant to the topic of this book.

A basic example of a sector instrument applies only a magnetic sector. Ions with mass m and z elementary charges e are accelerated with a voltage V into a magnetic field B, where they follow a path with a radius of curvature r. From the fundamental equation $m/z = B^2r^2e/2V$, describing the relationship between m/z and the experimental parameters, one can derive equations to describe how the separation of ions with different m/z can be achieved in three different ways. By variation of the radius of curvature, ions with different m/z are separated in space; an array of detectors is needed to detect the ions and acquire the mass spectrum. In a more practical approach, ions of different m/z can be detected one after another by means of a single-point detector (e.g., an EM) at a fixed position by variation of either B or V (de Hoffmann & Stroobant, 2007). The performance of the sector instrument in terms of mass resolution can be greatly improved by combining the magnetic sector with an electrostatic analyzer, resulting in a double-focusing instrument, which provides HRAM determination. Several geometries of double-focusing instruments have been described. Since the mid-1990s, the sector instrument has been replaced as the instrument of choice for HRMS and HRAM-MS by alternatives that are easier to operate and less expensive, for example, instruments based on time-of-flight or orbitrap technology.

In an FT-ICR-MS instrument, the ions are trapped in a strong magnetic field B (up to 15 T). An ICR cell consists of

two opposite trapping plates, two opposite excitation plates, and two opposite receiver plates. Both cylindrical and cubic ICR cells have been produced. In the magnetic field, ions with m/z describe cyclotron motions with a radius r perpendicular to the magnetic field lines. The ions moving in this way induce an image current at the receiver plate with a cyclotron frequency of $\omega_c = 2\pi f = v/r = Bez/m$, where f is the frequency in hertz. The cyclotron frequency is thus inversely proportional to the m/z value. In a typical FT-ICR-MS experiment, the ions, trapped in their cyclotron motion in the cell, are excited by means of an RF pulse on the excitation plates. This increases the radius of the cyclotron motion and, more importantly, the ions with the same m/z values start to move in phase. This coherent movement of the ions generates an image current at the receiver plates, which decays in time because of disturbance of the coherency of the ion movement in time. The time-domain signal from the receiver plates contains the frequency information of all the ions present in the cell. By Fourier transformation, the time-domain signal can be transformed into a frequency-domain signal and subsequently converted into a mass spectrum (Marshall et al., 1998; Scigelova et al., 2011). Similar to the orbitrap mass spectrometer, the resolution in FT-ICR-MS increases with measurement time; longer measurement times require extreme high vacuum in the ICR cell ($\approx 10^{-4}$ Pa; $\approx 10^{-6}$ mbar). FT-ICR-MS instruments can provide (m/z-dependent) ultra-high resolution, typically in excess of 10^5 (FWHM). A high-resolution spectrum can be achieved in a shorter time in instruments with a higher magnetic field strength. Commercial FT-ICR-MS systems are available that provide a resolution of ≈650,000 (at m/z 400, FWHM) with 1 spectrum s^{-1}.

1.4 TANDEM MASS SPECTROMETRY

1.4.1 Introduction

MS–MS involves the combination of two mass analyzers in series with a reaction chamber in between, enabling first-stage mass analysis in MS_1 and second-stage mass analysis in MS_2. A basic MS–MS experiment (product-ion analysis) consists of three steps. In the first step, a precursor ion with a particular m/z is selected from the population of ions generated in the ion source. In the second step, the precursor ion is fragmented, in most cases using CID. In the third step, the product ions formed in the CID of the precursor ion are mass analyzed.

The two mass analyzers can be combined either in space or in time (Johnson et al., 1990). There are tandem-in-space mass spectrometers, where the two mass analyzers are of the same type, for example, a TQ instrument, and tandem-in-space mass spectrometers, where the two mass analyzers are different, the so-called hybrid instruments, for example, a quadrupole–time-of-flight (Q–TOF) hybrid instrument with a quadrupole mass analyzer for MS_1 and a time-of-flight mass analyzer for MS_2. In tandem-in-space instruments, the three steps of the MS–MS process (precursor-ion selection, CID, mass analysis of product ions) are performed in spatially separated devices. The ion-trap instrument is an example of a tandem-in-time mass spectrometer, where the three steps are performed one after another in the same device. The reaction chamber in the tandem-in-space instrument is a collision cell, whereas in the tandem-in-time instrument CID is performed in the same region as the mass analysis, although dual-cell ion-trap instrument have been developed as well (Olsen et al., 2009).

In an MS–MS instrument, the m/z values of ions are measured before and after the collision cell. In practice, as most MS–MS instruments have only one ion detector, two separate experiments have to be performed, one involving the acquisition of the MS spectrum (without collision energy and collision gas) and another involving the acquisition of the product-ion MS–MS spectrum (with collision energy and gas). In most cases, the reaction in the collision cell leads to a change in m/z. For positive ions, the precursor or parent ion m_p^+ is converted into the product or daughter ion m_d^+ by the loss of a neutral fragment m_n. Thus, fragmentation of the precursor ion occurs. Although the neutral fragment m_n itself is not detected, its mass can be deduced from the m/z difference of m_p^+ and m_d^+. In principle, the fragmentation observed for a particular ionized molecule is compound specific. Even the protonated or deprotonated molecules of the same compound often show different fragmentation behavior.

1.4.1.1 Ion Dissociation Techniques In most analytical applications of MS–MS, the fragmentation reactions are induced by ion collisions with a neutral target gas, that is, helium (He), nitrogen (N_2), or argon (Ar), which is present in the collision cell at a pressure of typically 10^{-2}–0.1 Pa (10^{-4}–10^{-3} mbar). In the region between MS_1 and the collision cell (tandem-in-space instrument), the precursor ion selected in MS_1 is accelerated by a potential difference (V), which is generally called the collision energy. As a result, the ions have increased translation energy. Part of this translation energy is converted into vibrational energy of the ions upon the collisions. Thus, the ions are collisionally activated, which means that they are at higher vibrational states (larger amplitudes in the stretching and bending vibrational modes of the molecule). These excited ions can then fragment in a compound-specific way. Depending on the available internal energy and the structural features of the precursor ion, several competitive unimolecular fragmentation pathways may be available, thus leading to different fragment ions. At low collision energy, only the weakest bonds in the ion can be cleaved. By increasing the collision energy, an increasing number of pathways may be available. At very high collision energy, extensive C—C bond cleavages occur, resulting in uncontrolled fragmentation. In addition, scattering of ions

reduces the transmission of ions under these conditions. The process in the collision cell is generally called CID. One should be aware of the fact that CID is a two-step process: the actual collision is an ultrafast event ($\approx 10^{-15}$ s, i.e., the Franck–Condon approximation applies), followed by the unimolecular decomposition of the excited ions in competing reaction pathways, happening 10^{-10}–10^{-5} s after ion excitation. In between the two steps of the CID process, energy redistribution within the ion may take place.

CID can be performed in two different energy regimes (Sleno & Volmer, 2004). In most instruments, low-energy CID is performed with (laboratory) collision energies between 10 and 100 eV. One should discriminate between collision-cell CID and ion-trap CID. In collision-cell CID, applicable to TQ and Q–TOF instruments, multiple ion collisions are performed with N_2 or Ar. Typical residence time of the ions in a collision cell is 10–20 μs. In ion-trap CID, collisions are performed with a smaller target (He instead of Ar) and ion excitation is achieved by means of an *m*/*z*-dependent RF waveform pulse; the interaction time is in the ms range in ion-trap CID (Jonscher & Yates, 1997). At the first stage of fragmentation, ion-trap CID is generally softer than collision-cell CID, that is, less fragment ions are formed. In sector and TOF–TOF instruments, high-energy CID can be performed, involving single keV collisions with He as target gas. In high-energy collisions, more informative but often more complex product-ion MS–MS spectra may be obtained because a wider range of fragmentation pathways is opened. The mass spectral data discussed in Chapter 4 were acquired using low-energy CID in either collision-cell CID or ion-trap CID. In the discussion on fragmentation rules in Chapter 3, some data from high-energy CID are included as well.

It should be mentioned that fragmentation can also be induced in a process called in-source or up-front CID. By increasing the voltage applied to the ion-sampling orifice (or the voltage difference between orifice and skimmer), the ions experience more energetic collisions with neutrals in the high-pressure region. The resulting gain in internal energy in the ion can result in fragment ions, which can be mass analyzed. Because all ions present in the source can be fragmented in this way, the method only leads to useful, interpretable data if either pure compounds or well-separated analytes in not-too-complex matrices are analyzed. In-source CID initially found application in general unknown screening in toxicology (Marquet & Lachâtre, 1999; Marquet et al., 2000; Weinmann et al., 1999), but has since been replaced by MS–MS-based procedures (Section 5.5).

Next to CID, several other ion activation methods have been used, mostly in specific applications and/or instruments (Sleno & Volmer, 2004; Laskin & Futrell, 2005). As performing CID in the ultra-high-vacuum ICR cell of an FT-ICR-MS may compromise its performance, especially in terms of resolution and sensitivity, several alternative methods have been developed to induce fragmentation in FT-ICR-MS instruments, for example, infrared multiphoton photodissociation (IRMPD), sustained off-resonance irradiation (SORI), and black-body infrared radiative dissociation (BIRD) (Sleno & Volmer, 2004; Laskin & Futrell, 2005). Other ion-activation methods such as surface-induced dissociation and laser photodissociation have been mostly used by a limited number of research groups. Currently, the most widely applied alternative ion-activation methods are electron-capture dissociation (ECD) and electron-transfer dissociation (ETD) (Kim & Pandey, 2012; Zhurov et al., 2013), which are especially important in the fragmentation of multiply-charged ions of peptide, proteins, glycopeptides, and phosphorylated peptides. ECD can be applied in FT-ICR-MS, whereas ETD can be implemented on other types of mass analyzers such as ion-trap, Q–TOF, and orbitrap instruments.

1.4.1.2 Product-Ion Analysis The most straightforward operational mode of the tandem mass spectrometer is the product-ion analysis mode, where the precursor ion m_p^+ is selected in MS_1, while the product (or daughter) ions m_d^+ are mass analyzed in MS_2 and then detected (Yost & Enke, 1978; Busch et al., 1988). The resulting mass spectrum, called the product-ion mass spectrum, provides structural information on the precursor ion and thus on the compound analyzed. The selection of precursor ions in most MS–MS instruments is done either with unit-mass resolution or with somewhat degraded resolution to transmit the complete isotope pattern of the precursor ion. In the latter case, the presence of particular elements in the precursor ion, for example, Cl, Br, and/or S, can be followed in the product ions.

The interpretation of the product-ion mass spectra is the topic of this book, and especially using protonated molecules $[M+H]^+$ or deprotonated molecules $[M-H]^-$ as precursor ions. In order to learn about the fragmentation reactions and to derive general fragmentation rules (Chapter 3), the fragmentation in MS–MS of a large number of compounds from a wide variety of compound classes (mainly drugs and pesticides) was studied. These compounds were analyzed either in positive-ion mode as $[M+H]^+$ or in negative-ion mode as $[M-H]^-$, or in some cases as both. If the fragmentation pathways of a number of compounds from the same structural class are compared, often both class-specific (or group-specific) fragmentation and compound-specific fragmentation can be recognized. The class- or group-specific fragmentation is observed for all members of that particular group or class and may involve the observation of particular product ions and/or of particular neutral losses. Ample examples of such features are discussed in Chapter 4. Compound-specific fragmentation is only observed for a

particular compound, and thus involves structural features by which that particular compound differs from other members of the group or class.

1.4.1.3 Development of MS–MS Instruments Historically, the starting point of MS–MS was in the 1940s with the observation and subsequent explanation of metastable ions in magnetic sector instruments (Hipple et al., 1946; Busch et al., 1988; de Hoffmann & Stroobant, 2007). Metastable ions are ions with sufficient internal energy to fragment, but which survive long enough to be extracted from the ion source before they fragment. When fragmentation occurs, they do so in the mass analyzer region before reaching the detector. The charged fragments of metastable ions that dissociate in the reaction region of the instrument may be detected. It was discovered that the abundance of the metastable ions can be increased by energetic collisions of the ions with a neutral bath gas in a collision cell. This observation led to the development of MS–MS instruments, initially based on sector instruments, where high-energy CID (keV collisions) is applied (Section 3.4).

The extensive use of MS–MS in analytical applications can be attributed to the introduction by Yost and Enke of the so-called triple-quadrupole instruments in 1978, featuring two analytical quadrupole mass analyzers and a collision cell in an RF-only quadrupole, which works as an ion guide that does not provide *m*/*z* separation (Section 1.3.2) (Yost & Enke, 1978). As in many modern instruments, the RF-only quadrupole collision cell has been replaced by other types of RF-only multipole collision cells, for example, hexapoles, octapoles, ion tunnels, and travelling-wave stacked-ring ion tunnels; nowadays, the term tandem quadrupole (TQ) is preferred over triple-quadrupole.

Subsequently, the possibility of multistage MS–MS (MS^n) in ion-trap instruments was introduced by the group of Stafford in 1987 (Louris et al., 1987). With the increased analytical application of MS–MS instruments, which in part is the result of the introduction of new soft ionization techniques (e.g., FAB, TSI, and ESI), several hybrid MS–MS instruments were introduced, also providing additional analytically interesting features, such as HRAM determination. Thus, Q–TOF (Morris et al., 1996), hybrid Q–LIT instruments (Hager, 2002), hybrid LIT–orbitrap instruments (Hu et al., 2005; Makarov et al., 2006), and hybrid quadrupole–orbitrap instruments (Michalski et al., 2011) were introduced. These instruments are more cost effective and easier to operate than sector instruments.

MS–MS has become an indispensable tool in fundamental studies on ion generation, ion–molecule reactions, unimolecular fragmentation reactions, and the identity of ions. It plays an important role both in qualitative analytical applications of MS involving the online coupling of MS to GC or LC, for example, identification of drug metabolites (Section 5.7.1), and in quantitative analytical applications based on selected-reaction monitoring (Section 1.5.2).

1.4.2 Tandem Quadrupole Instruments

The most widely used MS–MS configuration is the TQ instrument. Initially, triple-quadrupole instruments were used where mass analysis is performed in the first and third quadrupoles and CID in the second quadrupole (collision cell), that is, in a $Q–q_{coll}–Q$ configuration (Yost & Enke, 1978). The gas-filled collision cell, operated in RF-only mode to transmit all ions without mass analysis, provides refocusing of ions scattered by the collisions and thereby somewhat reduces the transmission losses. Alternative RF-only collision cells have been developed in order to further reduce such transmission losses (e.g., RF-only hexapoles or octapoles). In a linear-acceleration high-pressure collision cell (LINAC), an axial voltage and tilted rods are used to reduce the residence time of the ions in the collision cell and to reduce crosstalk (Mansoori et al., 1998). A stacked-ring collision cell, featuring an axial travelling-wave or transient DC voltage, has been reported to reduce the transit times in the collision cell as well (Giles et al., 2004). Compared to the sector instruments used for MS–MS prior to 1978, the TQ instrument yielded significantly better product-ion resolution and greatly facilitated the acquisition of product-ion mass spectra.

The extent of fragmentation in collision-cell CID, as applied in TQ (and also in Q–TOF instruments), is determined by the gas pressure in the collision cell, the *m*/*z* of the precursor ion, and can be readily controlled by the collision energy, that is, the potential applied to the ions upon entering the collision cell. Optimization of the relevant instrumental parameters is needed for a particular application. For structure elucidation, it can be useful to acquire product-ion mass spectra at several collision energies. A plot of the relative abundance of the various product ions observed as a function of the collision energy is referred to as a breakdown curve; it plays an important role in optimizing collision energy conditions for optimizing SRM transitions. The optimum collision energy for a particular SRM transition, where one aims at preferably one intense product ion, is often not the optimum collision energy for structure elucidation, where one aims at a range of structure-informative fragment ions. One should be aware that setting a particular value for the collision energy in a particular instrument does not reflect the actual internal energy gained by the precursor ion. Setting the same collision energy for the fragmentation of the precursor ion of a particular compound in instruments from different manufacturers may yield widely different product-ion mass spectra, especially in terms of relative abundance of the product

ions. For doubly-charged peptide ions, that is, $[M+2H]^{2+}$, a linear relationship is observed between the optimum collision energy and its *m*/*z*-value, where the slope of the curve is instrument-dependent (Haller et al., 1996; Holman et al., 2012). Some instruments allow ramping the collision energy during the acquisition of the product-ion mass spectrum: higher collision energies are applied when scanning for low *m*/*z* and lower collision energies for the high *m*/*z*.

In the past, TQ instruments were frequently used in confirmation of identity and structure elucidation of unknowns. This role has diminished, on the one hand, due to its limitations in terms of resolution, mass accuracy, and full-spectrum sensitivity and, on the other hand, due to the introduction of other, more powerful alternatives. However, at present, the TQ instrument is still first choice in routine-targeted quantitative analysis where it is operated in SRM mode (Section 1.5.2) (van Dongen & Niessen, 2012).

1.4.3 Ion-Trap Instruments

In a typical ion-trap MS^2 experiment, one starts with a population of ions, generated in the ion source (e.g., by ESI) from which the precursor ion is selected, excited, and fragmented. This results in a new population of (product or daughter) ions. The latter population either can be scanned out to be detected or can serve in a new series of subsequent steps of the process: selection of a product ion as precursor ion in a new MS^n experiment, which is to be excited and fragmented, and leads to a new population of (granddaughter) ions. Note that the term MS–MS is applied to denote collision-cell CID, as achieved in TQ and Q–TOF instruments, whereas MS^n is applied in the case of ion-trap CID in ion-trap instruments.

The selection of a precursor ion from a population of ions can be done in several ways. A combination of DC and RF potentials can be applied, which drive the precursor ion to the apex of the stability diagram (Figure 1.20), where the motion of the ions with *m*/*z* values other than the *m*/*z* value to be selected becomes unstable. Alternatively, the amplitude of the fundamental RF voltage can be scanned in a reverse-then-forward manner, while applying a resonant supplementary voltage. In this way, ions with *m*/*z* values higher than the *m*/*z* of the precursor ion are ejected first, followed by ejection of ions with smaller *m*/*z* values.

In the next step of the process, the fundamental RF voltage applied to the ring electrode is lowered and a resonant RF potential is applied to the end-cap electrodes with such an amplitude that ion trajectory is enlarged but not to such an extent as to eject the ion out of the trap. This ion excitation results in more energetic collisions with the He bath gas and may lead to CID of the precursor ions. With a sufficiently high number of collisions, the ions gain sufficient internal energy to cause fragmentation of the precursor ions into product ions, generally with relatively high efficiency. Depending on the fundamental RF voltage, product ions can be trapped. Often, product ions with *m*/*z* values below 25–33% of the *m*/*z* of the precursor ion cannot be trapped and are ejected and lost without detection. This may result in limitations if CID of the precursor ion forms predominantly low-*m*/*z* product ions, as is the case for tramadol (Hakala et al., 2006). Different from collision-cell CID, the voltage (amplitude) of the *m*/*z* selective RF potential applied as collision energy results in an on/off situation. When the voltage is too low, no fragmentation is observed. If by increasing the voltage the onset of fragmentation is reached, further increase in the voltage does not change the appearance of the product-ion spectrum anymore.

Either the population of product or daughter ions produced by CID can be ejected and detected to obtain the MS^2 spectrum, or one of the product ions may be selected to serve as precursor ion in subsequent sequence of excitation and fragmentation. The resulting population of granddaughter ions (secondary product ions) can be scanned out and detected to obtain the MS^3 spectrum or again one of the product ions may be selected to serve as precursor ion in subsequent sequence of excitation and fragmentation. Most ion-trap MS^n instruments allow for $n = 10$, although due to sensitivity limitations in most cases a maximum of only six stages can be achieved. A nice example of six stages of ion-trap MS^n has been demonstrated in the negative-ion ESI-MS analysis of glycosylated saponins (Wolfender et al., 1998). Step-wise fragmentation involving subsequent losses of sugar monomers in subsequent MS^n steps is achieved. Step-wise fragmentation in MS^n has been obtained for other compound classes as well, for example, chlorpromazine (Section 4.2.1), citalopram (Section 4.2.3.3), simvastatin (Section 4.4.3.2), dicloxacillin (Section 4.8.3.1), and chlorotriazines (Section 4.11.1.1). The ion-trap CID provides fragmentation with effectively lower energy involved. As such, it facilitates the acquisition of a wealth of structural information, for example, by step-wise fragmentation and the generation of fragmentation trees (Kind & Fiehn, 2010; van der Hooft et al., 2011). A fragmentation tree is generated by further fragmenting selected fragment ions of a particular stage of MS^n into a next stage, that is, MS^{n+1}. Another interesting feature of ion-trap CID is the ability to fragment sodiated molecules $[M+Na]^+$, which is often not possible in collision-cell CID. This difference may be due to the longer residence time of ions in an ion-trap (ms) compared to their residence time in an RF-only collision cell (10–20 μs). Fragmentation of $[M+Na]^+$ may result in different information, compared to the fragmentation of $[M+H]^+$. This has been nicely demonstrated in the MS analysis of the iridoid glycoside globularin (Section 3.8) (Es-Safi et al., 2007) and by the ability to obtain linkage information in the fragmentation of $[M+Na]^+$ of disaccharides (Asam & Glish, 1997). Ion-trap MS^n of $[M+Na]^+$ is also important in the structure elucidation of compound classes such as avermectins (Section 4.10.1.2) and polyether ionophores (Section 4.10.2.3).

As discussed earlier (Section 1.3.3), 2D or linear ion traps (LITs) have been introduced as an alternative to 3D ion traps. In principle, they provide the same features in MS^n but with improved full-spectrum sensitivity (Douglas et al., 2005). LIT-MS^n systems as stand-alone devices have been widely used in combination with LC–MS in a wide range of application areas. In addition, LITs have been employed as part of hybrid systems, such as the second stage of mass analysis in a Q–LIT hybrid system (Hager, 2002), as well as a first-stage mass analyzer (eventually also providing CID) in combination with an orbitrap and an FT-ICR. In the latter type of hybrid instruments, the ion-trap MS^n features in MS_1 are combined with HRMS and accurate-mass determination in MS_2 (Hu et al., 2005; Makarov et al., 2006; Zubarev & Makarov, 2013) (Section 1.4.6). Another interesting development is the introduction of dual-pressure LIT instruments (Olsen et al., 2009). The first high-pressure (0.5 Pa, 5×10^{-3} mbar) ion trap provides storage of ions, selection of precursor ions, their excitation, and fragmentation. Threefold reduction of ion fragmentation time (10 ms) can be achieved. The fragment ions are then transferred to the second reduced-pressure (0.035 Pa; 3.5×10^{-4} mbar) ion trap to enable very high scan speeds.

1.4.4 Quadrupole–Linear Ion-Trap Hybrid Instruments

The hybrid Q–LIT instrument, introduced in 2002, has the general layout of a TQ instrument, but MS_2 can be operated (under software control) as either a normal linear quadrupole or a linear ion trap (Hager, 2002). For full-spectrum product-ion spectrum acquisition, the Q–LIT instrument shows several advantages. Precursor-ion fragmentation can be performed using collision-cell CID (in the LINAC, Section 1.4.2). The resulting product ions are accumulated in the LIT, providing enhanced product-ion (EPI) spectra with improved full-spectrum sensitivity. If necessary, additional MS^3 experiments can be done by selection of one of the product ions in the LIT as a precursor ion for subsequent excitation, fragmentation (ion-trap CID), and detection. Since its introduction in 2002, hardware, electronics, and software control of the Q–LIT instruments have been further optimized to provide a wide variety of MS–MS operating modes and to allow very rapid switching between various MS and MS–MS experiments (Hopfgartner et al., 2004). Because MS_2 can be rapidly switched between linear quadrupole and LIT mode of operation, combination of SRM and full-spectrum product-ion analysis can be achieved (Section 1.5.4).

1.4.5 Quadrupole–Time-of-Flight Hybrid Instruments

Similar to the Q–LIT hybrid, discussed in Section 1.4.4, the Q–TOF hybrid mass spectrometer can be considered as a modified TQ instrument, where the MS_2 quadrupole has been replaced by an orthogonal-acceleration reflectron-TOF mass analyzer (Morris et al., 1996). The first commercially available Q–TOF instrument was especially developed to facilitate peptide sequencing analysis, but the instrument found much wider application, especially in small-molecule structure elucidation studies. Thus, in MS mode, the quadrupole (MS_1) is operated in RF-only mode and the RF-only collision cell with low collision energy, whereas in MS–MS mode the quadrupole MS_1 performs the selection of the precursor ion with unit-mass resolution, and fragmentation of the precursor ion is achieved by collision cell CID. In both modes, the ions are orthogonally accelerated into the flight tube and HRAM analysis is performed in the reflectron-TOF analyzer (MS_2). Q–TOF instruments are now available from several instrument manufacturers (Xie et al., 2012). They are widely used in structure elucidation, metabolite identification, and sequencing of peptides. Because collision-cell CID is applied, the fragmentation characteristics are the same as in TQs. In structure elucidation, a significant advantage of Q–TOF is the ability to perform accurate-mass determination (<3 ppm) for both precursor and product ions. Principles and applications of Q–TOF hybrid instruments have been reviewed (Chernushevich et al., 2001; Campbell & Le Blanc, 2012).

In the context of this book, the use of Q–TOF instruments for structure elucidation is important, given the fact that the most important source of (HRAM) mass spectral data for Chapter 4 was a mass spectral library generated on a Q–TOF instrument.

1.4.6 Orbitrap Hybrid Instruments for MS–MS and MS^n

The initial instrumental setup of a commercial orbitrap mass spectrometer consisted of a hybrid LIT–orbitrap configuration, featuring an LIT to control the number of ions transferred to the orbitrap and to perform MS^n, a C-trap to direct the package of ions into the orbitrap, and the orbitrap itself (Figure 1.24) (Hu et al., 2005; Makarov et al., 2006). In this instrument, the orbitrap is used to perform HRAM analysis. Any precursor-ion selection and/or precursor-ion fragmentation is performed prior to delivering the ions to the orbitrap. Initially, precursor-ion selection and fragmentation, in order to generate MS^n product-ion mass spectra, are performed in the LIT. As the LIT in the commercial instrument is equipped with two separate off-axis detectors, simultaneous acquisition of precursor-ion HRAM mass spectrum and (several) unit-mass resolution product-ion MS^n mass spectra can be achieved. If both precursor-ion and product-ion mass spectra are acquired using the orbitrap, high resolution (≈100,000, FWHM) is used for the precursor ions, whereas medium resolution (≈15,000–30,000, FWHM) is generally sufficient for the HRAM analysis of the product ions of a well-characterized precursor ion.

Subsequently, it was demonstrated that CID could be achieved in the gas-filled quadrupole C-trap (Olsen et al., 2007). The fragmentation behavior in the C-trap is more similar to collision-cell CID. In commercial instruments, this was implemented by means of the installation of a separate RF-only collision octapole device (higher-energy collision-induced dissociation, HCD) to optimize the use of this feature. In the resulting system, fragmentation can be achieved in the LIT, featuring ion-trap MS^n, as well as in the HCD cell, featuring collision-cell CID. Additional hardware to perform ETD has been made available as well. The introduction of the HCD cell enabled the development of the stand-alone orbitrap, providing all-ion fragmentation without prior precursor-ion selection (Geiger et al., 2010). In addition, a quadrupole–orbitrap hybrid system was developed (Michalski et al., 2011). The configuration of this system comprises a quadrupole mass analyzer, a C-trap, an HCD cell, and an orbitrap mass analyzer. In MS mode, ions are passed through the quadrupole, operated in RF-only mode, to the C-trap, from where they are transferred into the orbitrap mass analyzer for HRAM analysis. In MS–MS mode, a precursor ion is selected in the quadrupole mass analyzer, transferred through the C-trap into the HCD cell for fragmentation. The fragment ions are transported back to the C-trap and then transferred into the orbitrap for HRAM product-ion analysis. Compared to the initially introduced LIT-orbitrap hybrid, the quadrupole-orbitrap hybrid is much faster, for example, with full-spectrum analysis with 140,000 resolution (FWHM, at m/z 200) within 1 s, and up to 12 full-spectrum product-ion mass spectra at 17,500 resolution (FWHM) within 1 s.

Most recently, more advanced orbitrap-based systems have been introduced, featuring both a quadrupole mass analyzer, a HCD cell, and a LIT system, next to the C-trap and orbitrap (Senko et al., 2013). In MS^n with a commercial version of this system, the precursor-ion selection is performed in the quadrupole mass analyzer. The ions are transferred through the C-trap to the high-pressure cell of a dual-cell LIT for excitation and fragmentation, eventually performing multistage MS^n. For multiply-charged peptide ion fragmentation, ETD can also be performed in the high-pressure LIT either as a separate experiment or in combination with HCD fragmentation. The fragment ions are transported back to the C-trap and from there transferred into the orbitrap for HRAM product-ion analysis.

Any orbitrap hybrid system for MS–MS or MS^n provides HRAM analysis at present with 140,000 or 280,000 resolution (FWHM for m/z 200) and with a mass accuracy of typically $\leq$1 ppm. As orbitrap technology is relatively young, further developments and improvements are to be expected in the future. Orbitrap-based instruments play an important role in metabolite identification, in peptide sequencing, and in solving other structure elucidation problems. They have been used in elucidating the identity of fragment ions of drugs such as furosemide (Section 4.1.4.3) and stanozolol (Section 4.6.4).

1.4.7 Other Instruments for MS–MS and MS^n

In the previous sections, the most widely used system configurations for MS–MS and/or MS^n in combination with ESI have been discussed. Two other tandem mass spectrometry configurations should be briefly mentioned: ion-trap–time-of-flight (IT–TOF) hybrid instruments and MS–MS on FT-ICR-MS instruments.

In addition to the ion-trap-based hybrid systems discussed so far, that is, Q–LIT and LIT–orbitrap instruments, another ion-trap-based hybrid system became commercially available, with an ion-trap as MS_1 and a TOF as MS_2, that is, the IT–TOF hybrid system. IT–TOF systems have been pioneered by the group of Lubman (Michael et al., 1992, 1993). It has subsequently become commercially available for both MALDI and ESI applications (Liu, 2012). Unlike CID in other ion-trap devices where He is used to stabilize the ion trajectories and as collision gas, in the IT–TOF instrument pulses of Ar are used to prevent precursor ions to be lost from the trap and to perform MS^n. It readily provides high-resolution MS and MS^n data, and currently it finds extensive use. However, the mass resolution of the commercial instrument (up to $\approx$15,000, FWHM) is not as good as in Q–TOF hybrid instruments (up to $\approx$60,000, FWHM). The fragmentation of the anabolic steroid norethisterone (Section 4.6.4) has been studied using an IT–TOF hybrid instrument.

An FT-ICR-MS instrument shows attractive features for use in MS–MS or MS^n, that is, its ultra-high resolution and accurate-mass capabilities, as well as the possibility of selectively trapping targeted ions in the ICR cell, while unwanted ions can be eliminated by the application of RF pulses. Thus, the MS^n procedures in an FT-ICR-MS instrument greatly resemble those in an ion-trap instrument. However, the extreme low pressures ($\leq 10^{-7}$ Pa; $\leq 10^{-9}$ mbar) required in the FT-ICR cell exclude the use of CID in the FT-ICR cell (Marshall et al., 1998). This problem can be solved in several ways, that is, the FT-ICR cell serves as MS_2 either in a hybrid system while fragmentation is performed in MS_1 or in a collision cell in between MS_1 and MS_2. To this end, LIT–FT-ICR hybrid systems have been introduced enabling MS^n of a selected precursor ion prior to transferring the product ions to the FT-ICR cell (Wu et al., 2004). Alternatively, Q–FT-ICR hybrid systems can be used (Patrie et al., 2004; Syka et al., 2004). Both types of instrument have become commercially available. FT-ICR-MS instruments have been used to elucidate the fragmentation of drugs such as galantamine (Section 4.5.4), anabolic steroids (Section 4.6.4), and polyether ionophores (Section 4.10.2.3). Due to the success of orbitrap technology, the product line of LIT–FT-ICR has recently been discontinued.

Another solution to the problem with CID in FT-ICR-MS is the use of alternative ion-activation methods to induce fragmentation in the FT-ICR. To this end, ion-activation methods such as infrared multiphoton photodissociation (IRMPD) and sustained off-resonance irradiation (SORI) have been introduced (Sleno & Volmer, 2004; Laskin & Futrell, 2005). More recently, ECD has been used as a powerful ion dissociation tool in FR-ICR-MS, which is applicable to multiply-charged ions of peptides and proteins (Kim & Pandey, 2012; Zhurov et al., 2013).

Another instrumental development that may have large impact on the way structure elucidation by MS–MS is performed is the commercial introduction of hybrid MS–MS systems featuring IMS. IMS is a powerful analytical tool routinely applied for field detection of explosives, drugs, and chemical weapons (e.g., at airports and in field forensics). In its simplest form, a drift-tube ion-mobility spectrometer measures how fast a given ion moves in a uniform electric field through a given atmosphere, for example, a (counter-current) buffer gas (He, N_2, Ar). Thus, an ion-mobility system separates ions by shape and charge. The hyphenation of IMS and MS combines a separation technique based of the analysis of molecular conformation and shape as performed in IMS, with the analysis of *m/z* and the gathered information on molecular structural features as performed in MS. IMS–MS has been pioneered by the groups of Bowers (Wyttenbach et al., 1996) and Clemmer (Clemmer & Jarrold, 1997; Srebalus et al., 1999). In IMS–MS, IMS provides a rapid gas-phase separation step prior to MS analysis, enabling the identification of ions with different drift times, thus with different collisional cross sections. There are several ways to implement IMS in IMS–MS (Kanu et al., 2008; Wyttenbach et al., 2014).

The groups of Bowers and Clemmer use the type of drift tubes also applied in stand-alone IMS. The conventional drift-tube approach is the oldest method to perform ion mobility in combination with MS, whereas drift-tube IMS–MS systems have become commercially available only very recently. The first commercial implementation of IMS–MS was based on the use of traveling-wave stacked-ring ion guides, which were initially developed to replace RF-only hexapole ion guides in vacuum interfaces for API or as collision cells (Giles et al, 2004; Pringle et al., 2007). The collision-cell region of a hybrid Q–IMS–TOF instrument features three traveling-wave stacked-ring ion guides, of which the middle one is used as a ion-mobility drift tube, operated at pressures up to 100 Pa (1 mbar) and with up to 200 mL min^{-1} of N_2 gas, whereas the other two may be used as a collision cell, operated at 1 Pa (10^{-2} mbar) when applicable (Pringle et al., 2007). A third way to perform IMS–MS is high-field asymmetric waveform ion mobility spectrometry (FAIMS), which involves the gas-phase mobility separation of ions in an electric field at atmospheric pressure. The FAIMS device is positioned in the API source in between the ESI needle and the vacuum interface (Kolakowski & Mester, 2007; Tsai et al., 2012). Commercially available FAIMS devices are primarily applied to improve sensitivity and to reduce matrix effects in quantitative analysis using LC–ESI-MS (Tsai et al., 2012; Xia et al., 2008). An IMS–MS system with separation in the ion tunnel area of atmospheric-pressure-to-vacuum interfaces is also under development. An application of IMS–MS in structure elucidation of hydroxylated metabolites is discussed in Section 5.7.1.

1.4.8 MS–MS and MS^n in the Analysis of Drugs and Pesticides

This book focuses on the interpretation of product-ion MS–MS and MS^n mass spectra of drugs, pesticides, and related compounds. The basic data sets comprised mass spectral libraries acquired using TQ and Q–LIT hybrid instruments and especially Q–TOF hybrid instruments. However, the interpretation of the product-ion mass spectra in these libraries were complemented with extensive literature data, which were acquired not only with the three aforementioned instrument types, but also with ion-trap MS^n, IT–TOF MS^n, LTQ–orbitrap, and various FT-ICR-MS systems. Obviously, an important issue in the reliable interpretation of product-ion mass spectra is the availability of accurate-mass data. If in some instances the interpretation was not supported by accurate-mass data, it is mentioned in the text. No attempt was made to explicitly show the differences on the information content of the product-ion mass spectra between collision-cell CID and ion-trap CID. Given the instruments used to acquire the product-ion mass spectra in the mass spectral libraries, most of the data refers to collision-cell CID. However, when comparison between the two CID modes could be made, in most cases the same information content was found, except for ions with low *m/z* (Section 1.4.2).

1.5 DATA ACQUISITION

1.5.1 Introduction

The two general modes of mass spectrometric data acquisition, that is, the full-spectrum mode and the selected-ion mode, have already been introduced in Section 1.3.1.1. The full-spectrum mode in single-MS and the full-spectrum product-ion analysis mode in MS–MS and MS^n (Section 1.4.1.2) have been explained in sufficient detail. In this section, additional and more advanced modes of data acquisition are briefly discussed. A more extensive discussion on the application of these modes follows in Chapter 5.

For a proper understanding of the possibilities and limitations of data acquisition in MS, one should be aware of the fact that, when equipped with one ion-detection system,

a mass spectrometer can perform only one experiment at a time. Several experiments in different acquisition modes can be performed in series. Functions may be defined to perform a series of such experiments repeatedly. Given the speed of current data acquisition and processing systems, decisions for a next step in a series of experiments may be based on the data acquired in the previous experiment, that is, data-dependent acquisition (DDA). The time required for individual MS experiments very much depends on the type of instrument used (and its model). Due to the huge progress in electronics, modern instruments can perform much faster than older ones.

1.5.2 Selected-Ion and Selected-Reaction Monitoring

The selected-ion acquisition mode, that is, selected-ion monitoring (SIM) in single-MS instruments and selected-reaction monitoring (SRM) in MS–MS instruments, is a powerful tool especially with beam instruments, that is, quadrupole and sector instruments, to improve S/N in targeted analysis by elongating the dwell time at a particular *m/z*. Ion-trapping devices, both ion-traps and FT-ICR-MS systems, can perform a selected-ion acquisition mode as well, but the gain in S/N will be generally less than that in beam instruments under similar conditions as no significant gain in dwell time is achieved.

In TQ instruments, SRM is a powerful tool to greatly enhance selectivity, and thereby achieve excellent lower limits of quantification in targeted quantitative analysis. In the SRM mode, both stages of mass analysis perform the selection of ions with a particular *m/z* value, that is, in MS_1 a precursor ion, mostly $[M+H]^+$ or $[M-H]^-$ of the target analyte is selected, subjected to dissociation in the collision cell, while in MS_2 a preferably structure-specific product ion of the selected precursor is selected and detected (Figure 1.25). The SRM mode makes the TQ instrument as the instrument of choice in routine quantitative analysis of target compounds in complex (biological) matrices (van Dongen & Niessen, 2012). Recently, it has also been implemented in quantitative analytical strategies using GC–MS as well (e.g., Cherta et al., 2013; Pang et al., 2015). In many instances, SRM is referred to as MRM, multiple-reaction monitoring, to indicate that multiple product ions of one precursor ion are monitored, even if only one product ion is monitored. Given the fact that SRM stands for selected-reaction monitoring (and not single-reaction monitoring), the term MRM is neither useful nor needed and it is therefore deprecated.

An SRM transition is a combination of a precursor ion *m/z*, a product ion *m/z*, and all MS parameters, for example, collision energy, required to measure this transition with the best sensitivity in a particular TQ instrument (and eventually the chromatographic retention time of the compound with which the SRM transition is defined). Important practical aspects, applications, as well as advantages and limitations of SRM are discussed in more detail in Section 5.3.

1.5.3 Structure-Specific Screening: Precursor-Ion and Neutral-Loss Analysis

Apart from full-spectrum product-ion analysis mode and the SRM mode, a TQ instrument has two additional modes of operation that can be useful as structure-specific screening procedures, for example, the precursor-ion analysis (PIA) and the neutral-loss analysis (NLA) modes (Hunt et al., 1983; Johnson & Yost, 1985).

In the PIA mode, MS_1 is operated in full-spectrum mode, whereas MS_2 is operated in selected-ion mode to monitor a structure-specific product ion. In PIA mode, a signal is detected if an ion transmitted in MS_1 upon CID generates the common product ion selected in MS_2. In the resulting mass spectrum, the peaks are labeled with their precursor-ion *m/z* value. An early example of PIA involved the screening for phthalate plasticizers in environmental samples by means of the common fragment ion with *m/z* 149 due to protonated phthalic anhydride (Hunt et al., 1983). The PIA mode can be used to determine from which precursor ion(s) a particular product ion originates. It may thus help answering the question whether a particular product ion is formed from a particular precursor ion in a one-step dissociation reaction or whether an intermediate fragmentation step is involved. As such, the PIA mode enables more detailed studies on fragmentation pathways, as for instance demonstrated for morphine and related opiates (Section 4.7.5) (Bijlsma et al., 2011).

In the NLA mode, both MS_1 and MS_2 are operated in scanning mode, but with a fixed *m/z* offset corresponding to a

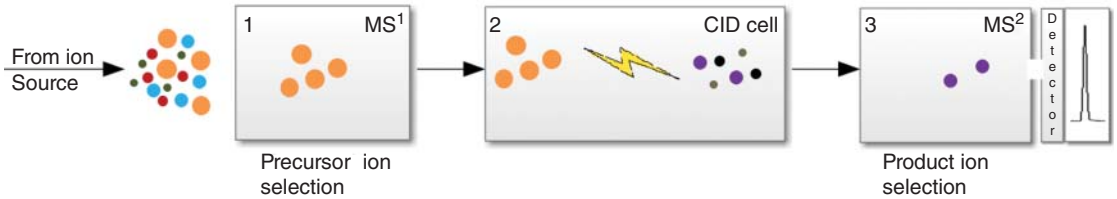

FIGURE 1.25 Schematic representation of selected-reaction monitoring (SRM) in a tandem-quadrupole instrument.

structure-specific neutral loss in the fragmentation reaction. In the NLA mode, a signal is detected if an ion transmitted in MS_1 upon CID loses a neutral molecule with a mass matching the fixed *m*/*z* difference. An early example of NLA is the monitoring of CO_2 losses from deprotonated aromatic carboxylic acids (Hunt et al., 1983).

The PIA and NLA modes of acquisition in TQ instruments have been successfully applied for structure-specific screening, that is, to search for specific compound classes in complex matrices. This can be demonstrated by the screening for anthocyanins in black raspberries, red raspberries, highbush blueberries, and grapes (Tian et al., 2005) and for two classes of designer drugs in urine (Montesano et al., 2013). The PIA and NLA modes are also frequently applied in drug metabolism studies (Kostiainen et al., 2003), especially using the constant neutral losses of 80 and 176 Da, characteristic for phase II sulfate and glucuronate conjugation, and for glutathione and cyanide-trapped reactive drug metabolites (Jian et al., 2012) (Section 5.7.1).

1.5.4 Data-Dependent Acquisition

The data-dependent acquisition (DDA) mode (also called information dependent acquisition) is another powerful mode of MS data acquisition (Stahl et al., 1996; Wenner & Lynn, 2004; Ma & Chowdhury, 2013). In DDA, the instrument performs a rule-based automatic switching between a survey and a dependent mode. In the most widely applied DDA mode, the instrument switches between full-spectrum MS mode and a full-spectrum product-ion (MS–MS) analysis mode. The switching is controlled by the intensity of a possible precursor ion observed and eventually by additional criteria such as isotope pattern, charge state, or specific *m*/*z* values on an inclusion or an exclusion list. In this way, highly efficient data acquisition is possible: MS and MS–MS data of unknown compounds in a mixture are acquired simultaneously in one chromatographic run. The DDA mode is widely applied in metabolite identification strategies (Section 5.7.1), in proteomics (Stahl et al., 1996; Wenner & Lynn, 2004), in general unknown screening in (clinical) toxicology (Oberacher & Arnhard, 2015), among other areas. In the MS analysis of complex LC chromatograms of digested proteomes, multiple precursor ions, for example, the 4–10 most abundant precursor ions in a survey MS spectrum, may be used to perform product-ion analysis in the dependent scan, that is, one survey MS spectrum followed by 4–10 product-ion MS–MS spectra before returning to the survey MS mode (ddTopN with $N = 4–10$). Switching between a targeted SRM method as the survey mode and product-ion analysis as the dependent mode has also been demonstrated, for example, in metabolite identification (Li et al., 2005; Soglia et al., 2004). As an example, general unknown screening in toxicology has been described involving data-dependent switching between scheduled-SRM, using ≈1250 SRM transitions, and full-spectrum product-ion analysis (Sections 5.3.3.4 and 5.5) (Dresen et al., 2009; Dresen et al., 2010).

1.5.5 Data-Independent Acquisition

An alternative to DDA is data-independent acquisition (DIA), where scan-wise switching between MS and MS–MS is performed to obtain fragments for all precursor ions present. This is especially useful in combination with HRAM instruments. DIA modes have been described in several ways, for example, as MS^E for Q–TOF instrument (Plumb et al., 2006) and as such widely applied, as MS^M for LIT–orbitrap instruments (Cho et al., 2012), and SWATH for another type of Q–TOF instrument (Arnhard et al., 2015). Examples of these data-acquisition modes are given in Section 5.5.

1.6 SELECTED LITERATURE ON MASS SPECTROMETRY

In this section, useful references are given to general books on mass spectrometry, which are considered relevant to the current discussion.

General mass spectrometry

- Busch KL, Glish GL, McLuckey SA. 1988. Mass spectrometry–mass spectrometry. Techniques and applications of tandem mass spectrometry. VCH Publishers, Inc, New York, NY. ISBN: 978-0-895-73275-0.
- Harrison AG. 1992. Chemical ionization mass spectrometry, 2nd ed. CRC Press, Boca Raton, FL. ISBN: 978-0-849-34254-7.
- Chapman JR. 1993. Practical organic mass spectrometry, 2nd ed. John Wiley & Sons, Ltd., Chichester, UK. ISBN: 978-0-471-92753-8.
- Sparkman OD. 2006. Mass spectrometry desk reference, 2nd ed. ISBN: 978-0-966-08139-8.
- de Hoffmann E, Stroobant V. 2007. Mass spectrometry. Principles and applications, 3rd ed. John Wiley & Sons, Ltd., Chichester, UK. ISBN: 978-0-470-03310-4.
- Watson JT, Sparkman OD. 2007. Introduction to mass spectrometry, 4th ed. Wiley Interscience, Hoboken, NJ. ISBN: 978-0-470-51634-8.
- Boyd RK, Basic C, Bethem RA. 2008. Trace quantitative analysis by mass spectrometry. Wiley Interscience, Hoboken, NJ. ISBN: 978-0-470-05771-1.
- Gross JH. 2011. Mass spectrometry, 2nd ed. Springer-Verlag Berlin-Heidelberg. ISBN: 978-3-642-10711-5.
- Carey FA, Sundberg RJ. 2007. Advanced organic chemistry, 5th ed. Springer New York, NY. ISBN: 978-0-387-44897 (part A) and ISBN: 978-0-387-68350 (part B).

Fragmentation in mass spectrometry

- McLafferty FW, Tureček F. 1993. Interpretation of mass spectra, 4th ed. University Science Books, Mill Valley, CA. ISBN: 978-0-935702-25-3.
- Kinter M, Sherman NE. 2000. Protein sequencing and identification using tandem mass spectrometry. Wiley Interscience, NY. ISBN: 978-0-47132-249-8.
- Smith RM. 2004. Understanding mass spectra. A basic approach, 2nd ed. Wiley Interscience, Hoboken, NJ. ISBN: 978-0-471-42949-4.
- Ham BM. 2008. Even electron mass spectrometry with biomolecule applications. Wiley Interscience, Hoboken, NJ. ISBN: 978-0-470-11802-3.

Liquid chromatography–mass spectrometry

- Cole RB (Ed.). 2010. Electrospray and MALDI mass spectrometry, fundamentals, instrumentation & applications, 2nd ed. Wiley Interscience, Hoboken, NJ. ISBN: 978-0-471-74107-7.
- Lee MS. 2002. LC/MS applications in drug development, 2nd ed. Wiley Interscience, Hoboken, NJ. ISBN: 978-0-471-40520-7.
- Ardrey RE. 2003. Liquid chromatography-mass spectrometry: An introduction. John Wiley & Sons, Ltd., Chichester, UK. ISBN: 978-0-471-49799-8.
- Niessen WMA. 2006. Liquid chromatography-mass spectrometry, 3rd ed. CRC Press, Boca Raton, FL. ISBN: 978-0-824-74082-5.
- Ferrer I, Thurman EM. (Ed.). 2009. Liquid chromatography time of flight mass spectrometry. Wiley Interscience, Hoboken, NJ. ISBN: 978-0-470-13797-0.
- Li W, Zhang J, Tse FLS. (Ed.). 2013. Handbook of LC-MS bioanalysis. Wiley Interscience, Hoboken, NJ. ISBN: 978-1-118-15924-8.

REFERENCES

Allen FH, Watson DG, Brammer L, Orpen AG, Taylor R. 2006. Typical interatomic distances: Organic compounds. Int Tables Crystallogr C 9.5: 790–811.

Allen JS. 1947. An improved electron multiplier particle counter. Rev Sci Instrum 18: 739–749.

Angel PM, Caprioli RM. 2013. Matrix-assisted laser desorption ionization imaging mass spectrometry: In situ molecular mapping. Biochemistry 52: 3818–3828.

Arnhard K, Gottschall A, Pitterl F, Oberacher H. 2015. Applying 'Sequential Windowed Acquisition of All Theoretical Fragment Ion Mass Spectra' (SWATH) for systematic toxicological analysis with liquid chromatography-high-resolution tandem mass spectrometry. Anal Bioanal Chem 407: 405–414.

Arpino PJ, Guiochon G. 1982. Optimization of the instrumental parameters of a combined LC–MS, coupled by an interface for DLI. III. Why the solvent should not be removed in LC–MS interfacing methods. J Chromatogr 251: 153–164.

Arpino P. 1989. Combined liquid chromatography mass spectrometry. Part I. Coupling by means of a moving belt interface. Mass Spectrom Rev 8: 35–55.

Arpino PJ. 1990 Combined liquid chromatography mass spectrometry. Part II. Techniques and mechanisms of thermospray. Mass Spectrom Rev 9: 631–669.

Arpino PJ. 1992. Combined liquid chromatography mass spectrometry. Part III. Applications of thermospray. Mass Spectrom Rev 11: 3–40.

Asam MR, Glish GL. 1997. Tandem mass spectrometry of alkali cationized polysaccharides in a quadrupole ion trap. J Am Soc Mass Spectrom 8: 987–995.

Atwater BL, Stauffer DB, McLafferty FW, Peterson DW. 1985. Reliability ranking and scaling improvements to the probability based matching system for unknown mass spectra. Anal Chem 57: 899–903.

Ausloos P, Clifton CL, Lias SG, Mikaya AI, Stein SE, Tchekhovskoi DV, Sparkma OD, Zaikin V, Zhu D. 1999. The critical evaluation of a comprehensive mass spectral library. J Am Soc Mass Spectrom 10: 287–299.

Banks JF Jr., Shen S, Whitehouse CM, Fenn JB. 1994. Ultrasonically assisted electrospray ionization for LC/MS determination of nucleosides from a transfer RNA digest. Anal Chem 66: 406–414.

Barber M, Bordoli RS, Sedgwick RD, Tyler AN, Whalley ET. 1981. Fast atom bombardment mass spectrometry of bradykinin and related oligopeptides. Biomed Mass Spectrom 8: 337–342.

Beckey HD. 1977. Principles of field ionization and field desorption mass spectrometry. Pergamon, Oxford, UK. ISBN 978-0-080-20612-3.

Bélanger J, Paré JRJ. 1986. Fast atom bombardment mass spectrometry in the pharmaceutical analysis of drugs. J Pharm Biomed Anal 4: 415–441.

Bijlsma L, Sancho JV, Hernández F, Niessen WMA. 2011. Fragmentation pathways of drugs of abuse and their metabolites based on QTOF MS/MS and MSE accurate-mass spectra. J Mass Spectrom 46: 865–875.

Blakley CR, McAdams MJ, Vestal ML. 1978. Crossed-beam liquid chromatograph–mass spectrometer combination, J Chromatogr 158: 261–276.

Blakley CR, Carmody JJ, Vestal ML. 1980. A new soft ionization technique for mass spectrometry of complex molecules. J Am Chem Soc 102: 5931–5933.

Blakley CR, Vestal ML. 1983. Thermospray interface for liquid chromatography/mass spectrometry. Anal Chem 55: 750–754.

Blanksby SJ, Ellison GB. 2003. Bond dissociation energies of organic molecules. Acc Chem Res 36: 255–263.

Bos SJ, van Leeuwen SM, Karst U. 2006. From fundamentals to applications: Recent developments in atmospheric pressure photoionization mass spectrometry. Anal Bioanal Chem 384: 85–99.

Bowie JH. 1984. The formation and fragmentation of negative ions derived from organic molecules. Mass Spectrom Rev 3: 161–207.

Bruins AP, Covey T, Henion JD. 1987. Ion spray interface for combined liquid chromatography/atmospheric pressure ionization mass spectrometry. Anal Chem 59: 2642–2646.

Bruins AP. 1998. Mechanistic aspects of electrospray ionisation. J Chromatogr A 794: 345–357.

Bruno TJ, Svoronos DN. 2010. CRC handbook of basic tables for chemical analysis. 3rd ed. CRC Press. Boca Raton, FL. ISBN: 978-1-420-08042-1.

Busch KL, Glish GL, McLuckey SA. 1988. Mass spectrometry–mass spectrometry. Techniques and applications of tandem mass spectrometry. VCH Publishers, Inc, New York, NY. ISBN 978-0-895-73275-0.

Cai SS, Syage JA. 2006. Comparison of atmospheric pressure photoionization, atmospheric pressure chemical ionization, and electrospray ionization mass spectrometry for analysis of lipids. Anal Chem 78: 1191–1199.

Cai SS, Hanold KA, Syage JA. 2007. Comparison of atmospheric pressure photoionization and atmospheric pressure chemical ionization for normal-phase LC/MS chiral analysis of pharmaceuticals. Anal Chem 79: 2491–2498.

Cai Y, Kingery D, McConnell O, Bach AC, II. 2005. Advantages of atmospheric pressure photoionization mass spectrometry in support of drug discovery. Rapid Commun Mass Spectrom 19: 1717–1724.

Campbell JL, Le Blanc JCY. 2012. Using high-resolution quadrupole TOF technology in DMPK analyses. Bioanalysis 4, 487–500.

Cappiello A, Famiglini G, Palma P, Pierini E, Termopoli V, Trufelli H. 2011. Direct-EI in LC-MS: Towards a universal detector for small-molecule applications. Mass Spectrom Rev 30: 1242–1255.

Carles S, Le Garrec JL, Mitchel JBA. 2007. Electron and ion reactions with hexamethyldisoloxane and pentamethyldisiloxane. J Chem Phys 127: 144308.

Carroll DI, Dzidic I, Stillwell RN, Horning MG, Horning EC. 1974. Subpicogram detection system for gas-phase analysis based upon atmospheric-pressure ionization (API) mass spectrometry. Anal Chem 46: 706–710.

Carroll DI, Dzidic I, Stillwell RN, Haegele KD, Horning EC. 1975. Atmospheric-pressure ionization mass spectrometry: Corona discharge ion source for use in liquid chromatograph–mass spectrometer–computer analytical system. Anal Chem 47: 2369–2373.

Carroll DI, Dzidic I, Horning EC, Stillwell RN. 1981. Atmospheric-pressure ionization mass spectrometry. Appl Spectrosc Rev 17: 337–406.

Chandra AK, Uchimaru T. 2002. The O—H bond dissociation energies of substituted phenols and proton affinities of substituted phenoxide ions: A DFT study. Int J Mol Sci 3: 407–422.

Chernushevich IV, Loboda AV, Thomson BA. 2001. An introduction to quadrupole–time-of-flight mass spectrometry. J Mass Spectrom 36: 849–865.

Cherta L, Portolés T, Beltran J, Pitarch E, Mol JG, Hernández F. 2013. Application of gas chromatography-(triple quadrupole) mass spectrometry with atmospheric pressure chemical ionization for the determination of multiclass pesticides in fruits and vegetables. J Chromatogr A 1314: 224–240.

Chervet JP, Ursem M, Salzman, JP. 1996. Instrumental requirements for nanoscale liquid chromatography. Anal Chem 68: 1507–1512.

Cho R, Huang Y, Schwartz JC, Chen Y, Carlson TJ, Ma J. 2012. MS^M, an efficient workflow for metabolite identification using hybrid linear ion trap orbitrap mass spectrometer. J Am Soc Mass Spectrom 23: 880–888.

Clark AE, Kaleta EJ, Arora A, Wolk DM. 2013. Matrix-assisted laser desorption ionization-time of flight mass spectrometry: A fundamental shift in the routine practice of clinical microbiology. Clin Microbiol Rev 26: 547–603.

Clemmer DE, Jarrold MF. 1997. Ion mobility measurements and their applications to clusters and biomolecules. J Mass Spectrom 32: 577–592.

Cody RB, Laramée JA, Durst HD. 2005. Versatile new ion source for the analysis of materials in open air under ambient conditions. Anal Chem 77: 2297–2302.

Cole RB. 2010. Electrospray and MALDI mass spectrometry, 2nd ed. John Wiley & Sons, Hoboken, NJ. ISBN 978-0-471-74107-7.

Covey TR, Lee ED, Henion JD. 1986. High-speed liquid chromatography tandem mass spectrometry for the determination of drugs in biological samples. Anal Chem 58: 2453–2480.

Covey TR, Bonner RF, Shushan BI, Henion JD. 1988. The determination of protein, oligonucleotide and peptide molecular weights by ion-spray mass spectrometry. Rapid Commun Mass Spectrom 2: 249–256.

Covey TR, Jong R, Javahari H, Liu C, Thomson C, LeBlanc Y. 2001. Design optimization of APCI instrumentation, Proceedings of the 49th ASMS Conference on Mass Spectrometry and Allied Topics, May 27–32, 2001, Chicago, IL.

Creaser CS, Stygall JW. 1993. Particle beam liquid chromatography – mass spectrometry: Instrumentation and aplications. A review. Analyst 118: 1467–1480.

Creaser CS, Ratcliffe L. 2006. Atmospheric pressure matrix-assisted laser desorption/ionization mass spectrometry: A review. Curr Anal Chem 2: 9–15.

de Hoffmann E, Stroobant V. 2007. Mass spectrometry. Principles and applications, 3rd ed. John Wiley & Sons, Ltd., Chichester, UK. ISBN 978-0-470-03310-4.

Demtröder W. 2010. Atoms, molecules and photons, 2nd ed. Springer, Heidelberg. ISBN 978-3-642-10297-4.

Dole M, Mack LL, Hines RL, Mobley RC, Ferguson LD, Alice MB. 1968. Molecular beams of macroions. J Chem Phys 49: 2240–2249.

Doroshenko VM, Cotter RJ. 1989. Ideal velocity focusing in a reflectron time-of-flight mass spectrometer. J Am Soc Mass Spectrom 10: 992–999.

Dougherty RC. 1981. Negative chemical ionization mass spectrometry. Anal Chem 53: 625A-636A.

Douglas DJ, Frank AJ, Mao D. 2005. Linear ion traps in mass spectrometry. Mass Spectrom Rev 24: 1–29.

Dresen S, Gergoc M, Politi, L, Halter C, Weinmann W. 2009. ESI-MS–MS library of 1,253 compounds for application in forensic and clinical toxicology. Anal Bioanal Chem 395: 2521–2526.

Dresen S, Ferreirós N, Gnann H, Zimmermann R, Weinmann W. 2010. Detection and identification of 700 drugs by multi-target screening with a 3200 QTRAP® LC–MS–MS system and library searching. Anal Bioanal Chem 396: 2425–2434.

Es-Safi NE, Kerhoas L, Ducrot PH. 2007. Fragmentation study of iridoid glucosides through positive and negative electrospray ionization, collision-induced dissociation and tandem mass spectrometry. Rapid Commun Mass Spectrom 21: 1165–1275.

Fenn JB, Mann M, Meng CK, Wong SF, Whitehouse CM. 1989. Electrospray ionization for mass spectrometry of large biomolecules. Science 246: 64–71.

Fenn JB. 1993. Ion formation from charged droplets: Roles of geometry, energy, and time. J Am Soc Mass Spectrom 4: 524–535.

Fenselau C, Cotter RJ. 1987. Chemical aspects of fast atom bombardment. Chem Rev 87: 501–512.

Fernández de la Mora J, Loscertales IG. 1994. The current emitted by highly conducting Taylor cones. J Fluid Mech 260: 155–184.

Foltz RL. 1992. Recent applications of mass spectrometry in forensic toxicology. Int J Mass Spectrom Ion Processes 118/119: 237–263.

Gallagher RT, Balogh MP, Davey P, Jackson MR, Southern LJ. 2003. Combined electrospray ionization−atmospheric pressure chemical source for use in high-throughput LC-MS applications. Anal Chem 75: 973–977.

Garcia-Ac A, Segura PA, Viglino L, Gagnon C, Sauvé S. 2011. Comparison of APPI, APCI and ESI for the LC-MS/MS analysis of bezafibrate, cyclophosphamide, enalapril, methotrexate and orlistat in municipal wastewater. J Mass Spectrom 46: 383–390.

Geiger T, Cox J, Mann M. 2010. Proteomics on an orbitrap benchtop mass spectrometer using all-ion fragmentation. Mol Cell Proteomics 9: 2252–2261.

Gilbert W. 1600. De Magnete. Peter Short, London. Translation by Mottelay PF. 1958. Dover Publications Inc., New York. ISBN: 978-0-486-26761-X (unabridged and unaltered republication of the John Wiley & Sons, New York, 1893 edition).

Giles K, Pringle SD, Worthington KR, Little D, Wildgoose JL, Bateman RH. 2004. Applications of a travelling wave-based radio-frequency-only stacked ring ion guide. Rapid Commun Mass Spectrom 18: 2401–2414.

Goodsell DS. 2009. The machinery of life, 2nd ed. Copernicus Books, Springer, New York. ISBN 978-0-387-84924-9.

Green KM, Lebrilla CB. 1997. Ion-molecule reactions as probes of gas-phase structures of peptides and proteins. Mass Spectrom Rev 16: 53–71.

Grimm RL, Beauchamp, JL. 2002. Evaporation and discharge dynamics of highly charged droplets of heptane, octane, and *p*-xylene generated by electrospray ionization. Anal Chem 74: 6291–6297.

Guilhaus M, Selby D, Mlynski V. 2000. Orthogonal acceleration time-of-flight mass spectrometry. Mass Spectrom Rev 19: 65–107.

Hadley JS, Fradin A, Murphy RC. 1988. Electron capture negative ion chemical ionization analysis of arachidonic acid. Biomed Environ Mass Spectrom 15: 175–178.

Hager JW. 2002. A new linear ion trap mass spectrometer. Rapid Commun Mass Spectrom 16: 512–526.

Hakala KS, Kostiainen R, Ketola RA. 2006. Feasibility of different mass spectrometric techniques and programs for automated metabolite profiling of tramadol in human urine. Rapid Commun Mass Spectrom 20: 2081–2090.

Haller I, Mirza UA, Chait BT. 1996. Collision induced decomposition of peptides. Choice of collision parameters. J Am Soc Mass Spectrom 7: 677–681.

Hanold KA, Fischer SM, Cormia PH, Miller CE, Syage JA. 2004. Atmospheric pressure photoionization. 1. General properties for LC/MS. Anal Chem 76: 2842–2851.

Harrison AG. 1992. Chemical ionization mass spectrometry, 2nd ed. CRC Press, Boca Raton, FL. ISBN-978-0-849-34254-7.

Hipple JA, Fox RE, Condon EU. 1946. Metastable ions formed by electron impact in hydrocarbon gases. Phys Rev 69: 347–356.

Hirabayashi A, Sakairi M, Koizumi H. 1994. Sonic spray ionization method for atmospheric pressure ionization mass spectrometry. Anal Chem 66: 4557–4559.

Hirabayashi A, Sakairi M, Koizumi H. 1995. Sonic spray mass spectrometry. Anal Chem 67: 2878–2882.

Hiraoka K, Fukasawa H, Matsushita F, Aizawa K. 1995. High-flow liquid chromatography/mass spectrometry interface using a parallel ion spray. Rapid Commun Mass Spectrom 9: 1349–1355.

Hiraoka K, Saito S, Katsuragawa J, Kudaka I. 1998. A new liquid chromatography mass spectrometry interface: Laser spray, Rapid Commun Mass Spectrom 12: 1170–1174.

Hiraoka K. 2003. Gas-phase ion/molecule reactions. in: fundamentals of mass spectrometry: 109–144. Springer Science+Business Media, New York. ISBN 978-1-461-47233-9.

Hirschfeld T. 1980. The Hy-phen-ated methods. Anal Chem 52: 297A-312A.

Holman SW, Sims PF, Eyers CE. 2012. The use of selected reaction monitoring in quantitative proteomics. Bioanalysis 4: 1763–1786.

Holmes J, Morrell F. 1957. Oscillographic mass spectrometric monitoring of gas chromatography. Appl Spectrosc 11: 86–87.

Holmgren E, Carlsson H, Goede P, Crescenzi C. 2005. Determination and characterization of organic explosives using porous graphitic carbon and liquid chromatography-atmospheric pressure chemical ionization mass spectrometry. J Chromatogr A 1099: 127–135.

Hopfgartner G, Varesio E, Tschäppät V, Grivet C, Bourgogne E, Leuthold LA. 2004. Triple quadrupole linear ion trap mass spectrometer for the analysis of small molecules and macromolecules. J Mass Spectrom 39: 845–855.

Horning EC, Horning MG, Carroll DI, Dzidic I, Stillwell RN. 1973. New picogram detection system based on a mass spectrometer with an external ionization source at atmospheric pressure. Anal Chem 45: 936–943.

Hu Q, Noll RJ, Li H, Makarov A, Hardman M, Cooks GR. 2005. The orbitrap: A new mass spectrometer. J Mass Spectrom 40: 430–443.

Huang MZ, Yuan CH, Cheng SC, Cho YT, Shiea J. 2010. Ambient ionization mass spectrometry. Annu Rev Anal Chem 3: 43–65.

Hübschmann HJ. 2015. Handbook of GC-MS, 3rd ed. Wiley-VCH Verlag GmbH & Co. ISBN 978-3-527-33474-2.

Huertas ML, Fontan J. 1975. Evolution times of tropospheric positive ions. Atmos Environ 9: 1018–1026.

Hunt DF, Stafford GC, Crow FW, Russell JW. 1976. Pulsed positive negative ion chemical ionization mass spectrometry. Anal Chem 48: 2098–2104.

Hunt DF, Shabanowitz J, Harvey TM, Coates ML. 1983. Analysis of organics in the environment by functional group using a triple quadrupole mass spectrometer. J Chromatogr 271: 93–105.

Hunter EPL, Lias SG. 1998. Evaluated gas phase basicities and proton affinities of molecules: An update. J Phys Chem Ref Data 27: 413–656.

Ibrahim Y, Tang K, Tolmachev AV, Shvartsburg AA, Smith RD. 2006. Improving mass spectrometer sensitivity using a high-pressure electrodynamic ion funnel interface. J Am Soc Mass Spectrom 17: 1299–1305.

Iribarne, JV, Thomson BA. 1976. Evaporation of small ions from charged droplets. J Chem Phys 64: 2287–2294.

Jarmusch AK, Musso AM, Shymanovich T, Jarmusch SA, Weavil MJ, Lovin ME, Ehrmann BM, Saari S, Nichols DE, Faeth SH, Cech NB. 2016. Comparison of electrospray ionization and atmospheric pressure photoionization liquid chromatography mass spectrometry methods for analysis of ergot alkaloids from endophyte-infected sleepygrass (*Achnatherum robustum*). J Pharm Biomed Anal 117: 11–17.

Jian W, Liu HF, Zhao W, Jones E, Zhu M. 2012. Simultaneous screening of glutathione and cyanide adducts using precursor ion and neutral loss scans-dependent product ion spectral acquisition and data mining tools. J Am Soc Mass Spectrom 23: 964–976.

Jiang Y, Cole RB. 2005. Oligosaccharide analysis using anion attachment in negative mode electrospray mass spectrometry. J Am Soc Mass Spectrom 16: 60–70.

Johnson JV, Yost RA. 1985. Tandem mass spectrometry for trace analysis. Anal Chem 57: 758A-768A.

Johnson JV, Yost RA, Kelley PE, Bradford DC. 1990. Tandem-in-space and tandem-in-time mass spectrometry: Triple quadrupoles and quadrupole ion traps. Anal Chem 62: 2162–2172.

Jonscher KR, Yates JR, III, 1997. The quadrupole ion trap mass spectrometer – a small solution to a big challenge. Anal Biochem 244: 1–15.

Kanu AB, Dwivedi P, Tam M, Matz L, Hill HH, Jr., 2008, Ion mobility-mass spectrometry. J Mass Spectrom 43: 1–22.

Karancsi T, Slégel P. 1999. Reliable molecular mass determination of aromatic nitro compounds: Elimination of gas-phase reduction occurring during atmospheric pressure chemical ionization. J Mass Spectrom 34: 975–977.

Karas M, Hillenkamp F. 1988. Laser desorption ionization of proteins with molecular masses exceeding 10,000 Daltons. Anal Chem 60: 2299–2301.

Karas M. 1996. Matrix-assisted laser desorption ionization mass spectrometry: A progress report. Biochem Soc Trans 24: 897–900.

Karas M, Krüger R. 2003. Ion formation in MALDI: The cluster ionisation mechanism. Chem Rev 103: 427–439.

Karasek FW. 1974. Plasma chromatography. Anal Chem 46: 710A-720A.

Katta V, Rockwood AL, Vestal ML. 1991. Field limit for ion evaporation from charged thermospray droplets. Int J Mass Spectrom Ion Processes 103: 129–148.

Kauppila TJ, Kostiainen R, Bruins AP. 2004a. Anisole, a new dopant for atmospheric pressure photoionization mass spectrometry of low proton affinity, low ionization energy compounds. Rapid Commun Mass Spectrom 18: 808–815.

Kauppila TJ, Kotiaho T, Kostiainen R, Bruins AP. 2004b. Negative-ion atmospheric pressure photoionization mass spectrometry. J Am Soc Mass Spectrom 15: 203–211.

Kebarle P, Verkerk UH. 2009. Electrospray: From ions in solution to ions in the gas phase, what we know now. Mass Spectrom Rev 28: 898–917.

Kelly RT, Tolmachev AV, Page, JS, Tang K, Smith RD. 2010. The ion funnel: Theory, implementations, and applications. Mass Spectrom Rev 29: 294–312.

Kim M-S, Pandey A. 2012. Electron transfer dissociation mass spectrometry in proteomics. Proteomics 12: 530–542.

Kind T, Fiehn O. 2010. Advances in structure elucidation of small molecules using mass spectrometry. Bioanal Rev 2: 23–60.

Knochenmuss R. 2006. Ion formation mechanisms in UV-MALDI. Analyst 131: 966–986.

Kolakowski BM, Mester Z. 2007. Review of applications of high-field asymmetric waveform ion mobility spectrometry (FAIMS) and differential mobility spectrometry (DMS). Analyst 132: 842–864.

Koo I, Kim S, Zhang X. 2013. Comparative analysis of mass spectral matching-based compound identification in gas chromatography–mass spectrometry. J Chromatogr A 1298: 132–138.

Kostiainen R, Kotiaho T, Kuuranne T, Auriola S. 2003. Liquid chromatography/atmospheric pressure ionization-mass spectrometry in drug metabolism studies. J Mass Spectrom 38: 357–372.

Lacorte S, Fernandez-Alba AR. 2006. Time of flight mass spectrometry applied to the liquid chromatographic analysis of pesticides in water and food. Mass Spectrom Rev 25: 866–880.

Laskin J, Futrell JH. 2005. Activation of large ions in FT-ICR mass spectrometry. Mass Spectrom Rev 24: 135–167.

Lattimer RP, Schulten H-R. 1989. Field ionization and field desorption mass spectrometry: Past, present, and future. Anal Chem 61: 1201A-1215A.

Leinonen A, Kuuranne T, Kostiainen R. 2002. LC–MS in anabolic steroid analysis - optimization and comparison of three ionization techniques: Electrospray ionization, atmospheric pressure chemical ionization and atmospheric pressure photoionization. J Mass Spectrom 37: 693–698.

Leis HJ, Windischhofer W. 2012. (*S*)-(−)-*N*-(Pentafluorobenzylcarbamoyl)prolyl chloride: A chiral derivatisation reagent designed for gas chromatography/negative ion chemical ionisation

mass spectrometry of amino compounds. Rapid Commun Mass Spectrom 26: 592–598.

Lépine F, Boismenu D, Milot S, Mamer O. 1999. Collision of molecular anions of benzenedicarboxylic esters with oxygen in a triple quadrupole mass spectrometer. J Am Soc Mass Spectrom 10: 1248–1252.

Li AC, Alton D, Bryant MS, Shou WZ. 2005. Simultaneously quantifying parent drugs and screening for metabolites in plasma pharmacokinetic samples using selected reaction monitoring information-dependent acquisition on a QTrap instrument. Rapid Commun Mass Spectrom 19: 1943–1950.

Li DX, Gan L, Bronja A, Schmitz OJ. 2015. Gas chromatography coupled to atmospheric pressure ionization mass spectrometry (GC-API-MS): Review. Anal Chim Acta 891: 43–61.

Lias SG, Liebman JF, and Levin RD. 1984. Evaluated gas phase basicities and proton affinities of molecules; heats of formation of protonated molecules. J Phys Chem Ref Data: 13: 695–808.

Lien GW, Chen CY, Wang GS. 2009. Comparison of electrospray ionization, atmospheric pressure chemical ionization and atmospheric pressure photoionization for determining estrogenic chemicals in water by liquid chromatography tandem mass spectrometry with chemical derivatizations. J Chromatogr A 1216: 956–966.

Lim KH, Su Z, Foltz RL. 1993. Stereoselective disposition: Enantioselective quantitation of 3,4-(methylenedioxy)methamphetamine and three of its metabolites by gas chromatography/electron capture negative ion chemical ionization mass spectrometry. Biol Mass Spectrom 22: 403–411.

Linden HB. 2004. Liquid injection field desorption ionization: A new tool for soft ionization of samples including air-sensitive catalysts and non-polar hydrocarbons. Eur J Mass Spectrom 10: 459–468.

Liu ZY. 2012. An introduction to hybrid ion trap/time-of-flight mass spectrometry coupled with liquid chromatography applied to drug metabolism studies. J Mass Spectrom 47: 1627–1642.

Louris JN, Cooks RG, Syka JEP, Kelley PE, Stafford GC, Jr., Todd JFJ. 1987. Instrumentation, applications, and energy deposition in quadrupole ion-trap tandem mass spectrometry. Anal Chem 59: 1677–1685.

Ma S, Chowdhury SK. 2013. Data acquisition and data mining techniques for metabolite identification using LC coupled to high-resolution MS. Bioanalysis 5: 1285–1297.

Mack LL, Kralik P, Rheude A, Dole M. 1970. Molecular beams of macroions. II. J Chem Phys 52: 4977-4986.

Makarov A, Denisov E, Kholomeev A, Balschun W, Lange O, Strupat K, Horning S. 2006. Performance evaluation of a hybrid linear ion trap/orbitrap mass spectrometer. Anal Chem 78: 2113–2120.

Mann M, Meng CK, Fenn JB. 1989. Interpreting mass spectra of multiply charged ions. Anal Chem 61: 1702–1708.

Mann M, Talbo G. 1996. Developments in matrix-assisted laser desorption/ionization peptide mass spectrometry. Curr Opin Biotechnol 7: 11–19.

Mansoori BA, Dyer EW, Lock CM, Bateman K, Boyd RK, Thomson BA. 1998. Analytical performance of a high-pressure radiofrequency-only quadrupole collision cell with an axial field applied by using conical rods. J Am Soc Mass Spectrom 9: 775–788.

March RE. 1997. An introduction to quadrupole ion trap MS. J Mass Spectrom 32: 351–369.

Marchi I, Rudaz S, Veuthey J-L. 2009. Atmospheric pressure photoionization for coupling liquid-chromatography to mass spectrometry: A review. Talanta 78: 1–18.

Märk TD, Dunn GH. 1985. Electron impact ionisation. Springer Verlag. Wien. ISBN 978-3-709-14030-7.

Marquet P, Lachâtre G. 1999. Liquid chromatography–mass spectrometry: Potential in forensic and clinical toxicology. J Chromatogr B 733: 93–118.

Marquet P, Venisse N, Lacassie É, Lachâtre G. 2000. In-source CID mass spectral libraries for the "general unknown" screening of drugs and toxicants. Analusis 28: 925–934.

Marshall A, Hendrickson CL, Jackson GS. 1998. Fourier transform ion cyclotron resonance mass spectrometry: A primer. Mass Spectrom Rev 17: 1–35.

Matuszewski BK, Constanzer ML, Chavez-Eng CM. 2003. Strategies for the assessment of matrix effect in quantitative bioanalytical methods based on HPLC-MS/MS. Anal Chem 75: 3019–3030.

Matuszewski BK. 2006. Standard line slopes as a measure of a relative matrix effect in quantitative HPLC-MS bioanalysis. J Chromatogr B 830: 293–300.

McEwen CN, McKay RG, Larsen BS. 2005 Analysis of solids, liquids, and biological tissues using solids probe introduction at atmospheric pressure on commercial LC/MS instruments. Anal Chem 77: 7826–7831.

McLafferty FW, Tureček F. 1993. Interpretation of mass spectra, 4th ed. University Science Books, Mill Valley, CA. ISBN 978-0-935702-25-3.

Mesaros C, Lee SH, Blair IA. 2010. Analysis of epoxyeicosatrienoic acids by chiral liquid chromatography/electron capture atmospheric pressure chemical ionization mass spectrometry using [^{13}C]-analog internal standards. Rapid Commun Mass Spectrom 24: 3237–3247.

Michael SM, Chien BM, Lubman DM. 1992. An ion trap storage/time-of-flight mass spectrometer. Rev Sci Instrum 63: 4277–4284.

Michael SM, Chien BM, Lubman DM. 1993. Detection of electrospray ionization using a quadrupole ion trap storage/reflectron time-of-flight mass spectrometer. Anal Chem 65: 2614–2620.

Michalski A, Damoc E, Hauschild JP, Lange O, Wieghaus A, Makarov A, Nagaraj N, Cox J, Mann M, Horning S. 2011. Mass spectrometry-based proteomics using Q Exactive, a high-performance benchtop quadrupole orbitrap mass spectrometer. Mol Cell Proteomics 10, M111.011015, 1–12.

Miller PE, Denton MB. 1986. The quadrupole mass filter: Basic operating concepts. J Chem Educ 63: 617–622.

Montalti M, Credi A, Prodi L, Gandolfi MT. 2006. Handbook of photochemistry, 3rd ed. Taylor & Francis Group, LLC, Boca Raton, FL. ISBN 978-0-824-72377-5.

Montesano C, Sergi M, Moro M, Napoletano S, Romolo FS, Del Carlo M, Compagnone D, Curini R. 2013. Screening of methylenedioxyamphetamine- and piperazine-derived designer

drugs in urine by LC-MS/MS using neutral loss and precursor ion scan. J Mass Spectrom 48: 49–59.

Moore C, Rana S, Coulter C, Feyerherm F, Prest H. 2006. Application of two-dimensional gas chromatography with electron capture chemical ionization mass spectrometry to the detection of 11-nor-Δ^9-tetrahydrocannabinol-9-carboxylic acid (THC-COOH) in hair. J Anal Toxicol 30: 171–177.

Morris HR, Paxton T, Dell A, Langhorne J, Berg M, Bordoli RS, Hoyes J, Bateman RH. 1996. High-sensitivity collisionally-activated decomposition tandem mass spectrometry on a novel quadrupole–orthogonal acceleration time-of-flight mass spectrometer. Rapid Commun Mass Spectrom 10: 889–896.

Munson MSB. 2000. Development of chemical ionization mass spectrometry. Int J Mass Spectrom 200: 243–251.

Nguyen S, Fenn JB. 2007. Gas-phase ions of solute species from charged droplets of solutions. Proc Natl Acad Sci U S A 104: 1111–1117.

Nollet JA. 1754. Recherches sur les causes particulières des phénomènes électriques, Nouvelle Ed. H.L. Guerin & L.F. Delatour, Paris. (Modern re-edition ISBN: 978-1-276-08135-9).

Oberacher H, Arnhard K. 2015. Compound identification in forensic toxicological analysis with untargeted LC-MS-based techniques. Bioanalysis 7: 2825–2840.

Olsen JV, Macek B, Lange O, Makarov A, Horning S, Mann M. 2007. Higher-energy C-trap dissociation for peptide modification analysis. Nat Methods 4: 709–712.

Olsen JV, Schwartz JC, Griep-Raming J, Nielsen ML, Damoc E, Denisov E, Lange O, Remes P, Taylor D, Splendore M, Wouters ER, Senko M, Makarov A, Mann M, Horning S. 2009. A dual pressure linear ion trap orbitrap instrument with very high sequencing speed. Mol Cell Proteomics 8: 2759–2769.

Page JS, Kelly RT, Tang K, Smith RD. 2007. Ionization and transmission efficiency in an electrospray ionization-mass spectrometry interface. J Am Soc Mass Spectrom 18: 1582–1590.

Pang GF, Fan CL, Cao YZ, Yan F, Li Y, Kang J, Chen H, Chang QY. 2015. High throughput analytical techniques for the determination and confirmation of residues of 653 multiclass pesticides and chemical pollutants in tea by GC/MS, GC/MS/MS, and LC/MS/MS: Collaborative study, first action 2014.09. J AOAC Int 98: 1428–1454.

Patrie SM, Charlebois JP, Whipple D, Kelleher NL, Hendrickson CL, Quinn JP, Marshall AG, Mukhopadhyay B. 2004. Construction of a hybrid quadrupole–Fourier transform ion cyclotron resonance mass spectrometer for versatile MS–MS above 10 kDa. J Am Soc Mass Spectrom 15: 1099–1108.

Paul W, Steinwedel H. 1953. Ein neues Massenspektrometer ohne Magnetfeld. Z Naturforsh A 8: 448–450.

Paul W, Raether M. 1955. Das elektrische Massenfiler. Z Phys 140: 262–271.

Paul W. 1990. Electromagnetic traps for charged and neutral particles (Nobel lecture). Angew Chem Int Ed Engl 29: 739–748.

Plumb RS, Johnson KA, Rainville P, Smith BW, Wilson ID, Castro-Perez JM, Nicholson JK. 2006. UPLC/MS^E; A new approach for generating molecular fragment information for biomarker structure elucidation. Rapid Commun Mass Spectrom 20: 1989–1994.

Pringle SD, Giles K, Wildgoose JL, Williams JP, Slade SE, Thalassinos K, Bateman RH, Bowers MT, Scrivens JH. 2007. An investigation of the mobility separation of some peptide and protein ions using a new hybrid quadrupole/travelling wave IMS/oa-ToF instrument. Int J Mass Spectrom 261: 1–12.

Raffaelli A, Saba A. 2003. Atmospheric pressure photoionization mass spectrometry. Mass Spectrom Rev 22: 318–331.

Rauha J-P, Vuorela H, Kostiainen R. 2001. Effect of eluent on the ionization efficiency of flavonoids by ion spray, atmospheric pressure chemical ionization, and atmospheric pressure photoionization mass spectrometry. J Mass Spectrom 36: 1269–1280.

Rayleigh JWS. 1882. On the equilibrium of liquid conducting masses charged with electricity. Philos Mag series 5. 14: 184–186.

Ramm LE, Whitlow MB, Mayer MM. 1985. The relationship between channel size and the number of C9 molecules in the C5b-9 complex. J Immunol 134: 2594–2599.

Robb DB, Covey TR, Bruins AP. 2000. Atmospheric pressure photoionization: An ionization method for liquid chromatography–mass spectrometry. Anal Chem 72: 3653–3659.

Robb DB, Blades MW. 2005. Effects of solvent flow, dopant flow, and lamp current on dopant-assisted APPI for LC–MS. Ionization via proton transfer. J Am Soc Mass Spectrom 16: 1275–1290.

Robb DB, Blades MW. 2008. State-of-the-art in atmospheric pressure photoionization for LC/MS. Anal Chim Acta 627: 34–49.

Rosenfelder N, Vetter W. 2009. Gas chromatography coupled to electron capture negative on mass spectrometry with nitrogen as the reagent gas – an alternative method for the determination of polybrominated compounds. Rapid Commun Mass Spectrom 23: 3807–3812.

Ross MS, Wong CS. 2010. Comparison of electrospray ionization, atmospheric pressure photoionization, and anion attachment atmospheric pressure photoionization for the analysis of hexabromocyclododecane enantiomers in environmental samples. J Chromatogr A 1217: 7855–7863.

Roy TA, Field FH, Lin YY, Smith LL. 1979. Hydroxyl ion negative chemical ionization mass spectra of steroids. Anal Chem 51: 272–278.

Schmelzeisen-Redeker G, Bütfering L, Röllgen FW. 1989. Desolvation of ions and molecules in thermospray mass spectrometry. Int J Mass Spectrom Ion Processes 90: 139–150.

Schmid S, Jecklin MC, Zenobi R. 2011. Electrosonic spray ionization–an ideal interface for high-flow liquid chromatography applications. J Chromatogr A 1218: 3704–3710.

Schulten HR. 1982. Off-line combination of liquid chromatography and field desorption mass spectrometry: Principles and environmental, medical and pharmaceutical applications. J Chromatogr 251: 105–128.

Schwartz JC, Senko MW, Syka JEP. 2002. A two-dimensional quadrupole ion trap mass spectrometer. J Am Soc Mass Spectrom 13: 659–669.

Scigelova M, Hornshaw M, Giannokopulos A, Makarov A. 2011. Fourier transform mass spectrometry. Mol Cell Proteomics 10: M111.009431.1-19.

Senko MW, Remes PM, Canterbury JD, Mathur R, Song Q, Eliuk SM, Mullen C, Earley L, Hardman M, Blethrow JD, Bui H, Specht A, Lange O, Denisov E, Makarov A, Horning S, Zabrouskov V. 2013. Novel parallelized quadrupole/linear ion trap/orbitrap tribrid mass spectrometer improving proteome coverage and Peptide identification rates. Anal Chem 85: 11710–11714.

Shahin MM. 1966. Mass-spectrometric studies of corona discharges in air at atmospheric pressures. J Chem Phys 45: 2600–2605.

Short LC, Cai SS, Syage JA. 2007. APPI-MS: Effects of mobile phases and VUV lamps on the detection of PAH compounds. J Am Soc Mass Spectrom 18: 589–599.

Singh G, Gutierrez A, Xu K, Blair AI. 2000. Liquid chromatography/electron capture atmospheric pressure chemical ionization/mass spectrometry: Analysis of pentafluorobenzyl derivatives of biomolecules and drugs in the attomole range. Anal Chem 72: 3007–3013.

Sleno L, Volmer DA. 2004. Ion activation methods for tandem mass spectrometry. J Mass Spectrom 39: 1091–1112.

Smith DPH. 1986. The electrohydrodynamic atomization of liquids. IEEE Trans Ind Appl 22: 527–535.

Smith RD, Loo JA, Edmonds CG, Barinaga CJ, Udseth HR. 1990. New developments in biochemical mass spectrometry: Electrospray ionization. Anal Chem 62: 882–899.

Smith RD, Loo JA, Ogorzalek Loo RR, Busman M, Udseth HR. 1991. Principles and practice of electrospray ionization-mass spectrometry for large polypeptides and proteins. Mass Spectrom Rev 10: 359–452.

Smith RM. 2004. Understanding mass spectra. A basic approach, 2nd ed. Wiley Interscience, Hoboken, NJ. ISBN 978-0-471-42949-4.

Soglia JR, Harriman SP, Zhao S, Barberia J, Cole MJ, Boyd JG, Contillo LG. 2004. The development of a higher throughput reactive intermediate screening assay incorporating micro-bore liquid chromatography-micro-electrospray ionization-tandem mass spectrometry and glutathione ethyl ester as an in vitro conjugating agent. J Pharm Biomed Anal 36: 105–116.

Sparkman OD, Penton ZE, Kitson FG. 2011. Gas chromatography and mass spectrometry. A practical guide, 2nd ed. Academic Press, Burlington, MA. ISBN 978-0-123-73628-4.

Srebalus CA, Li J, Marshall WS, Clemmer DE. 1999. Gas-phase separations of electrosprayed peptide libraries. Anal Chem 71: 3918–3927.

Stafford GC Jr., Kelley PE, Syka, JEP, Reynolds WE, Todd JFJ. 1984. Recent improvements in and analytical applications of advanced ion trap technology. Int J Mass Spectrom Ion Processes 60: 85–98.

Stafford GC Jr., 2002. Ion trap mass spectrometry: A personal perspective. J Am Soc Mass Spectrom 13 (2002) 589–596.

Stahl DC, Swiderek KM, Davis MT, Lee TD. 1996. Data-controlled automation of liquid chromatography/tandem mass spectrometry analysis of peptide mixtures. J Am Soc Mass Spectrom 7: 532–540.

Stein SE, Scott DR. 1994. Optimization and testing of mass spectral library search algorithms for compound identification. J Am Soc Mass Spectrom 5: 859–866.

Stemmeler EA, Diener JL, Swift A. 1994. Gas-phase reactions of $O_2^{-\bullet}$ with alkyl and aryl esters of benzenedicarboxylic acids. J Am Soc Mass Spectrom 5: 990–1000.

Stemmeler EA, Hites RA. 1988. The fragmentation of negative ions generated by electron capture negative ion mass spectrometry: A review with new data. Biomed Environ Mass Spectrom 17: 311–328.

Straube EA, Dekant W, Völkel W. 2004. Comparison of electrospray ionization, atmospheric pressure chemical ionization, and atmospheric pressure photoionization for the analysis of dinitropyrene and aminonitropyrene LC-MS/MS. J Am Soc Mass Spectrom 15: 1853–1862.

Syage JA, Evans MD, Hanold KA. 2000. Photoionization mass spectrometry. Am Lab 32: 24–29.

Syka JE, Marto JA, Bai DL, Horning S, Senko MW, Schwartz JC, Ueberheide B, Garcia B, Busby S, Muratore T, Shabanowitz J, Hunt DF. 2004. Novel linear quadrupole ion trap/FT mass spectrometer: Performance characterization and use in the comparative analysis of histone H3 post-translational modifications. J Proteome Res 3: 621–626.

Takáts Z, Wiseman JM, Cooks RG. 2005. Ambient mass spectrometry using desorption electrospray ionization (DESI): Instrumentation, mechanisms and applications in forensics, chemistry and biology. J Mass Spectrom 40: 1261–1275.

Tanaka K, Waki H, Ido Y, Akita S, Yoshida Y, Yoshida T. 1988. Protein and polymer analyses up to *m/z* 100 000 by laser ionization time-of-flight mass spectrometry. Rapid Commun Mass Spectrom 2: 151–153.

Taylor G. 1964. Disintegration of water drops in an electric field. Proc R Soc London Ser A 280: 383–397.

Tian Q, Giusti MM, Stoner GD, Schwartz SJ. 2005. Screening for anthocyanins using high-performance liquid chromatography coupled to electrospray ionization tandem mass spectrometry with precursor-ion analysis, product-ion analysis, common-neutral-loss analysis, and selected reaction monitoring. J Chromatogr A 1091: 72–82.

Tsai CW, Yost RA, Garrett TJ. 2012. High-field asymmetric waveform ion mobility spectrometry with solvent vapor addition: A potential greener bioanalytical technique. Bioanalysis 4: 1363–1375.

Tsuchiya M, Aoki E, Kuwabara H. 1989. Clusters of water under atmospheric pressure studied by field ionization and liquid ionization mass spectrometry. Int J Mass Spectrom Ion Processes 90: 55–70.

Tyler AN, Clayton E, Green BN. 1996. Exact mass measurement of polar organic molecules at low resolution using electrospray ionization and a quadrupole mass spectrometer. Anal Chem 68: 3561–3569.

Urban J, Afseth NK, Štys D. 2014. Fundamental definitions and confusions in mass spectrometry about mass assignment, centroiding and resolution. Trends Anal Chem 52: 126–136.

van Bavel B, Geng D, Cherta L, Nácher-Mestre J, Portolés T, Ábalos M, Sauló J, Abad E, Dunstan J, Jones R, Kotz A, Winterhalter H, Malisch R, Traag W, Hagberg J, Ericson Jogsten I, Beltran J, Hernández F. 2015. Atmospheric-pressure chemical ionization tandem mass spectrometry (APGC/MS/MS) an alternative

to high-resolution mass spectrometry (HRGC/HRMS) for the determination of dioxins. Anal Chem 87: 9047–9053.

Van Berkel GJ, Pasilis SP, Ovchinnikova O. 2008. Established and emerging atmospheric pressure surface sampling/ionization techniques for mass spectrometry. J Mass Spectrom 43: 1161–1180.

van der Hooft JJ, Vervoort J, Bino RJ, Beekwilder J, de Vos RC. 2011. Polyphenol identification based on systematic and robust high-resolution accurate mass spectrometry fragmentation. Anal Chem 83: 409–416.

van Dongen WD, Niessen WMA. 2012. LC-MS systems for quantitative bioanalysis. Bioanalysis 4: 2391–2399.

van Veldhuizen EM, Rutgers WR. 2001. Corona discharges: Fundamentals and diagnostics. Proceedings of Frontiers in Low Temperature Plasma Diagnostics IV, Rolduc, The Netherlands, March 2001: 40–49.

Vestal ML. 1983. Ionization techniques for nonvolatile molecules. Mass Spectrom Rev 2: 447–480.

Vestal ML, Fergusson GJ. 1985. Thermospray liquid chromatograph/mass spectrometer interface with direct electrical heating of the capillary. Anal Chem 57: 2373–2378.

Vestal ML, Juhasz P, Martin SA. 1995. Delayed extraction matrix-assisted laser desorption time-of-flight mass spectrometry. Rapid Commun Mass Spectrom 9: 1044–1050.

Wang C, Gardinali PR. 2012. Comparison of multiple API techniques for the simultaneous detection of microconstituents in water by on-line SPE-LC-MS/MS. J Mass Spectrom 47: 1255–1268.

Wang G, Hsieh Y, Korfmacher WA. 2005. Comparison of atmospheric pressure chemical ionization, electrospray ionization, and atmospheric pressure photoionization for the determination of cyclosporin A in rat plasma. Anal Chem 77: 541–548.

Weinmann W, Wiedemann A, Eppinger B, Renz M, Svoboda M. 1999. Screening for drugs in serum by electrospray ionization/collision-induced dissociation and library searching. J Am Soc Mass Spectrom 10: 1028–1037.

Well PR. 1968. Group electronegativities. Prog Phys Org Chem 6: 111–145.

Wenner BR, Lynn BC. 2004. Factors that affect ion trap data-dependent MS/MS in proteomics. J Am Soc Mass Spectrom 15: 150–1507.

Whitehouse CM, Dreyer RN, Yamashita M, Fenn JB. 1985. Electrospray interface for liquid chromatographs and mass spectrometers. Anal Chem 57: 675–679.

Wilm M, Mann M. 1994. Electrospray and Taylor-cone theory, Dole's beam of macromolecules. Int J Mass Spectrom Ion Processes 136: 167–180.

Wilm M, Mann M. 1996. Analytical properties of the nanoelectrospray ion source. Anal Chem 68: 1–8.

Wilm M. 2011. Principles of electrospray ionization. Mol Cell Proteomics 10(7): M111.009407-1-8.

Winger BE, Light-Wahl KJ, Ogorzalek Loo RR, Udseth HR, Smith RD. 1993. Observation and implications of high mass-to-charge ratio ions from electrospray ionization mass spectrometry. J Am Soc Mass Spectrom 4: 536–545.

Wiza JL. 1979. Microchannel plate detectors. Nucl Instrum Methods 162: 587–601.

Wolfender J-L, Rodriguez S, Hostettmann K. 1998. Liquid chromatography coupled to mass spectrometry and nuclear magnetic resonance spectroscopy for the screening of plant constituents. J Chromatogr A 794: 299–316.

Wong SF, Meng CK, Fenn JB. 1988. Multiple charging in electrospray ionization of poly(ethylene glycols). J Phys Chem 92: 546–550.

Wu SL, Jardine I, Hancock WS, Karger BL. 2004. A new and sensitive on-line liquid chromatography/mass spectrometric approach for top-down protein analysis: The comprehensive analysis of human growth hormone in an *E. coli* lysate using a hybrid linear ion trap/Fourier transform ion cyclotron resonance mass spectrometer. Rapid Commun Mass Spectrom 18: 2201–2207.

Wyttenbach T, von Helden G, Bowers MT. 1996. Gas-phase conformation of biological molecules: Bradykinin. J Am Chem Soc 118: 8355–8364.

Wyttenbach T, Pierson NA, Clemmer DE, Bowers MT. 2014. Ion mobility analysis of molecular dynamics. Annu Rev Phys Chem 65: 175–196.

Xia YQ, Wu ST, Jemal M. 2008, LC-FAIMS-MS/MS for quantification of a peptide in plasma and evaluation of FAIMS global selectivity from plasma components. Anal Chem 80: 7137–7143.

Xie C, Zhong D, Yu K, Chen X. 2012. Recent advances in metabolite identification and quantitative bioanalysis by LC-Q-TOF MS. Bioanalysis 4: 937–959.

Yamashita M, Fenn FB. 1984a. Electrospray ion source. Another variation on the free-jet theme. J Phys Chem 88: 4451–4459.

Yamashita M, Fenn FB. 1984b. Negative ion production with the electrospray ion source. J Phys Chem 88: 4671–4675.

Yang L, Amad M, Winnik WM, Schoen AE, Schweingruber H, Mylchreest I, Rudewicz PJ. 2002. Investigation of an enhanced resolution triple quadrupole mass spectrometer for high-throughput liquid chromatography/tandem mass spectrometry assays. Rapid Commun Mass Spectrom 16: 2060–2066.

Yost RA, Enke CG. 1978. Selected ion fragmentation with a tandem quadrupole mass spectrometer. J Am Chem Soc 100: 2274–2275.

Zaikin V, Halket J. 2009. A handbook of derivatives for mass spectrometry. IM Publications LLP, Charlton, Chichester. ISBN 978-1-901-01909-4.

Zhurov KO, Fornelli L, Wodrich MD, Laskay ÜA, Tsybin YO. 2013. Principles of electron capture and transfer dissociation mass spectrometry applied to peptide and protein structure analysis. Chem Soc Rev 42: 5014–5030.

Zubarev RA, Makarov A. 2013. Orbitrap mass spectrometry. Anal Chem 85: 5288–5296.